약학박사 학위논문

관동화 유래 세스퀴테르펜 화합물에 의한 Nrf2 활성화 매개 신경보호 및 항건선 효능 연구

Neuroprotective and anti-psoriatic activities of sesquiterpenoids from *Tussilago farfara* mediated through Nrf2 activation

2019년 2월

서울대학교 대학원
약학과 천연물과학 전공
이 주 희

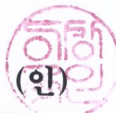# 관동화 유래 세스퀴테르펜 화합물에 의한 Nrf2 활성화 매개 신경보호 및 항건선 효능 연구

Neuroprotective and anti-psoriatic activities of sesquiterpenoids from *Tussilago farfara* mediated through Nrf2 activation

지도교수 김 영 식

이 논문을 약학박사 학위논문으로 제출함
2019 년 2 월

서울대학교 대학원
약학과 천연물과학 전공
이 주 희

이주희의 약학박사 학위논문을 인준함
2018 년 12 월

위 원 장: 이 상 국 (인)

부위원장: 박 성 혁 (인)

위   원: 노 민 수 (인)

위   원: 김 현 표 (인)

위   원: 김 영 식 (인)

Abstract

Neuroprotective and anti-psoriatic activities of sesquiterpenoids from *Tussilago farfara* mediated through Nrf2 activation

Joohee Lee

Natural Products Science

College of Pharmacy

The Graduate School

Seoul National University

Oxidative stress plays a key role in neurodegenerative diseases, such as Alzheimer's and Parkinson's disease. It is responsible for the dysfunction or death of neuronal cells that contribute to disease pathogenesis. Skin is the major target of oxidative stress, as it is continuously exposed to exogenous stressors, such as UV radiation and other environmental stresses producing reactive oxygen species. Thus, an efficient antioxidative strategy stimulating an endogenous defense mechanism is important for treatment of neurodegenerative diseases and psoriasis, a chronic inflammatory skin disease. Pharmacological activation of Nrf2, a master regulator of the antioxidant response, can be a beneficial therapeutic strategy. The present study demonstrates that 7β-(3′-ethyl-*cis*-crotonoyloxy)-1α-(2′-methylbutyryloxy)-3,14-dehydro-Z-notonipetranone (ECN) and tussilagonone (TGN),

sesquiterpenoids isolated from the medicinal plant *Tussilago farfara*, are potent, naturally occurring Nrf2 activators. Furthermore, the underlying mechanisms of Nrf2-mediated neuroprotection by ECN and amelioration of psoriatic features by TGN were investigated.

Phytochemicals are potent antioxidants and act as activators of Nrf2 inducing phase II detoxification enzymes and cytoprotective genes. Terpenoids, including sesquiterpenoids, activate Nrf2 through the Michael reaction of reactive cysteine residues on the Keap1 protein. Because of this common feature, various terpenoids have been reported to possess protective effects. However, Nrf2-mediated pharmacological activities of ECN and TGN have yet to be elucidated. The objective of this study was to i) assess the potency of ECN and TGN as Nrf2 activators and ii) investigate the molecular mechanisms underlying neuroprotective activities of ECN and anti-psoriatic properties of TGN both *in vitro* and *in vivo*.

ECN had a protective effect against oxidative stress-induced cell damage. ECN up-regulated Nrf2 and heme oxygenase-1 (HO-1) expression in PC12 cells at the transcriptional level and induced phosphorylation of Akt for Nrf2 activation. Knockdown of Nrf2 by small interfering RNA (siRNA) abrogated the protective effects of ECN, indicating that a neuroprotective effect of ECN against oxidative stress is mediated by Nrf2/HO-1 signaling. In a 6-OHDA-induced mouse model of Parkinson's disease, administration of ECN ameliorated motor impairments and dopaminergic neuronal damage.

TGN showed HO-1-mediated anti-inflammatory properties in macrophages and reduced the expression of inflammatory mediators in a 12-*O*-tetradecanoylphorbol-13-acetate (TPA)-induced skin inflammation mouse model.

Furthermore, TGN inhibited NF-kB and STAT3 activation, leading to attenuation of psoriasis-related inflammatory genes and hyperproliferation of keratinocytes. It was identified that inhibition of NF-κB and STAT3 by TGN is mediated through Nrf2 activation. Topical TGN treatment ameliorated imiquimod (IMQ)-induced psoriasis-like skin inflammation in mice. Moreover, TGN reduced inflammatory immune genes and epidermal hyperproliferation in IMQ-induced skin homogenates.

Taken together, these results suggest that ECN and TGN, as potent Nrf2 activators, could be attractive therapeutic candidates for the neuroprotection or treatment of neurodegenerative diseases and psoriasis.

CONTENTS

vii

LIST OF FIGURES

xii

I. INTRODUCTION

1. Neurodegenerative diseases

Neurodegenerative diseases, such as Alzheimer's disease (AD), Parkinson's disease (PD), and amyotrophic lateral sclerosis (ALS), are characterized by the progressive loss of structure or function of neuronal cells in distinct regions of the central nervous system (CNS) **(Fig. 1)**, resulting in cognitive and motor dysfunction [1]. Although the exact cause of each disease remains unclear, many lines of evidence suggest that neuroinflammation, oxidative stress, and mitochondrial dysfunction play a key role in the pathogenesis of neurodegeneration [2, 3].

Microglia, the resident immune cells of the CNS, is activated by pro-inflammatory stimuli, such as lipopolysaccharide (LPS) and neurotoxins. Activated microglia release pro-inflammatory mediators including nitric oxide (NO), prostaglandin E_2 (PGE_2), interleukin 1β (IL-1β), tumor necrosis factor α (TNF-α), and reactive oxygen species (ROS), which act as neurotoxins and cause neuronal loss. Microglia can become over-activated and remain in a chronic inflammatory state by neuronal damage and consequent reactive microgliosis, accelerating neurodegeneration **(Fig. 2)** [4, 5].

In the brain, reactive oxygen species (ROS), which cause oxidative stress, are mainly generated by dopamine metabolism, mitochondrial dysfunction, aging, and neuroinflammation. Several proteins related to the pathogenesis of AD and PD, such as amyloid-β peptide (Aβ), amyloid precursor protein (APP), α-synuclein,

parkin, PTEN-induced kinase1 (PINK1), DJ-1, and leucine-rich repeat kinase (LRRK2) are also associated with oxidative stress and mitochondrial dysfunction [6, 7]. Taken together, modulation of neuroinflammation and oxidative stress can be an effective pharmacological strategy for the prevention or treatment of neurodegenerative disorders.
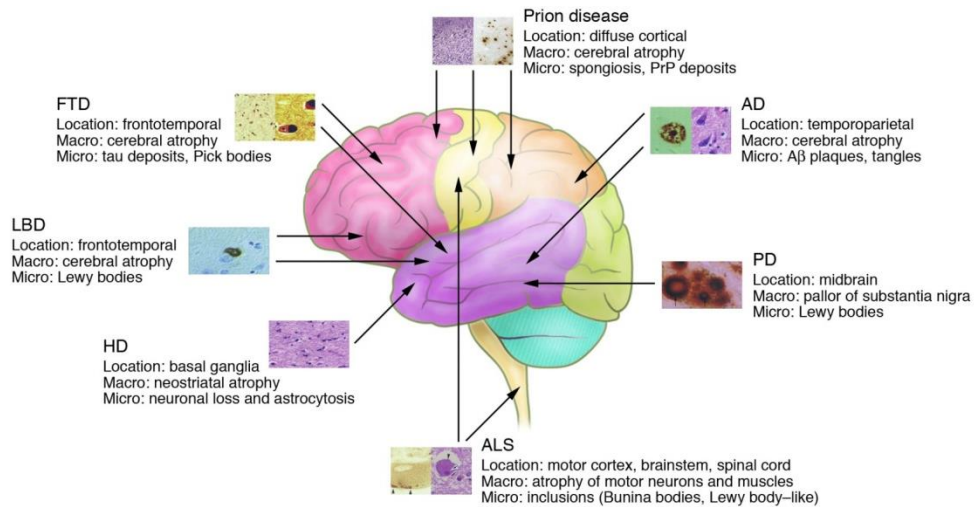
Figure 1. Overview of the anatomical location of and macroscopic and microscopic changes characteristic of the neurodegenerative disorders (adapted from ref. [8])

AD, Alzheimer disease; ALS, amyotrophic lateral sclerosis; FTD, frontotemporal dementia; HD, Huntington disease; LBD, Lewy body dementia; PD, Parkinson disease.
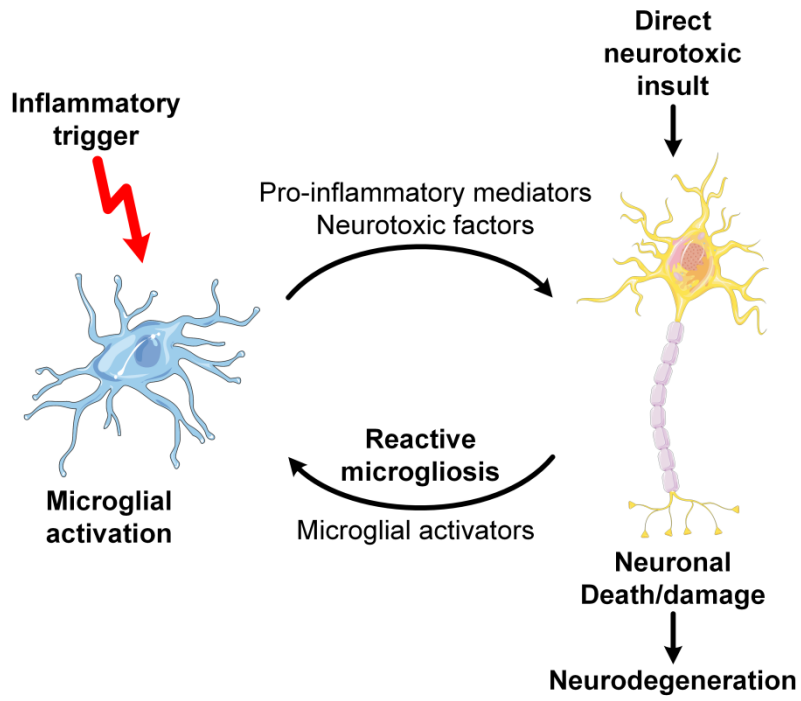
Figure 2. Neuronal damage driven by reactive microgliosis (slightly modified from ref. [3])

1.1. Parkinson's disease

PD is the second-most common neurodegenerative disorder with a prevalence of 1–2% in the elderly population. It is characterized by a selective loss of dopamine-producing neurons in the substantia nigra pars compacta (SNpc) and consequent depletion of dopamine levels as well as dopaminergic nerve terminals in the striatum **(Fig. 3)**, which causes motor symptoms, such as tremors, rigidity, and slowness of movement. Motor symptoms appear when more than half the dopaminergic nerve terminals degenerate, causing a 70–80% depletion of dopamine levels in the dorsal striatum [9, 10].

Current treatments for PD are symptomatic and do not slow or reverse the progressive loss of dopaminergic neurons. Levodopa, the chemical precursor of dopamine, is the most widely used and effective drug to treat motor symptoms of PD [11]. While dopamine cannot cross the blood brain barrier (BBB), levodopa can penetrate the BBB and is converted to dopamine by dopa decarbocylase (DDC). To inhibit levodopa metabolism prior to its transport across the BBB, a DDC inhibitor is combined with levodopa **(Fig. 4)**. Additionally, coadministration of catechol-*O*-methyltransferase (COMT) inhibitors block levodopa methylation into 3-*O*-methyldopa and prolong its duration of action in the CNS [11, 12]. In the striatum, levodopa, dopamine agonists, and monoamine oxidase type B (MAO-B) inhibitors all increase the amount of dopamine [12].

Neurotoxin-based models induced by 6-hydroxydopamine (6-OHDA) and 1-methyl-4-phenyl-1,2,3,6-tetrahydropyridine (MPTP) are widely used animal

models of PD. A common feature of these models is that they can induce the rapid death of dopaminergic neurons in the SNpc by producing oxidative stress [13]. MPTP enters the brain by crossing the BBB after systemic administration and is metabolized into its active form, MPP+, in astrocytes by MAO-B. MPP+ is transported into dopaminergic neurons through the dopamine transporter (DAT) and can be stored in mitochondria or synaptic vesicles via the vesicular monoamine transporter (VMAT). Unlike MPTP, 6-OHDA should be injected stereotaxically into the SNpc, medial forebrain bundle (MFB), or the striatum due to its inability to cross the BBB [14, 15]. Inside neurons, 6-OHDA exerts neurotoxicity via 1) its intra- or extracellular auto-oxidation, which produces hydrogen peroxide (H_2O_2) and superoxide and hydroxyl radicals; 2) formation of H_2O_2 by MAO-B, and 3) direct inhibition of mitochondrial respiratory chain complex I and participation in the formation of superoxide free radicals [16]. Recent studies have examined the neuroprotective effects of compounds by using these neurotoxin models of PD, supporting the fact that neurotoxin-induced animal models of PD are useful tools to investigate potential treatments for PD [17-20].

A
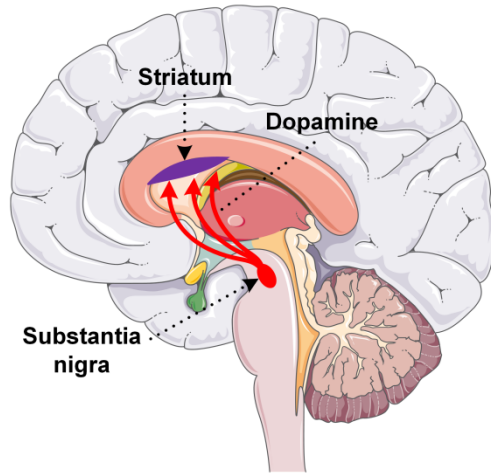
B
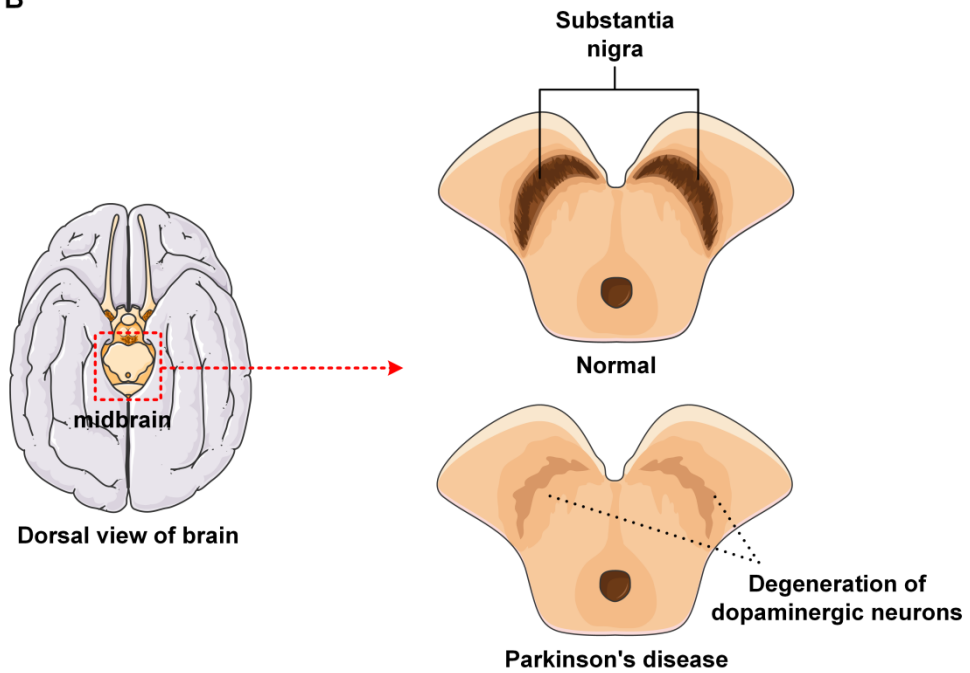
Figure 3. Brain regions affected by PD

(A) Nigrostriatal dopamine pathway (B) Diminished dopamine production in substantia nigra
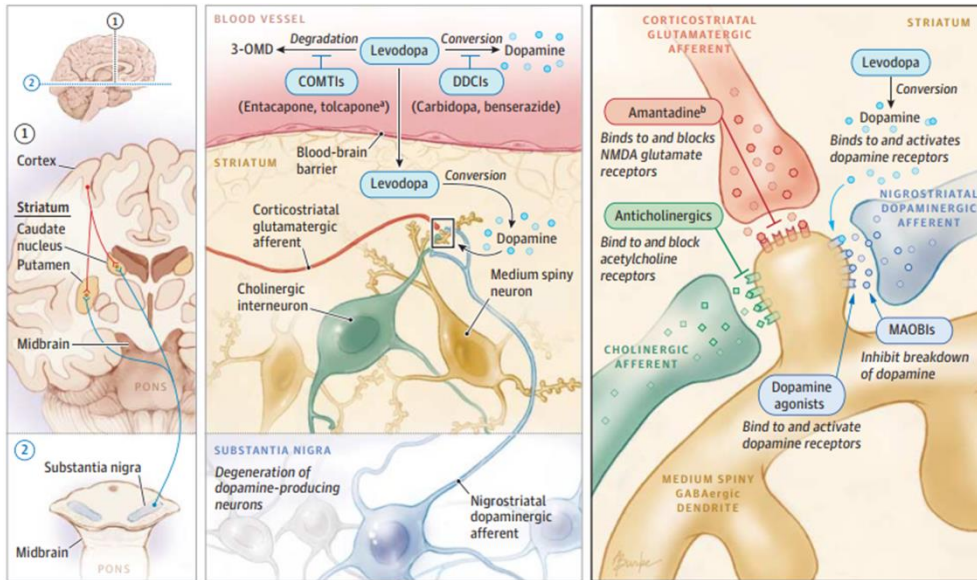
Figure 4. Schematic illustration of neurologic pathways affected in PD and sites of action of medications for the treatment of motor symptoms (adapted from ref. [12])

1.2. Phytochemicals for neuroprotection

Current treatments for neurodegenerative diseases provide only symptomatic relief but not reversal of disease progression. To overcome the limitations of current treatments, pharmacological approaches using phytochemicals for treating neurological disorders have emerged as new therapeutic strategies. Phytochemicals are biologically active secondary metabolites from plants and play a key role in protecting cells from inflammation and oxidative stress, which are major features of neurodegenerative diseases [21, 22]. Polyphenols constitute the largest group of phytochemicals and have therapeutic effects for chronic diseases as powerful antioxidants due to their multiple hydroxyl groups. Resveratrol, a polyphenolic stilbene, has been shown to have neuroprotective properties in various models of neurological disorders, not only by antioxidant and anti-inflammatory actions but also by improving mitochondrial functions and biogenesis through SIRT1/AMPK/PGC1α pathway [21-24]. Curcumin, one of the notable curcuminoids of turmeric, reduced the pathogenesis of AD by attenuating neurotoxic beta amyloid pathology and gliosis and provided protection against neuronal and brain mitochondrial damages in PD models [21-23, 25]. A recent study demonstrated that curcumin protected oxidative stress-induced injury in PD rats by activating the Wnt/β-catenin signaling pathway [26]. Berberine, an isoquinoline alkaloid with PI3K-activating activity, ameliorated the 6-OHDA-induced dopaminergic neuron loss and behavior movement deficiency in zebrafish mediated by upregulated PI3K/AKT/Bcl-2 cell survival and Nrf2/HO-1 antioxidative signaling pathways [26]. Carnosic acid, a diterpene from rosemary,

10

increased parkin protein in 6-OHDA-treated SH-SY5Y cells and rats, enhancing the ubiquitin-proteasome system, promoting a-synuclein degradation, and, consequently, preventing cell death [27]. Phytochemicals that have neuroprotective effects against neuronal damage by different mechanisms can be an attractive and promising strategy to prevent and treat neurodegenerative diseases **(Fig. 5)**.
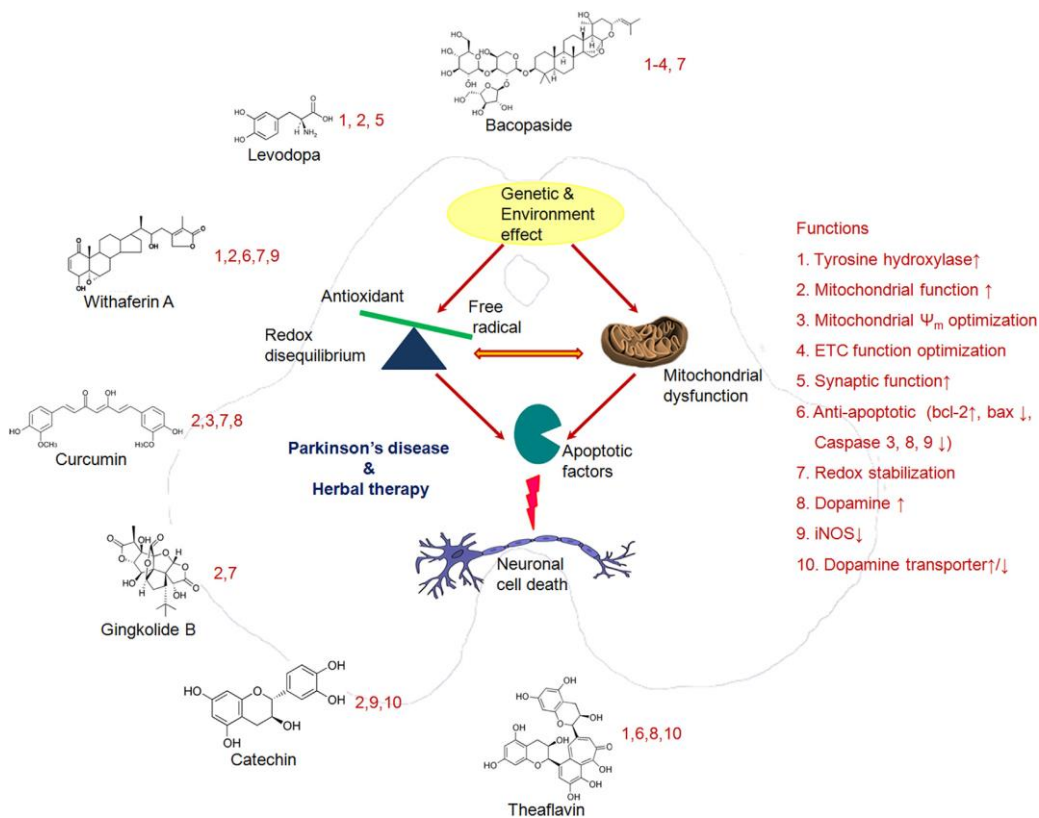
Figure 5. Illustration of role of the important constituents of different medicinal herbs and the possible cellular targets in PD therapy (adapted from ref. [25])

2. Psoriasis

Psoriasis is a chronic immune-mediated skin disease with a prevalence of 2-3% in the world's population. It is manifested as scaly plaques of red and thickened skin **(Fig. 6)** derived from epidermal hyperproliferation, hyperparakeratosis (retention of nuclei in the stratum), acanthosis (thickened epidermis) with elongated rete ridges, and immune cell infiltration **(Fig. 7)**. Patients with psoriasis experience low quality of life as a result of the economic and psychosocial burdens and are at risk of complications such as arthritis and cardiovascular disease [28].

Although the underlying cellular and molecular pathogenesis of psoriasis is complex and not fully understood, many lines of current evidence suggest that this skin disorder is mediated by the crosstalk between epidermal keratinocytes and immune cells [29, 30]. Psoriatic keratinocytes induce inflammatory mediators including cytokines (IL-6, IL-1β, TNF-α, and granulocyte–macrophage colony-stimulating factor), chemokines (CXCL1, CXCL2, CCL20, and CXCL8), and antimicrobial peptides (AMPs; S100A proteins, and β-defensin). These mediators contribute to the activation of immune cells and feed back into the proinflammatory disease cycle, inducing psoriatic keratinocyte phenotypes and infiltration of dermal immune cells [31].

The dysregulated Th17 pathway including the IL23/IL17 axis has been demonstrated to play a key role in the immunopathogenesis of psoriasis [29, 32, 33]. An external stimulus, such as stress, trauma, infection, drugs, and damage-

associated molecular patterns (DAMPs), can activate inflammatory and resident myeloid dendritic cells and macrophages to produce IL-23, IL-1β, and other proinflammatory cytokines including IL-6 and TNF. These innate immunity mediators stimulate the activities of key T cell populations, such as T helper 1 (T_H1), T_H17, and T_H22 cells, which release additional cytokines and chemokines. In addition, skin infiltrating inflammatory cells, such as mast cells, neutrophils, and NK and NK T cells, also contribute to the disease development *via* producing cytokines (IL-17), antimicrobial peptides, and cytotoxic granules. The pro-inflammatory cytokines and chemokines act on keratinocytes to undergo hyperproliferation and impaired differentiation, leading to the development of psoriatic lesions **(Fig. 7)** [32-35].

The currently used mouse models of psoriasis can be divided into acute (direct induced), genetically engineered (transgenic), and xenograft (humanized). Although these models are useful *in vivo* tool for investigating genetic and immune mechanisms contributing to psoriasis, no current model fully recapitulates all features of human psoriasis [36]. The imiquimod (IMQ)-induced psoriasisform dermatitis model is the most widely used murine model for preclinical studies of psoriasis [37]. Daily application of IMQ on mouse back skin involves the induction of erythema, skin thickening, scaling, epidermal alterations, and inflammatory cell infiltration [38]. The advantages of this model are due to its ease of use, low cost, and quick and reproducible inflammatory skin induction. However, this model has limitations: 1) unintended consequences of topical treatment; (2) unclear mechanism of action; (3) limited IMQ treatment duration; (4) induction of limited

14

aspects of human psoriasis [37].
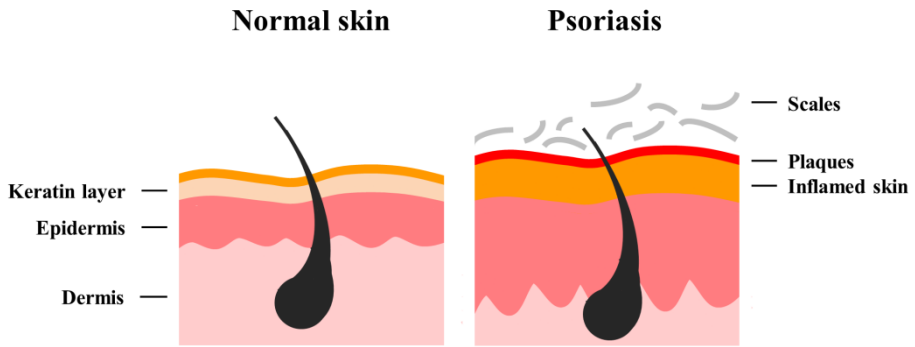
Figure 6. Illustration of the histopathological changes in psoriatic skin
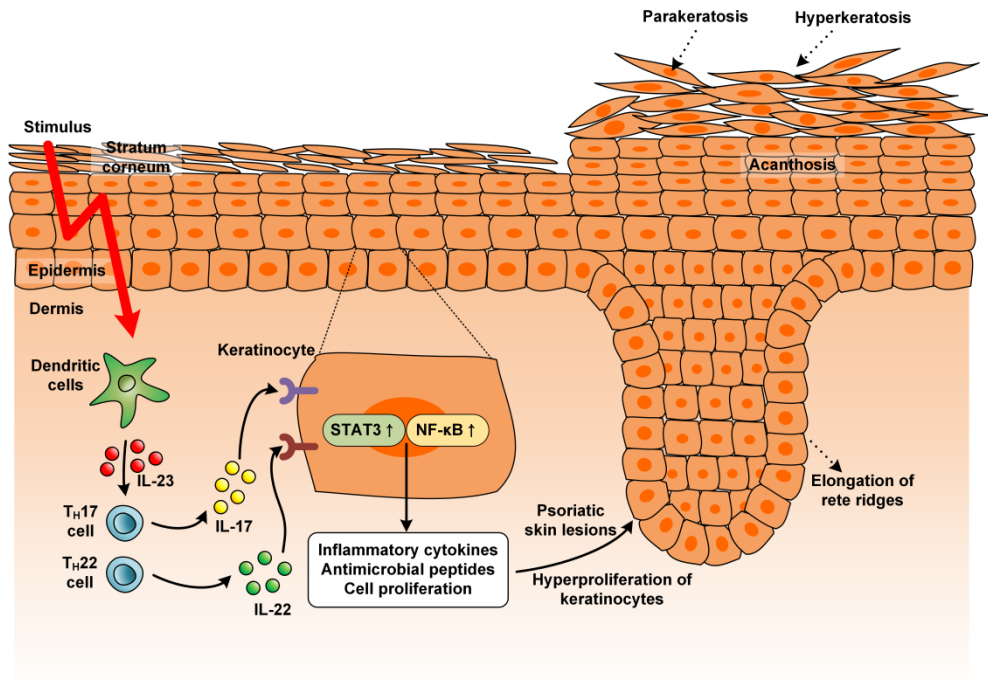
Figure 7. Mechanisms of psoriasis and psoriatic skin lesions

2.1. Inflammation

Inflammation is a complex defensive and adaptive response that removes harmful stimuli and restores homeostasis [39]. Macrophages have a major role in processing inflammatory responses, tissue repair and remodeling [40]. When toll-like receptor 4 (TLR4), a cell surface receptor, is activated by lipopolysaccharide (LPS) from gram-negative bacteria, macrophages are stimulated to initiate inflammatory signaling cascades *via* the nuclear factor (NF)-κB pathway [41]. In stimulated conditions, the p50 and p65 heterodimer of NF-κB is released from IκB, translocating from the cytoplasm to the nucleus, where it binds to specific promoter regions and triggers the expression of target genes. Inducible nitric oxide synthase (iNOS), cyclooxygenase-2 (COX-2) and proinflammatory cytokines such as TNF-α and IL-6 are regulated by NF-κB **(Fig. 8)** [42]. Therefore, the pharmacological inhibition of the NF-κB pathway plays a key role in preventing or treating inflammatory diseases and finding novel, potent plant-derived inhibitors of NF-κB is important for the field of anti-inflammatory drug discovery.

Heme oxygenase (HO) is a late limiting enzyme in heme metabolism that catalyzes heme degradation to carbon monoxide (CO), ferrous iron (Fe^{2+}), and biliverdin (BV), which is subsequently converted to bilirubin (BR) by BV reductase. These by-products of HO influence various biological events associated with inflammation [43]. Three distinct mammalian HO isoforms have been identified to date: HO-1, which is an inducible form, and HO-2 and HO-3, which are constitutively expressed forms [44, 45]. HO-1 exerts cytoprotective effects

against oxidative stress as a phase II detoxifying enzyme. Its expression is regulated through multiple signaling pathways, including phosphoinositide 3-kinase (PI3K)/protein kinase B (AKT), mitogen activated protein kinases (MAPKs), and the transcription factor nuclear factor-E2-related factor 2 (Nrf2) [46-48]. For example, carnosol, a diterpene derived from the herb rosemary, attenuates oxidative stress, leading to the up-regulation of HO-1 via the PI3K/AKT and Nrf2 pathways [49]. Resveratrol induces HO-1 expression by via through the AKT and extracellular signal regulated protein kinase 1/2 (ERK1/2) signaling pathways in PC12 cells [50]. HO-1 has also been considered to exhibit anti-inflammatory properties in several models of inflammation, including chronic arthritis, lung inflammation, liver ischemia/reperfusion injury, and inflammatory cardiovascular diseases [51-54]. Thus, HO-1 induction by natural phytochemicals is a beneficial therapeutic target for protection against oxidative stress and inflammatory disorders.
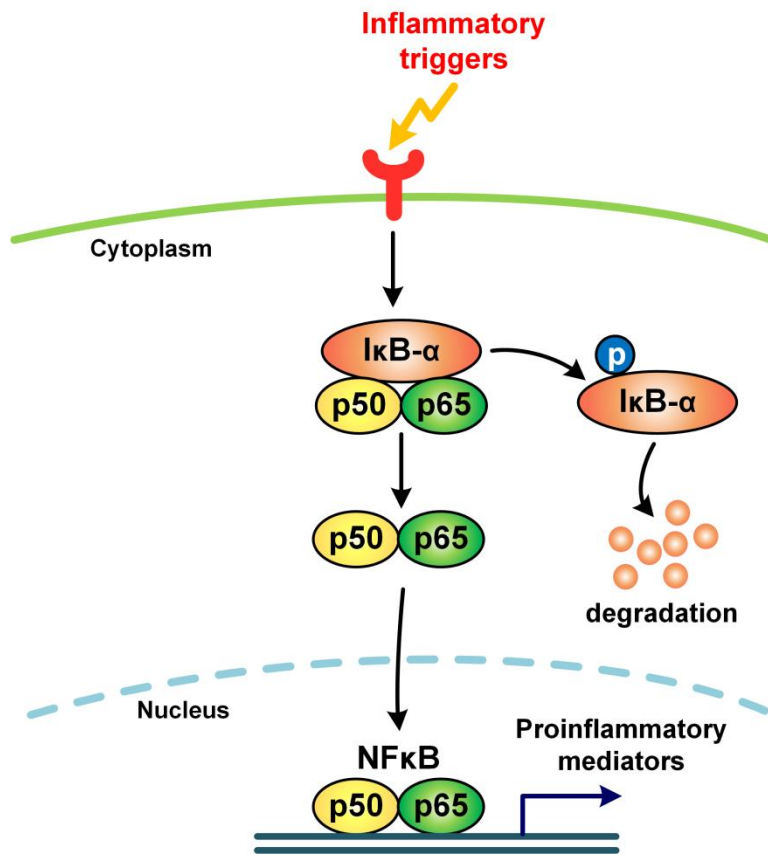
Figure 8. Activation of the NF-κB signaling pathway

2.2. Psoriasis treatment

Depending on the degree of psoriasis severity, different treatments are recommended. The main therapies are psoralen and ultraviolet A. (PUVA) photochemotherapy, topical treatment with corticosteroids, retinoids, immunosuppressants, vitamin D analogs, and biological therapies. Both corticosteroids and vitamin D analogs act by binding and activating hormone receptors that belong to the nuclear hormone receptor superfamily. In fact, these intracellular receptors act as ligand-dependent transcription factors and are the most frequently targets in the treatment of inflammatory pathologies, including skin diseases [28]. Corticosteroids are the most commonly used topical treatment for psoriasis of all grades, either as monotherapy or in combination with systemic treatment. Their therapeutic response is mediated by vasoconstriction, anti-inflammatory, and immunosuppressive effects; however, continuous treatments and/or high doses often cause severe systemic side effects, including hypertension, osteoporosis, cataracts, glaucoma, and diabetes, among others [55]. Regarding vitamin D analogs, they regulate genes involved in epidermal proliferation, inflammation, and keratinization. However, this treatment is also accompanied by side effects, as they can produce skin irritation and photosensitivity [55].

Systemic treatments involve the administration of drugs either orally or by injection. Specific biologic compounds were designed after the observation of improvement of psoriasis patients under immunosuppressive agents. General anti-psoriatic therapies target pro inflammatory pathways, which involve the use of

21

antibodies, soluble cytokine receptors, and fusion proteins. The first biological drugs for the treatment of psoriasis vulgaris were developed to target TNF-α, an important inflammatory cytokine belonging to the Th1-derived cytokines, which exerts pleiotropic effects and regulates inflammation and immune system [56]. However, as TNF-α is a major cytokine for the host defense, blocking this cytokine may cause side effects such as persistent fatigue and higher severity of infections, among others.

The IL-23 and IL-17 cytokines are important mediators of psoriasis and play a major role in the immunopathogenesis of psoriasis [57]. For this reason, the members of this axis have been considered as a potential target for the psoriasis treatment [29]. Several inhibitors of IL-23 and IL-17 have been recently tested in psoriasis patients. For instance, Ustekinumab, a monoclonal antibody that targets both IL-12 and IL-23 is used to treat moderate-to-severe psoriasis and results in the inhibition of the following downstream signaling pathway in T cells. Similarly, secukinumab and ixekizumab are also monoclonal antibodies that are approved for the treatment of the psoriasis that specifically bind to the IL-17 (**Fig. 9**). Additionally, monoclonal antibodies that are able to target IL-17 receptors were also developed [58].
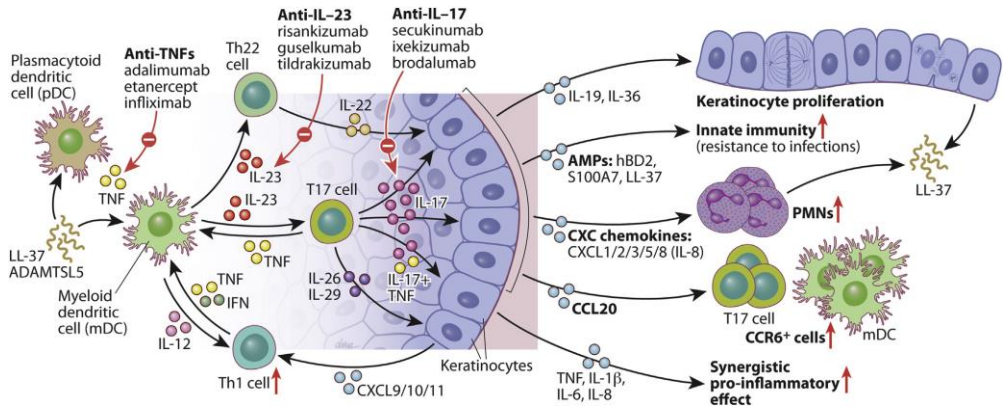
Figure 9. Biologics for the treatment of psoriasis (adapted from ref. [29])

Blocking targets of the biologics are TNF-α, IL-23, and IL-17.

3. Nuclear factor erythroid 2-related factor 2 (Nrf2)

Nuclear factor erythroid 2-related factor 2 (Nrf2) is a member of the "cap'n'collar" family of basic leucine zipper transcription factors, which also includes p45NF-E2, Nrf1, Nrf3, BACH1, and BACH2 [59]. It is an essential transcription factor that regulates antioxidant defense genes in maintaining cellular homeostasis. Under normal conditions, Nrf2 remains inactive in the cytoplasm by forming a complex with its inhibitory protein, Kelch-like ECH-associated protein 1 (Keap1), which promotes ubiquitination and the eventual degradation of Nrf2. Under stress conditions, Nrf2 activation occurs predominantly through conformational changes of Keap1, which are induced by electrophiles to this protein via the Michael addition. This results in the stabilization of Nrf2 and subsequent saturation of the Keap1 binding sites. In addition, it has been suggested that ROS activate certain kinases that induce Nrf2 phosphorylation, resulting in weakening of the Keap1–Nrf2 interaction. Newly synthetized Nrf2 translocates to the nucleus and dimerizes with small Maf proteins. These heterodimers bind to the antioxidant response element (ARE) in the promoter region of several cytoprotective genes, such as HO-1 and NAD(P)H quinone dehydrogenase 1 (NQO1), peroxiredoxins 1 and 6, and the glutathione biosynthesis enzymes glutamate-cysteine ligase (regulatory and catalytic subunits) and glutathione synthetase (**Fig. 10)** [60, 61].
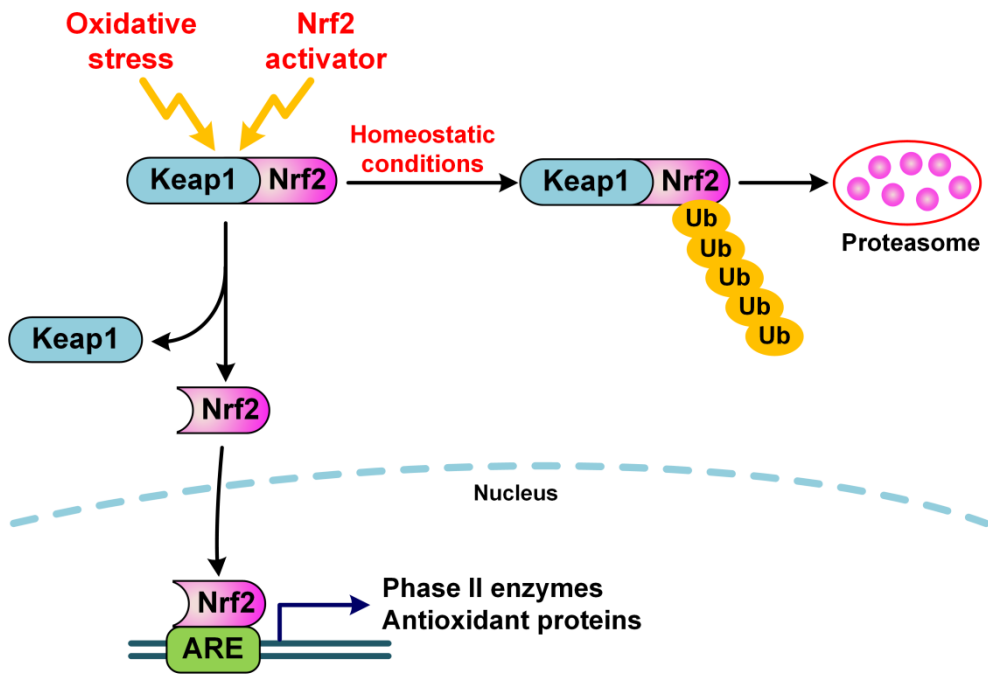
Figure 10. Activation of the Nrf2/ARE signaling pathway

Under normal conditions, Nrf2 remains inactive in the cytoplasm by forming a complex with its inhibitory protein Keap1, which promotes ubiquitination and the eventual degradation of Nrf2. Under stress conditions, Nrf2 is released from Keap1, translocates to the nucleus, and binds to the ARE in the promoter region of several cytoprotective genes.

3.1. Activation of the Nrf2 pathway for neuroprotection

The Nrf2 signaling pathway has been reported to be closely related to neurodegenerative diseases [61]. Nrf2 activation in astrocyte mediates neuroprotection against the 1-methyl-4-phenyl-1,2,3,6-tetrahydropyridine (MPTP)-induced neurotoxicity PD model in mice [62], and electrophilic compounds show protective effects both *in vitro* and *in vivo* against neuronal degeneration by activating the Keap1/Nrf2/HO-1 pathway [63]. Upregulation of HO-1, one of the target genes induced by Nrf2, plays a key role in neurodegenerative damage associated with AD and PD [64]. Therefore, the Nrf2/HO-1 pathway is a beneficial therapeutic target in the protection or treatment of neurodegenerative diseases.

Phytochemicals are potent antioxidants and act as activators of Nrf2 inducing phase II detoxification enzymes. Terpenoids, including mono-, sesqui-, di-, and triterpenoids, induce Nrf2 through the Michael reaction of reactive cysteine residues on the Keap1 protein. Because of this common feature, various terpenoids have been reported to possess protective effects [65, 66]. A previous study revealed that several sesquiterpenoids isolated from the buds of *Tussilago farfara* have anti-inflammatory actions in activated microglia and cytoprotective effects against LPS-induced neuronal cell death [67].

3.2. The role of Nrf2 in skin

Skin is the major target of oxidative stress, as it is continuously exposed to exogenous stressors, such as UV radiation and other environmental stresses producing ROS. Skin metabolism, chronic inflammation, and skin tissue damage are also endogenous stresses to generate ROS. Continued ROS might result in excessive oxidative stress leading to many skin diseases, including psoriasis [68]. Thus, an efficient antioxidative strategy stimulating an endogenous defense mechanism is important for treatment of psoriasis.

Many cytoprotective proteins, including HO-1 and NQO1, are under the control of Nrf2, a master regulator of the antioxidant response [69]. The activation of Nrf2 by several compounds was demonstrated to be beneficial in the prevention of skin carcinogenesis in a variety of animal studies [48]. In addition, Nrf2 activation was also investigated as a promising treatment strategy for allergic skin inflammation, atopic dermatitis, psoriasis, epidermal blistering disease, and vitiligo vulgaris [48].

4. *Tussilago farfara* L.

Tussilago farfara L **(Fig. 11A)**, commonly known as coltsfoot, is a perennial medicinal plant of the family Asteraceae that is widely distributed in Korea, China, Britain, Europe, North Africa, and sporadically in the United States. The dried flower buds of *T. farfara* (Farfarae Flos; **Fig. 11B**) have been used in traditional medicine to treat respiratory problems, such as cough, bronchitis, and asthma [70, 71]. A series of phytochemical studies on *T. farfara* have revealed that the plant contains a diverse number of compounds, including sesquiterpenes, polysaccharides, flavonoids, phenylpropanoids, chromones, and pyrrolizidine alkaloids, displaying several pharmacological properties, such as anti-inflammatory, antioxidative, and neuroprotective effects [72-75].

Figure 11. Pictures of *T. farfara* (adapted from google image)

The pictures of *T. farfara* (A) and the dried buds of *T. farfara* (B)

A
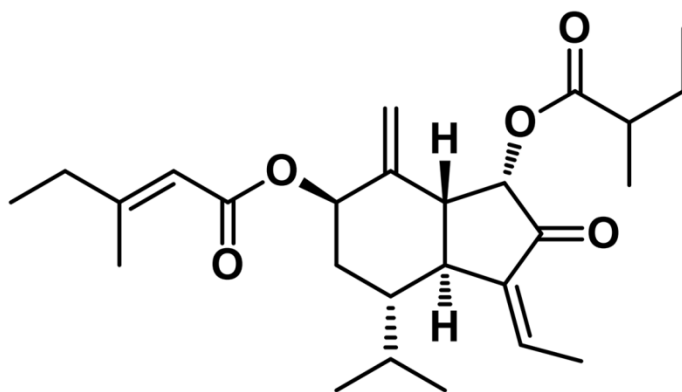
B
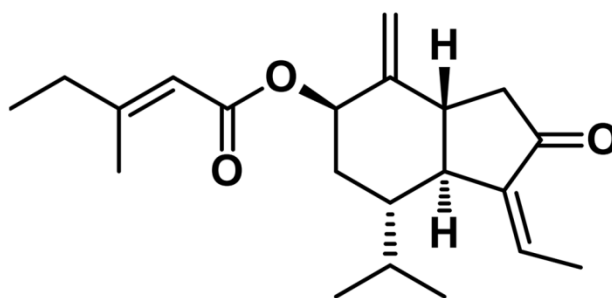
Figure 12. The chemical structures of sesquiterpenoids used in the present study

The chemical structures of 7β-(3-ethyl-cis-crotonoyloxy)-1α-(2-methylbutyryloxy)-3,14-dehydro-Z-notonipetranone (ECN) (A) and tussilagonone (TGN) (B) isolated from the dried buds of *T. farfara*

II. STATE OF THE PROBLEM

In this study, the molecular mechanisms underlying neuroprotective activities of 7β-(3-ethyl-cis-crotonoyloxy)-1α-(2-methylbutyryloxy)-3,14-dehydro-Z-notonipetranone (ECN) and anti-inflammatory and anti-psoriatic properties of tussilagonone (TGN) were investigated both *in vitro* and *in vivo*. Both ECN and TGN are sesquiterpenoids isolated from the buds of *Tussilago farfara* and act as Nrf2 activators.

A previous study revealed that several sesquiterpenoids isolated from the buds of *T. farfara*, including ECN, have anti-inflammatory actions in activated microglia and cytoprotective effects against LPS-induced neuronal cell death [73]. However, the Nrf2-mediated neuroprotective properties of ECN against oxidative stress and *in vivo* studies on the 6-OHDA-induced neurotoxicity in mice have yet to be elucidated. The objective of this study was, thus, to investigate cytoprotective activities against cell damage induced by oxidative stress and underlying molecular mechanisms of ECN. The potency of ECN to activate Nrf2 and induce HO-1 was also identified. In addition, this study aimed to determine whether ECN exerted any protective effects in an animal experimental model of neurodegeneration.

It has been reported that TGN exerts inhibitory effects on LPS-induced nitric oxide (NO) production, cytoprotective effects by activation of the Nrf2 pathway in HepG2 cells, and inhibitory effects on airway MUC5AC mucin gene expression and production [76-78]. However, the anti-inflammatory effects and underlying molecular mechanisms of TGN are not yet fully understood. The objective of this study was to investigate the potential crosstalk between HO-1

32

induction and the anti-inflammatory mechanisms induced by TGN in LPS-stimulated macrophages. The inhibitory effects of TGN on LPS-induced inflammatory responses and the signaling pathways mediating these processes were also identified. Furthermore, the *in vivo* effects of TGN on 12-*O*-tetradecanoylphorbol-13-acetate (TPA)-induced skin inflammation in mice were studied.

Although there are some biological agents for psoriasis that target pro-inflammatory cytokines, they are expensive and have some side effects [79]. Because of limitations of current therapies, multi-targeting phytochemicals can be beneficial for treatment of psoriasis. Based on the HO-1-mediated anti-inflammatory actions of TGN, it was hypothesized that TGN might be effective in other chronic inflammatory diseases, such as psoriasis, and that this effect could be mediated through the activation of the Nrf2 pathway. The main objective of the present research was to i) examine the therapeutic effect of TGN on psoriasis both *in vitro* and *in vivo* and ii) characterize the signaling crosstalk among Nrf2, NF-kB, and STAT3 in psoriasis. To prove the hypothesis of this study, the role of Nrf2 activation by TGN in regulating STAT3 and NF-κB activation in keratinocytes was examined. Additionally, an optimal mouse model of chronic psoriatic skin inflammation was achieved, and the therapeutic potential of TGN against psoriasis was elucidated.

III. RESULTS AND DISCUSSION

1. Neuroprotection against 6-OHDA toxicity in PC12 cells and mice through the Nrf2 pathway by ECN

1.1. ECN exerts protective effects against H_2O_2- or 6-OHDA-induced injury in PC12 cells

To investigate whether ECN is cytoprotective against oxidative stress, we used H_2O_2 or 6-OHDA. ECN alone did not show any cytotoxicity at concentrations of up to 10 μM **(Fig. 13A)**. Exposure to 500 μM H_2O_2 for 24 h decreased cell viability by $56.9 \pm 1.5\%$, while pretreatment of PC12 cells with ECN 10 μM increased cell viability of up to $91.8 \pm 6.6\%$ **(Fig. 13B)**. Incubation with 250 μM 6-OHDA for 24 h reduced cell viability to $50.6 \pm 2.4\%$. However, pretreatment with 5 and 10 μM ECN significantly abolished (***$P < 0.001$, compared with the 6-OHDA group) the cytotoxic effect of 6-OHDA, increasing cell viability to $80.7 \pm 2.3\%$ and $87.9 \pm 1.7\%$, respectively **(Fig. 13C)**. These results suggest that ECN has protective effects against oxidative stress-induced cell damage in PC12 cells.
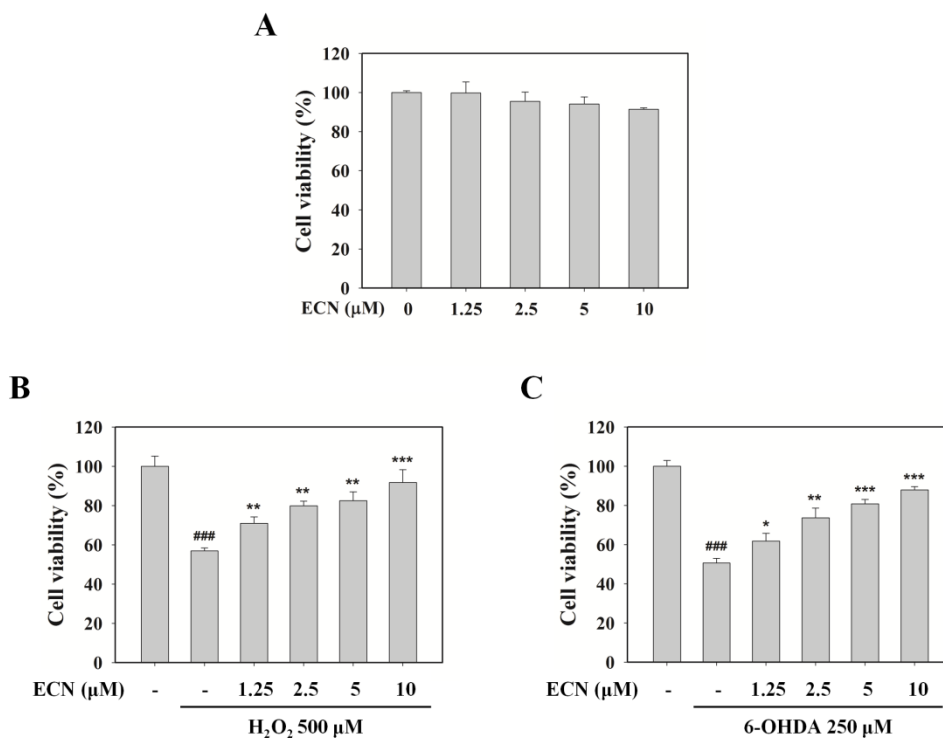
Figure 13. Cytoprotective effects of ECN on H_2O_2- and 6-OHDA-induced cell injury in PC12 cells

(A) PC12 cells were treated with the indicated concentrations of ECN for 24 h and cell viability was determined by an MTT assay. (B and C) Cells were preincubated with various concentrations of ECN for 24 h and then exposed to 500 μM H_2O_2 (B) or 250 μM 6-OHDA (C) for an additional 24 h. $^{###}P < 0.001$ indicates a significant difference from the untreated control group. $^*P < 0.05$, $^{**}P < 0.01$, and $^{***}P < 0.001$ indicate a significant difference compared with the H_2O_2- or 6-OHDA-only induced group.

36

1.2. ECN up-regulates Nrf2 and HO-1 expression in PC12 cells at the transcriptional level

The Nrf2 pathway is a valuable therapeutic target for neuroprotection [80]. Thus, it was examined whether ECN activates the Nrf2/HO-1 pathway. PC12 cells were treated with various concentrations of ECN (2.5, 5, or 10 μM) for 6 h or with 10 μM ECN from 1 h to 24 h, and protein levels of Nrf2 and HO-1 were determined by a Western blot analysis. As shown in **Fig. 14A**, ECN treatment upregulated Nrf2 and HO-1 protein expressions dose dependently. Sulforaphane (SFN), a well-known Nrf2 activator, was used as a positive control. Time course study showed that Nrf2 protein reached a maximum level 6 h after 10 μM ECN treatment, whereas Keap1 protein changed in the opposite expression pattern to that of Nrf2. HO-1 protein expression increased 3 h after ECN treatment **(Fig. 14B)**. We subsequently investigated whether the expression of both Nrf2 and HO-1 was regulated at the transcriptional level using real-time PCR. ECN treatment for 6 h induced a dose-dependent increase of both Nrf2 and HO-1 mRNA levels, showing 3.3- and 5.2-fold increase at 10 μM, respectively **(Fig. 14C)**. In the presence of actinomycin D (Act. D, 50 ng/ml) or cycloheximide (CHX, 10 μg/ml), upregulations of Nrf2 and HO-1 by ECN were reduced, indicating that ECN regulated Nrf2 and HO-1 expression at the transcriptional and translational levels **(Fig. 13D, E)**.
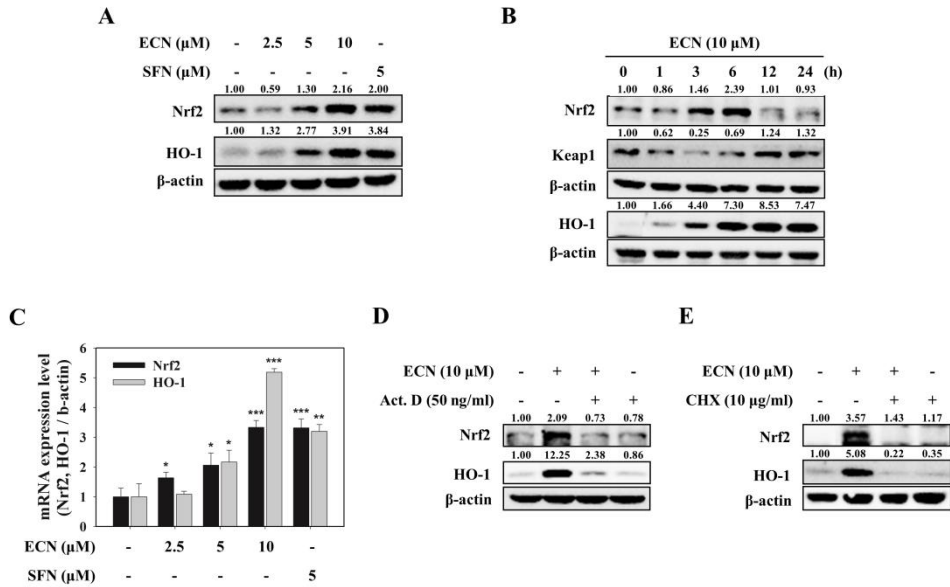
Fig. 14. Upregulation of Nrf2 and HO-1 expression at the transcriptional level in PC12 cells

(A) PC12 cells were treated with the indicated concentrations of ECN for 6 h. Total cell lysates were prepared for Western blot analysis to determine Nrf2 and HO-1 protein levels. SFN was used as a positive control. (B) Cells were treated with 10 μM ECN for the indicated times. (C) Cells were pretreated with the indicated concentrations of ECN for 6 h and mRNA levels of Nrf2 and HO-1 were analyzed by real-time PCR. (D and E) Cells were treated with 10 μM ECN for 6 h in the presence of actinomycin D (Act. D, 50 ng/ml) or cycloheximide (CHX, 10 μg/ml).

1.3. ECN-induced HO-1 expression is mediated through activation of Nrf2/ARE signaling

When Nrf2/ARE pathway is activated by Nrf2 inducers, Nrf2 translocates to the nucleus and ultimately induces its downstream target genes such as HO-1 [81]. Thus, it was identified whether ECN could enhance Nrf2 nuclear translocation and ARE-luciferase activity. ECN treatment increased the nuclear localization of Nrf2, as well as the expression of HO-1 in the cytoplasm **(Fig. 15A)**. Treatment of ECN upregulated ARE-luciferase activity time and dose dependently (up to 4.1-fold and 3.5-fold, respectively) **(Fig. 15B, C)**. To verify further whether ECN-induced HO-1 is mediated through activation of Nrf2, PC12 cells were transfected with siRNA targeting Nrf2. As shown in **Fig. 15D**, Nrf2 knockdown using siRNA blocked ECN-mediated HO-1 protein expression, suggesting that Nrf2 activation is crucial for ECN-induced HO-1 upregulation in PC12 cells.

A

ECN (10 μM)

	0	0.25	0.5	1	2	3	6	(h)
HO-1	1.00	1.21	1.24	3.33	3.61	14.99	30.98	Cytosol
β-actin								
Nrf2	1.00	1.37	1.91	10.07	17.34	16.28	17.05	Nucleus
PCNA								

B

C

D

	si Con		si Nrf2	
ECN (10 μM)	-	+	-	+
Nrf2	1.00	4.72	1.00	1.38
HO-1	1.00	10.66	1.00	0.71
β-actin				
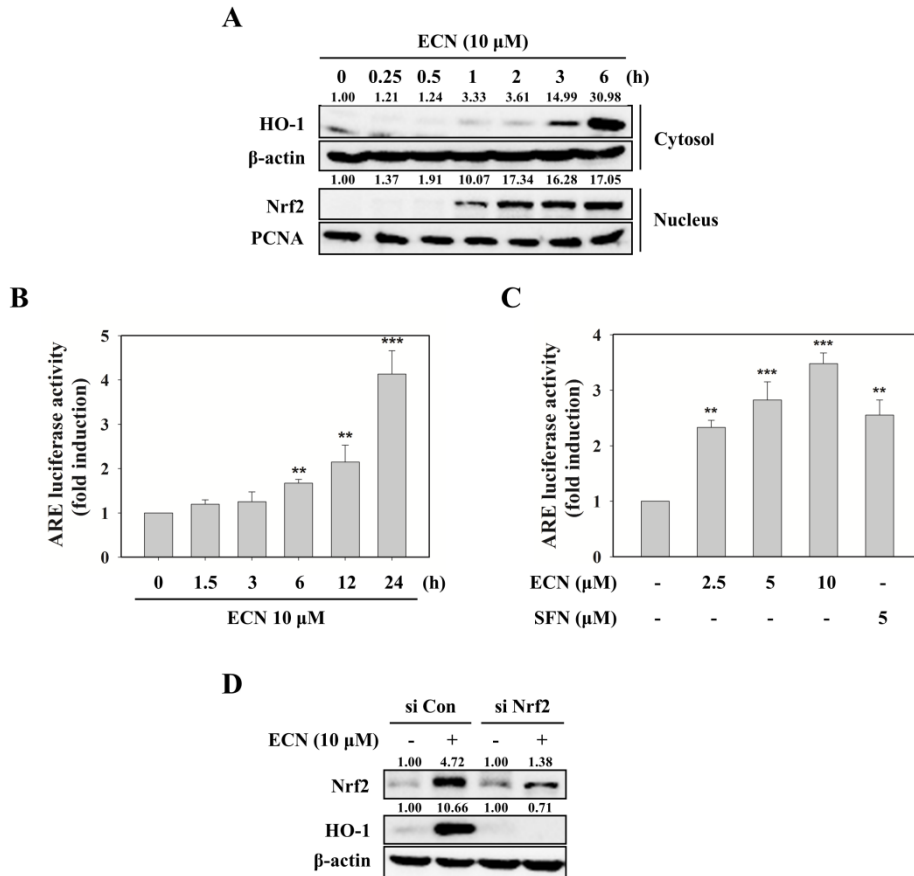
Figure 15. Effects of ECN on the activation of ARE/Nrf2 signaling

(A) PC12 cells were treated with 10 μM ECN for the indicated times. Nrf2 in the cytoplasm and nucleus and HO-1 in the cytoplasm were determined by Western blotting. (B and C) Cells were treated for the indicated times with 10 μM ECN (B) or 1 h with the indicated concentrations of ECN (C), and ARE-luciferase activity was measured. (D) Cells were transfected with 50 nM control siRNA (si Con) or Nrf2-targeted siRNA (si Nrf2) for 48 h and then treated with 10 μM ECN for 6 h.

1.4. ECN may directly modify thiols of Keap1 for Nrf2 activation

As it has been reported that mild oxidative or electrophilic stress can activate the Nrf2 pathway [82], it was examined if ECN activated the Nrf2/HO-1 signaling pathway by producing ROS. When PC12 cells were incubated with ECN for indicated time intervals, intracellular ROS levels measured by DCF-DA assay were increased time dependently until 1 h, and then decreased 2 h after treatment with ECN **(Fig. 16A)**. Preincubation with 5 mM NAC eliminated 10 μM ECN-caused ROS generation **(Fig. 16B)**. To elucidate further the role of ROS in ECN-induced Nrf2 and HO-1 activation, we used NAC (5 mM) and DTT (0.5 mM) as thiol reducing agents and Trolox (25 μM) as a non-thiol reducing antioxidant. Pretreatment with NAC or DTT abrogated ECN-induced HO-1 expression and Nrf2 transcriptional activity. However, Trolox did not reverse the effect of ECN on HO-1 and Nrf2 activation **(Fig. 16C, 17D)**. Collectively, these findings reveal that ECN may stabilize Nrf2 and upregulate Nrf2-mediated HO-1, by directly interacting with Keap1 and modifying critical cysteine thiols present in Keap1 rather than acting as a mild pro-oxidant.
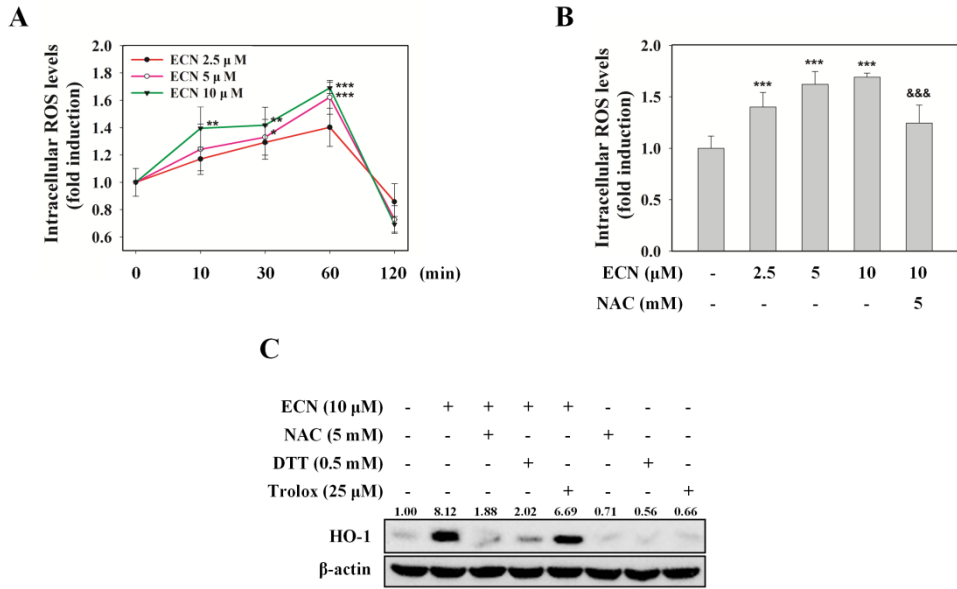
Figure 16. Role of ROS in Nrf2 activation

(A) PC12 cells were treated with ECN (2.5, 5, and 10 μM) for the indicated times and the levels of intracellular ROS were measured by DCFH-DA assay. $**P < 0.01$ and $***P < 0.001$ vs control (0 min). (B) Cells were treated with the indicated concentrations of ECN for 1 h. The antioxidant NAC served as a positive control. $***P < 0.001$ vs control group; $^{\&\&\&}P < 0.001$ vs ECN 10 μM treated group. (C) Cells were preincubated with various antioxidants for 1 h before treatment with ECN (10 μM) for 6 h to determine HO-1 levels.

42

1.5. ECN induces phosphorylation of Akt for Nrf2 activation

Next, it was investigated whether MAPKs or Akt contributed to the activation of Nrf2/HO-1. Pharmacological inhibition of Akt with LY294002, but not that of p38 (SB203580), JNK (SP600125), and ERK (U0126), inhibited ECN-induced HO-1 expression in PC12 cells **(Fig. 17A)**. In addition, ECN activated Akt phosphorylation at ser473 as early as 10 min after treatment **(Fig. 17B)**. Pretreatment with LY294002 abolished ECN-induced nuclear translocation of Nrf2 and ARE reporter gene activity **(Fig 17C, D)**. These results indicate that phosphorylation of Akt plays a role as an upstream signal in ECN-induced Nrf2/HO-1 activation.

A

ECN (μM)	-	10	10	10	10	10
LY294002 (μM)	-	-	20	-	-	-
SB203580 (μM)	-	-	-	20	-	-
SP600125 (μM)	-	-	-	-	20	-
U0126 (μM)	-	-	-	-	-	20
	1.00	2.14	0.93	1.76	1.68	1.68

HO-1

β-actin

B

ECN (10 μM)

	0	10	30	60	120	240 (min)
	1.00	2.97	3.37	2.72	2.10	1.60

p-Akt

| | 1.00 | 1.06 | 1.17 | 0.88 | 0.76 | 0.71 |

Akt

| | 1.00 | 1.17 | 1.36 | 2.50 | 2.60 | 3.28 |

Nrf2

β-actin

C

ECN (10 μM)	-	+	+	-
LY294002 (20 μM)	-	-	+	+
	1.00	2.59	0.38	0.25

Nrf2 (N)

PCNA

D

ARE luciferase activity (fold induction)

ECN (10 μM)	-	+	+	+	+	+	+
NAC (5 mM)	-	-	+	-	-	-	-
DTT (0.5 mM)	-	-	-	+	-	-	-
Trolox (25 μM)	-	-	-	-	+	-	-
LY294002 (20 μM)	-	-	-	-	-	+	-
SnPP (20 μM)	-	-	-	-	-	-	+

Figure 17. Role of Akt in Nrf2 activation

(A) Cells were preincubated with various kinase inhibitors for 1 h before treatment with ECN (10 μM) for 6 h to determine HO-1 levels. (B) Cells were treated with ECN (10 μM) for indicated intervals and then p-Akt and Nrf2 protein levels were determined. (C) Cells were pretreated with LY294002 for 1 h and then treated with ECN for 1 h. Nuclear levels of Nrf2 were analyzed. (D) Cells were pretreated with various antioxidants or kinase inhibitors for 1 h and then incubated with ECN for 24 h. [###]$P < 0.001$ vs control group; **$P < 0.01$ and ***$P < 0.001$ vs ECN 10 μM treated group.

44

1.6. Neuroprotective effect of ECN against oxidative stress is mediated by Nrf2/HO-1 signaling

To determine whether the neuroprotective effect of ECN against oxidative stress was attributed to Nrf2/HO-1 signaling, we used SnPP, a HO-1 activity inhibitor, and a knockdown of Nrf2 by siRNA transfection. Pretreatment with SnPP dose-dependently reversed the protective effect of 10 μM ECN **(Fig. 18A)**, and the Nrf2 siRNA transfection abolished the protective effect of ECN against 6-OHDA induced cell damage **(Fig. 18B)**. Taken together, these results indicate that activation of the Nrf2/HO-1 pathway is required for the neuroprotection of ECN in PC12 cells.

.
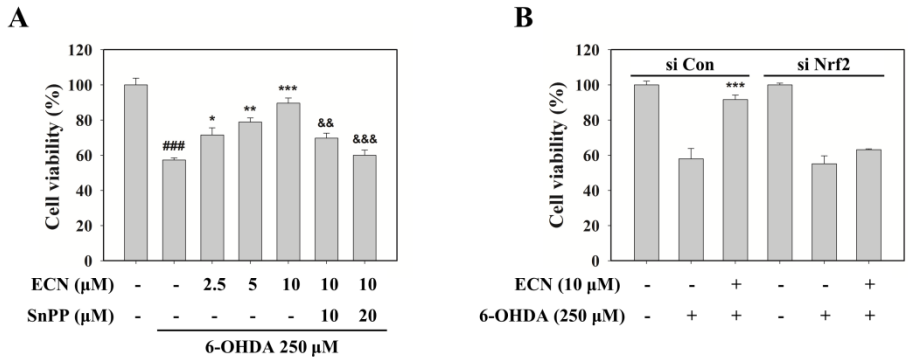
Figure 18. Nrf2/HO-1 signaling-mediated neuroprotective effects of ECN

(A) PC12 cells were pretreated with SnPP (10 or 20 μM) for 1 h before treatment with ECN (2.5, 5, and 10 μM) for 24 h and then exposed to 250 μM 6-OHDA for an additional 24 h. Cell viability was determined by the MTT assay. Data are presented as the mean ± SD. $^{###}P < 0.001$ indicates a significant difference from the 6-OHDA untreated control group; $^*P < 0.05$, $^{**}P < 0.01$, and $^{***}P < 0.001$ indicate a significant difference compared with the 6-OHDA-only exposed group; $^{&&}P < 0.01$ and $^{&&&}P < 0.001$ versus the 10 μM ECN plus 6-OHDA treated group. (B) Cells were transfected with 50 nM control siRNA (si Con) or Nrf2-targeted siRNA (si Nrf2) for 48 h and then treated with 10 μM ECN. After 24 h, cells were exposed to 250 μM 6-OHDA for an additional 24 h.

46

1.7. ECN ameliorates 6-OHDA-induced motor impairments

To demonstrate whether ECN functions as a potent neuroprotective agent on an *in vivo* model, the effects of ECN on a 6-OHDA-induced mouse model were examined **(Fig. 19A)**. Two kinds of behavior tests, rotarod test and apomorphine (APO)-induced rotation test, were conducted. The results from the rotarod test showed that the 6-OHDA injection impaired performance ($^{\#}P < 0.05$, compared with the control group). This was measured by the length of time that mice stayed on the rotating rod. However, ECN administration (5 mg/kg/day, for seven consecutive days) before 6-OHDA injection ameliorated this impairment, ($^{*}P < 0.05$) compared with the 6-OHDA-only group **(Fig. 19B)**. In the APO-induced rotation test, 6-OHDA significantly increased the number of rotations in 25 min ($^{\#\#\#}P < 0.001$, compared with the vehicle control), whereas pretreatment with ECN at 5 mg/kg/day considerably decreased the number of rotations ($^{**}P < 0.01$) compared with the 6-OHDA group **(Fig. 19C)**. These results indicate that ECN effectively improves 6-OHDA-induced movement impairments.
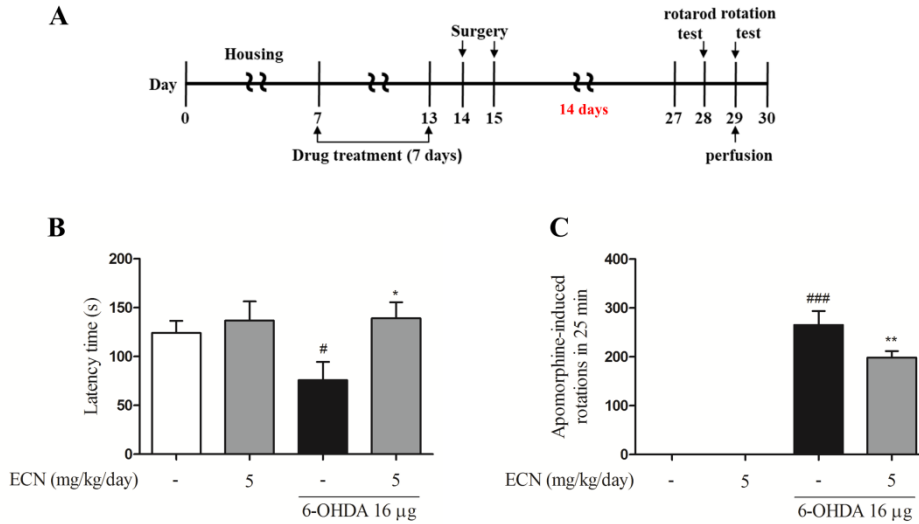
Figure 19. Effects of ECN on 6-OHDA-induced motor impairment in mice

(A) Schematic representation of the *in vivo* experimental design describing the treatment periods with 6-OHDA and ECN. ECN at 5 mg/kg dissolved in normal saline was administered for seven days. 6-OHDA was injected unilaterally via stereotaxic surgery in the right ST at one day after the last drug administration. (B) On the 14th day after 6-OHDA injection, latency time on the rotarod was tested. Data shown represent the three trial average time on the rotarod. (C) Contralateral rotations induced by APO were measured for 30 min 15 days after 6-OHDA lesion. $^{\#}P < 0.05$ and $^{\#\#\#}P < 0.001$ as compared with the saline-treated control group; $^{*}P < 0.05$ and $^{**}P < 0.01$ as compared with the 6-OHDA group.

1.8. ECN prevents 6-OHDA-induced dopaminergic neuronal damage in the ST and SN of the mouse brain

To confirm the neuroprotective effects of ECN against dopaminergic neuronal loss induced by 6-OHDA, immunostaining brain sections at the level of the SN and ST was conducted, for detecting TH and DAT—markers of dopaminergic neurons. Injection of 6-OHDA significantly reduced both TH-positive fibers and cells ($^{\#\#\#}P$ < 0.001) when compared with the control, while pretreatment with ECN at 5 mg/kg ameliorated this loss in the ST and SN ($^{**}P$ < 0.01 compared with the 6-OHDA group) **(Fig. 20A, B)**. A similar protective effect on DAT-positive fibers in the lesioned ST was also observed in the ECN-pretreated group **(Fig. 20C)**. Taken together, these results obtained from immunohistochemistry support the hypothesis that ECN can protect dopaminergic neuronal loss against neurotoxicity induced by 6-OHDA. Representative images for these data are shown in **Fig. 20D**.
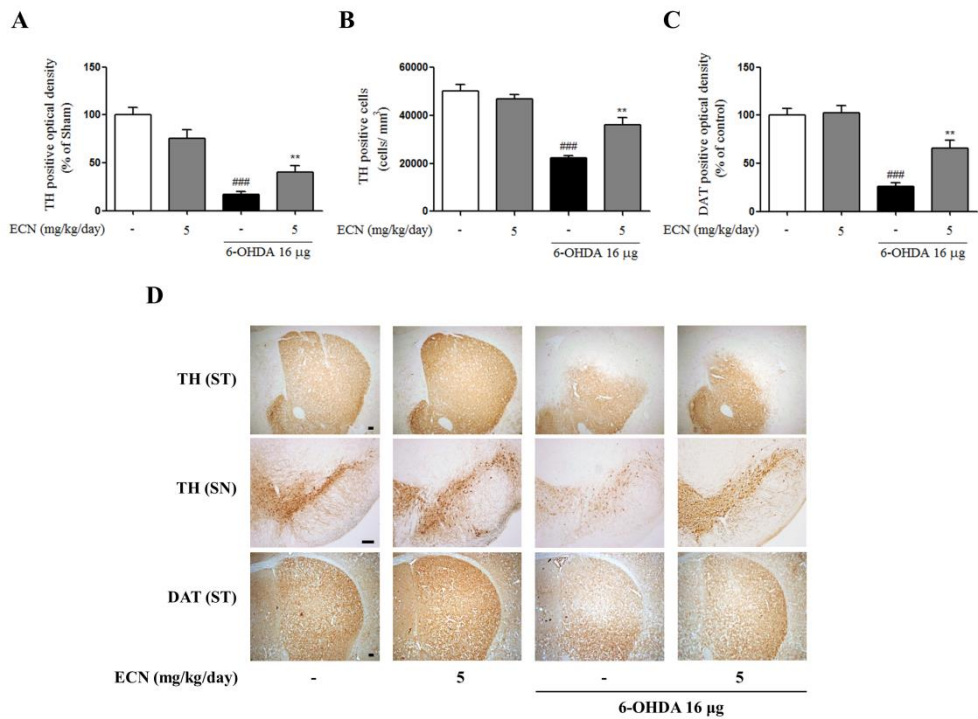
Figure 20. Protective effects of ECN on 6-OHDA-induced dopaminergic neuronal loss in the ST and SN of mice

(A) The optical density of TH-positive fibers in the ST was measured. (B) The numbers of TH-positive neurons in the SN were counted. (C) The optical density of DAT-positive fibers in the ST was measured. $^{\#\#\#}P < 0.001$ as compared with the sham group; $**P < 0.01$ as compared with the 6-OHDA group. (D) Representative immunostaining images are shown. Scale bar = 100 μm.

50

1.9. Discussion

The present study was designed to examine whether ECN provides Nrf2-mediated neuroprotective properties against oxidative stress. It was demonstrated that ECN activated the Nrf2/HO-1 signaling pathway and had the ability to protect PC12 cells from damage caused by oxidative stress. The beneficial effects of ECN were reversed by the inhibition of Nrf2/HO-1, supporting the hypothesis that Nrf2 activation is responsible for the neuroprotective effects of ECN **(Fig. 21)**. This is the first study to reveal that ECN is a potent natural Nrf2 activator and has protective effects on 6-OHDA-induced *in vivo* model.

Because oxidative stress is closely associated with neuronal damage in neurodegenerative diseases [83], pharmacological agents that activate Nrf2 have been reported to be potent for the treatment of neurodegenerative diseases in different experimental models [65, 80]. Dimethyl fumarate (DMF), an approved drug for the treatment of multiple sclerosis, activates the Nrf2 pathway showing a protective effect against α-synucleinopathy toxicity in the murine model of PD [84]. A natural alkaloid, berberine, protected PC12 cells against 6-OHDA-induced neurotoxicity through activating the Nrf2/HO-1 signaling pathway and improved 6-OHDA-induced dopaminergic neuron loss and behavior movement deficiency in zebrafish, which supported the potency of berberine for the prevention and treatment of neurodegenerative diseases [26]. Here, it was shown that ECN significantly activated Nrf2 and its target gene HO-1, which led to protective activity against oxidative stress in PC12 cells. Moreover, ECN alleviated motor

deficits and dopaminergic neuronal damage in the 6-OHDA mouse model. These results indicate that intraperitoneal administration of ECN has a protective effect against oxidative stress-induced neurotoxicity in the ST and SN of the mouse brain and PD-associated behavioral symptoms. Similar to other well-known Nrf2 activators such as curcumin and DMF [85], a structural feature of ECN that contains an α,β-unsaturated carbonyl moiety also supports the potential of ECN as a natural Nrf2 activator. Taken together, ECN may be a valuable pharmacological strategy for the treatment of oxidative stress-related neurodegenerative diseases, through activating the Nrf2 pathway.

Electrophiles and mild ROS have been demonstrated to induce Nrf2 activation and phase II enzymes [82, 86]. In addition, accumulated evidence supports that multiple protein kinases, including mitogen-activated protein kinases (MAPKs) and phosphatidylinositol-3-kinase (PI3K)/Akt, are associated with phosphorylation and nuclear accumulation of Nrf2 [87, 88]. For example, carnosol upregulated HO-1 through PI3K/Akt-dependent Nrf2 activation in PC12 cells [49]. Tussilagonone, one of the other sesquiterpenoids in *T. farfara*, phosphorylated MEK1/2 and ERK1/2 to induce Nrf2 nuclear accumulation and target genes showing cytoprotective effects in HepG2 cells [77]. The data obtained from this study indicate that ECN with electrophilic property can directly modify Keap1 cysteine thiols, thereby leading to Nrf2 stabilization and HO-1 induction. This finding is in agreement with a previous report, which showed that guggulsterone with an electrophilic center activated Nrf2 through direct modification of critical cysteine residues in Keap1 [89]. Further study is required to clarify which cysteine

residue is a direct target of ECN. It was also investigated whether upstream kinases are responsible for ECN-induced Nrf2 activation. Pretreatment of cells with PI3K/Akt LY294002 inhibited ECN-induced nuclear accumulation of Nrf2, ARE-luciferase activity, and HO-1 expression, suggesting the essential role of the Akt pathway in regulating the Nrf2-ARE pathway by ECN.

The neurotoxin 6-OHDA *in vivo* model is widely used to study the therapeutic potential of drugs to treat PD [26]. However, the neurotoxin-based animal models of PD often fall short in replicating the true aspects of idiopathic PD, thus, the results of animal studies have failed to translate into success in clinical trials [90-92]. Despite these limitations, 6-OHDA model is a useful tool for identifying neuroprotective effects associated with oxidative stress because it generates reactive oxygen species and mimics the neuropathological and biochemical features of neurodegeneration in PD, such as motor and behavioral deficits and the loss of dopaminergic neurons [93-95]. ECN administration ameliorated 6-OHDA-induced motor impairment and hypokinesia in the rotarod test and APO-induced rotation test. Because many studies have demonstrated a strong relationship between behavioral impairment and nigrostriatal dopaminergic neuronal loss [96-100], neuronal loss was investigated by measuring immunoreactivity of TH and DAT in the ST and SN of mice. TH, a rate-limiting enzyme of catecholamine biosynthesis, is a marker for dopaminergic neurons. In addition, DAT, a transmembrane transporter, is responsible for the re-uptake of extracellular dopamine into presynaptic neurons. Because PD is closely associated with dopamine metabolism, TH and DAT have been considered to be important

markers and therapeutic targets for PD [100-102]. A study in human brain tissues supports this notion by showing that there were reductions in TH and DAT staining in the nigrostriatal area of PD patients [103]. In this study, intrastriatal injection of 6-OHDA induced the loss of TH- and DAT-positive neurites in the ST- and TH-positive cells in the SNpc, which is consistent with the previous study [104]. However, the ECN-treated group recovered the down-regulated TH- and DAT-positive neurons of 6-OHDA-induced mice, which indicates that ECN-induced improvement of behavioral abnormalities in the mouse model is the result of a suppression of dopaminergic neuronal loss. Although further study is needed to evaluate whether ECN crosses the blood–brain barrier (BBB), several lines of evidence imply that bioavailability of ECN may make it pharmacologically effective *in vivo*. ECN, with a molecular weight of 430, has no ability to form hydrogen bonds with water according to the rules for hydrogen bonding [105], indicating that it possesses the physicochemical properties for BBB penetration [106]. Moreover, the estimated brain-to-plasma partition coefficient denoted by $K_{p,brain}$ value of ECN is 16.1 by an already known prediction method [107, 108], which means the total concentration of ECN in human brain tissue is predicted to be 16.1 fold higher than that in plasma.
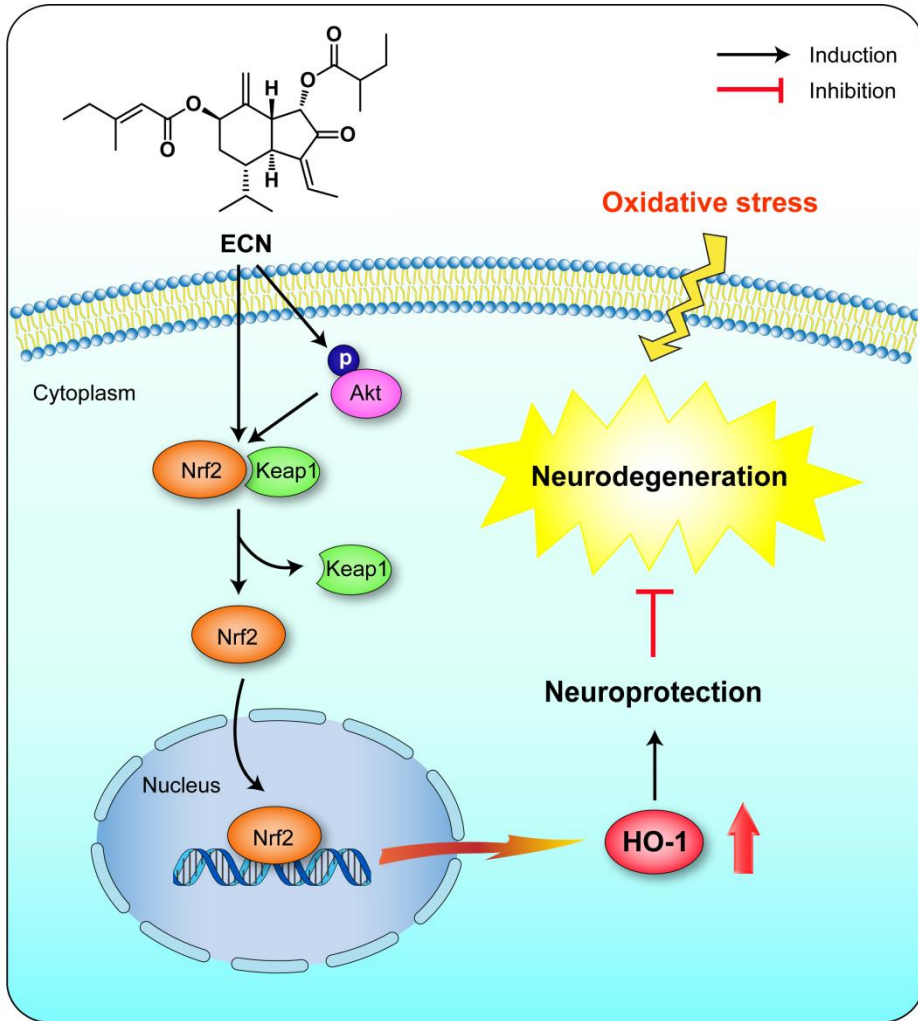
Figure 21. The proposed mechanism of Nrf2/ARE-mediated protective effects of ECN against oxidative stress-induced neurodegeneration

2. Amelioration of psoriasis-like skin lesions in keratinocytes and mice through Nrf2 activation by TGN

2.1. Heme oxygenase-1-mediated anti-inflammatory effects of TGN on macrophages and 12-*O*-tetradecanoylphorbol-13-acetate-induced skin inflammation in mice

2.1.1. TGN induces HO-1 expression in RAW 264.7 macrophages at the transcriptional level

HO-1 induction has been considered to have major anti-inflammatory therapeutic potential [109]. To determine whether TGN induces HO-1 expression in macrophages, RAW 264.7 cells were treated with different concentrations of TGN (2.5, 5 or 10 μM) for 6 h, and HO-1 protein expression was examined by Western blot analysis. TGN did not affect cell viability at concentrations up to 10 μM, as measured by MTT assay **(Fig. 22A)**. HO-1 protein levels were up-regulated in response to TGN treatment in a dose-dependent manner **(Fig. 22B)**. To examine the time course of HO-1 induction, cells were treated with 10 μM TGN from 1 to 24 h. HO-1 protein increased 3 h after TGN treatment, reaching maximum levels after 6-12 h and decreasing at 24 h **(Fig. 22C)**. Subsequently, it was examined whether TGN induced HO-1 expression at the transcriptional level. HO-1 mRNA levels were increased by TGN treatment for 3 h in a concentration-dependent manner, as

assessed by real-time PCR analysis **(Fig. 22D)**. To confirm that TGN-induced HO-1 expression is regulated at the transcriptional and translational levels, actinomycin D (Act. D), an inhibitor of DNA-dependent RNA polymerase, and cycloheximide (CHX), inhibitor of ribosomal protein synthesis, were used. Cotreatment of RAW 264.7 cells with TGN and Act. D or CHX blocked the HO-1 expression induced by TGN **(Fig. 22E, F)**. Taken together, these results suggested that HO-1 induction in response to TGN is primarily regulated at the level of gene transcription.
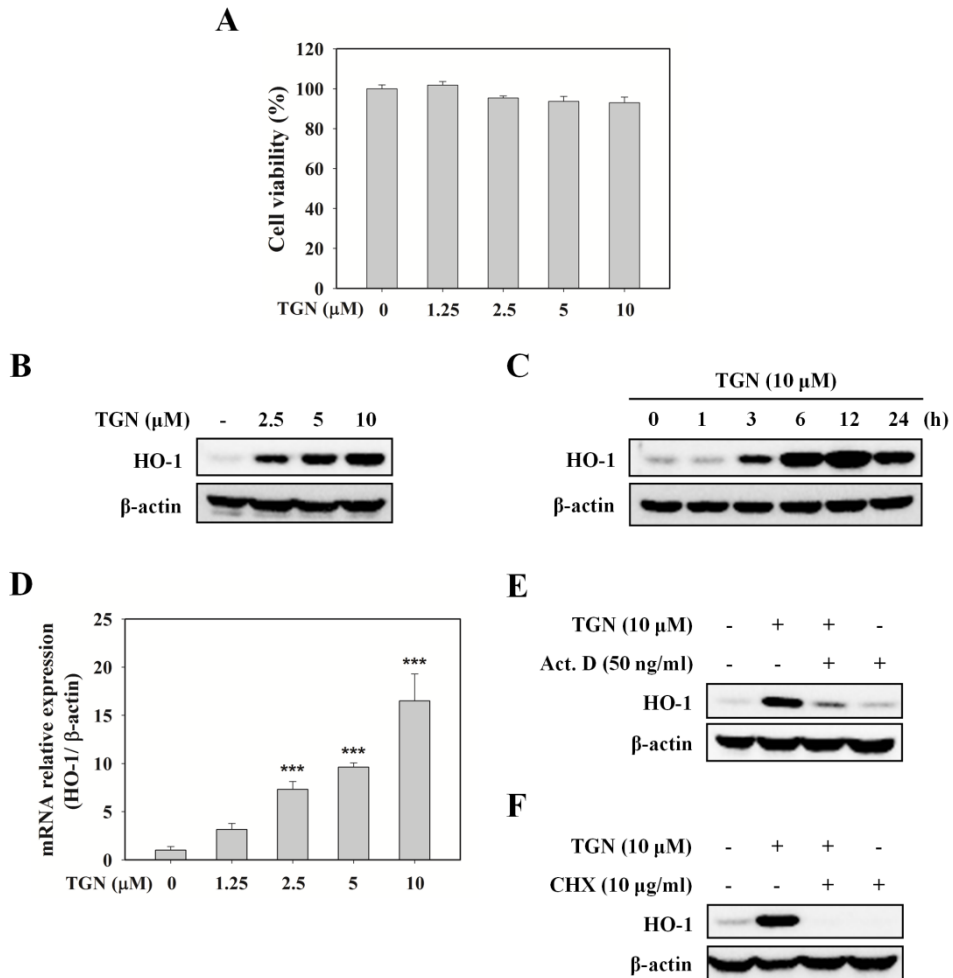
Figure 22. TGN induces HO-1 expression at the transcriptional level in RAW 264.7 cells.

(A) RAW264.7 cells were treated with the indicated concentrations of TGN for 24 h and cell viability was determined by an MTT assay. (B) Cells were incubated with various concentrations of TGN for 6 h. Total cell lysates were prepared for Western blot analysis to determine HO-1 expression levels. (C) Cells were treated with 10 μM TGN for the indicated periods of time. Whole lysates were prepared and HO-1 expression levels were determined by Western blot analysis. (D) RAW264.7 cells were treated with the indicated concentrations of TGN for 3 h.

Total RNAs were isolated and the relative HO-1 mRNA expression levels were evaluated by real-time PCR and calculated as $2^{-\Delta Ct}$, where $\Delta Ct = Ct_{(target\ gene)} - Ct_{(\beta\text{-}actin)}$. The values are expressed as the mean $\pm$ SD from three individual experiments. Asterisks indicate a significant difference (***$P<0.001$) from the untreated control. (E and F) Cells were treated with 10 µM TGN for 6 h in the presence of actinomycin D (Act. D, 50 ng/ml) or cycloheximide (CHX, 10 µg/ml), and then the cells were harvested for Western blot analysis of HO-1 expression levels.

2.1.2. TGN increases Nrf2 protein expression at the translational level in RAW 264.7 cells

Nrf2 is the major transcription factor that regulates HO-1 induction, and Nrf2 signaling is considered to be regulated by Keap1, which binds to and represses Nrf2 under normal conditions, leading to proteasomal degradation of Nrf2 [88]. Thus, it was determined whether TGN affects the Nrf2-Keap1 pathway by enhancing Nrf2 expression and causing Keap1 degradation. RAW 264.7 cells were treated with different concentrations of TGN (2.5, 5 or 10 μM) for 6 h, and then the total cell lysates were used for Western blot analysis. Nrf2 protein levels were significantly increased at the highest dose of TGN, whereas Keap1 protein levels were decreased **(Fig. 23A)**. Treatment with 10 μM TGN at various time intervals also revealed that the amount of Nrf2 increased within 1 h and reached its peak at 6 to 12 h after exposure to TGN, but Keap1 protein expression decreased in a time dependent manner **(Fig. 23B)**. To examine whether the increased Nrf2 expression was caused by increased Nrf2 transcription, we conducted real-time PCR. Nrf2 mRNA levels were unaffected by TGN treatment **(Fig. 23C)**. Moreover, Act. D failed to block TGN-induced Nrf2 protein expression **(Fig. 23D)**. In contrast, CHX reversed the Nrf2 protein level induced by TGN **(Fig. 23E)**. These results suggest that TGN activates the Nrf2-Keap1 pathway and that the Nrf2 protein level elevated by TGN is due to the regulation of Nrf2 translation.
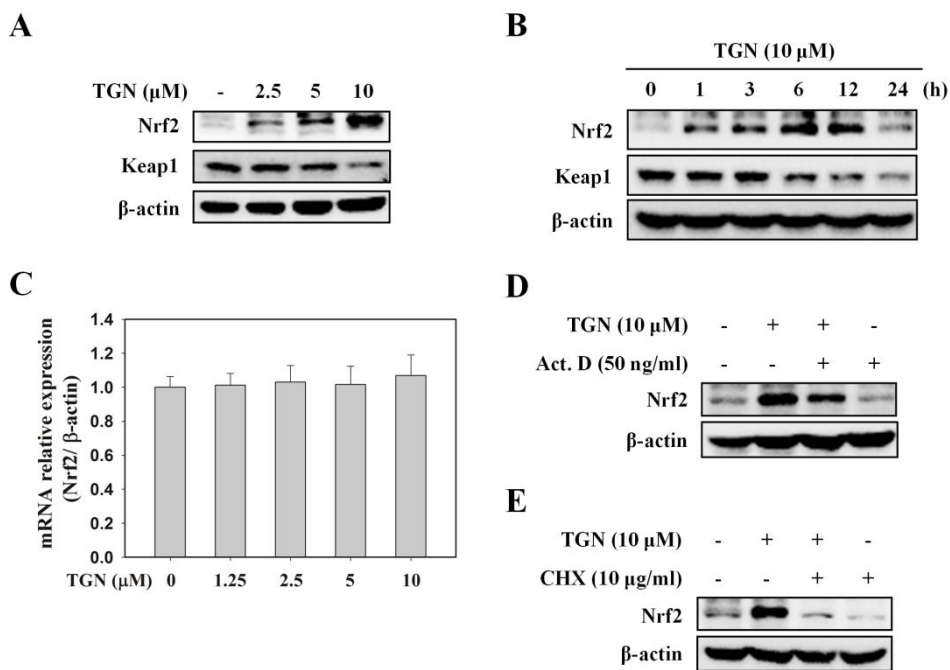
Figure 23. TGN induces Nrf2 activation at the translational level in RAW 264.7 cells.

(A) RAW 264.7 cells were treated with the indicated concentrations of TGN for 6 h. The whole cell extracts were prepared for Western blot analysis to determine Nrf2 and Keap1 protein levels. (B) Cells were treated with 10 μM TGN for the indicated times. Whole lysates were prepared and Nrf2 and Keap1 protein expression levels were determined by Western blot analysis. (C) RAW264.7 macrophages were treated with the indicated concentrations of TGN for 3 h. The cells were harvested for RNA preparation and the mRNA transcript levels of Nrf2 were analyzed by real-time PCR. The calculation method for the relative Nrf2 mRNA expressions was the same as described in Figure 1. ***$P<0.001$ indicates a significant difference from the untreated control. (D and E) Cells were treated with 10 μM TGN for 6 h in the presence of actinomycin D (Act. D, 50 ng/ml) or cycloheximide (CHX, 10 μg/ml) and then the Nrf2 protein levels were determined by western blot analysis.

2.1.3. TGN-induced HO-1 expression is mediated through activation of Nrf2

When cells are stimulated with Nrf2 inducers, Nrf2 dissociates from Keap1, translocates to the nucleus and ultimately activates the expression of phase II detoxifying enzymes such as HO-1 [81]. Therefore, it was examined the nuclear translocation of Nrf2 in cells treated with TGN using Western blot. Nrf2 translocation to the nucleus and nuclear accumulation was highest at 1 h after exposure to TGN and increased in a concentration-dependent manner. **(Fig. 24A, B)**. In addition, it was observed that HO-1 expression in the cytoplasmic fraction increased after Nrf2 translocation to the nucleus. To further confirm whether TGN-induced HO-1 expression was mediated by Nrf2 activation, small interfering RNA (siRNA) to target Nrf2 was used. Inhibited Nrf2 expression blocked TGN-mediated HO-1 expression **(Fig. 24C)**, suggesting that TGN induces HO-1 expression via Nrf2 activation.
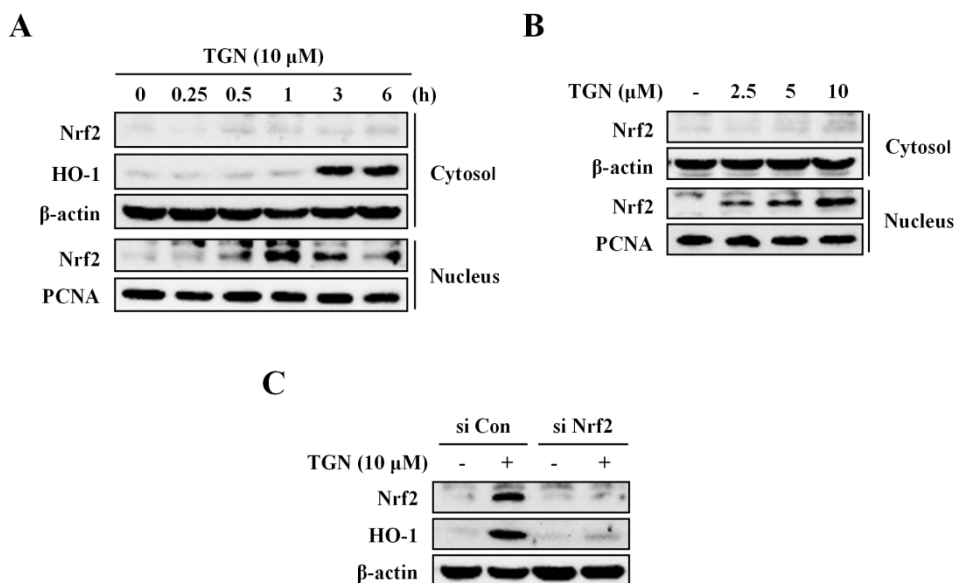
Figure 24. TGN up-regulates HO-1 expression through Nrf2 activation.

(A) RAW 264.7 cells were treated with 10 μM TGN for the indicated times. Nrf2 in the cytoplasm and nucleus and HO-1 in the cytoplasm were determined by Western blotting. PCNA and β-actin were used as markers for the nuclear and cytoplasmic extracts, respectively. (B) Cells were treated for 1 h with the indicated concentrations of TGN. The cytoplasmic and nuclear extracts were prepared for the Western blot analysis of Nrf2. (C) Cells were transfected with 50 nM control siRNA (si Con) or Nrf2-targeted siRNA (si Nrf2) for 48 h and then treated with 10 μM TGN for 6 h. The total protein extracts of cells were used for Western blotting to analyze Nrf2 and HO-1 expression levels. The data shown are representative of three independent experiments.

2.1.4. TGN inhibits the production of NO and PGE$_2$ as well as the expression of iNOS, COX-2, TNF-α and IL-6 in LPS-stimulated RAW 264.7 cells

To investigate the anti-inflammatory effect of TGN, we determined whether TGN inhibits the production of pro-inflammatory mediators, NO and PGE$_2$, in LPS-stimulated RAW 264.7 cells. The supernatants were collected to measure the amount of NO or PGE$_2$ with Griess reagent or an ELISA kit, respectively. Pretreatment of cells with TGN significantly inhibited both LPS-induced NO (IC$_{50}$ = 2.01 ± 0.2 μM) and PGE$_2$ production (IC$_{50}$ = 2.66 ± 0.67 μM) in a dose-dependent manner **(Fig. 25A, B)**. Consistent with these results, Western blot analysis also revealed that TGN inhibited iNOS and COX-2 protein expression in a concentration-dependent manner in LPS-stimulated RAW 264.7 cells **(Fig. 25C)**. In contrast, HO-1 expression was enhanced by increasing concentrations of TGN, regardless of LPS stimulation. LPS-induced mRNA expression of iNOS and COX-2 were attenuated in the presence of TGN **(Fig. 26A, B)**. These results indicate that TGN suppresses NO and PGE$_2$ production by affecting iNOS and COX-2 expression at the transcriptional level. Furthermore, mRNA expression of TNF-α and IL-6, pro-inflammatory cytokines that promote systemic inflammation was also investigated. TGN treatment inhibited the mRNA expression levels of these cytokines in a dose-dependent manner compared with those treated with LPS alone **(Fig. 26C, D)**.
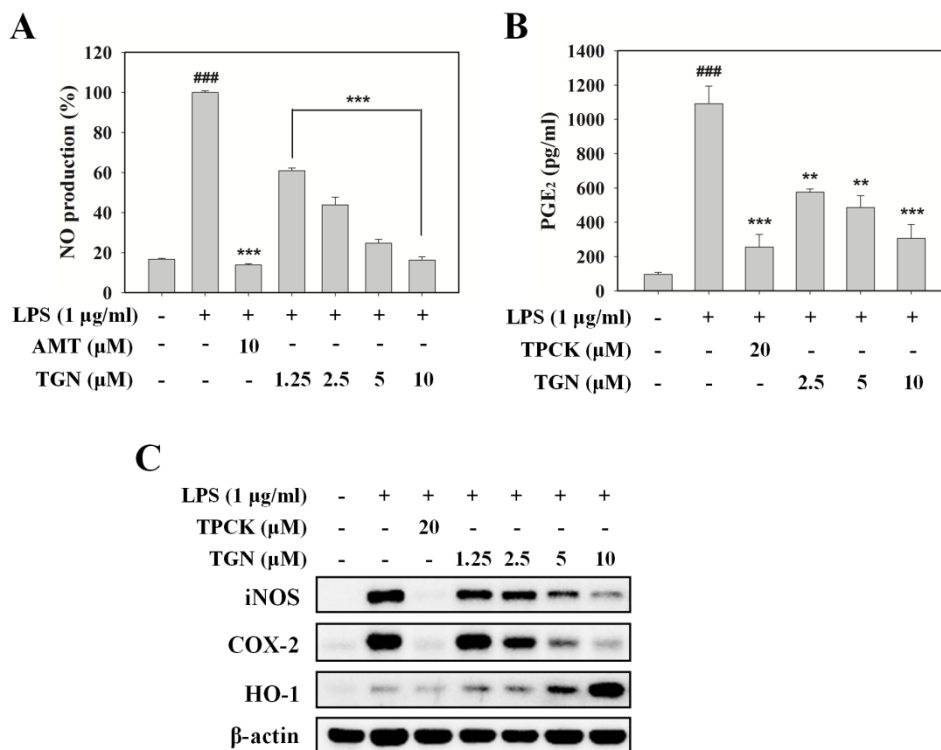
Figure 25. TGN inhibits LPS-induced inflammatory mediators.

(A and B) RAW 264.7 cells were preincubated with the indicated concentrations of TGN for 6 h, followed by stimulation with LPS (1 μg/ml) for 18 h. The amounts of NO (A) and PGE_2 (B) in the supernatants were quantified by the Griess reagent and a PGE_2 ELISA kit, respectively. In this experiment, 10 μM 2-amino-5,6-dihydro-6-methyl-4H-1,3-thiazine (AMT) (A) and 20 μM 2-N-p-tosyl-L-phenylalanine chloromethyl ketone (TPCK) (B) were used as positive controls. [###]$P<0.001$ indicates a significant difference from the unstimulated control group and **$P<0.01$ and ***$P<0.001$ indicate a significant difference from the LPS-only stimulated group. (C) Cells were pretreated with the indicated concentrations of TGN for 6 h and then stimulated with LPS (1 μg/ml) for 18 h. Whole cell lysates were prepared for Western blot analysis to determine the expression levels of iNOS, COX-2 and HO-1.

65
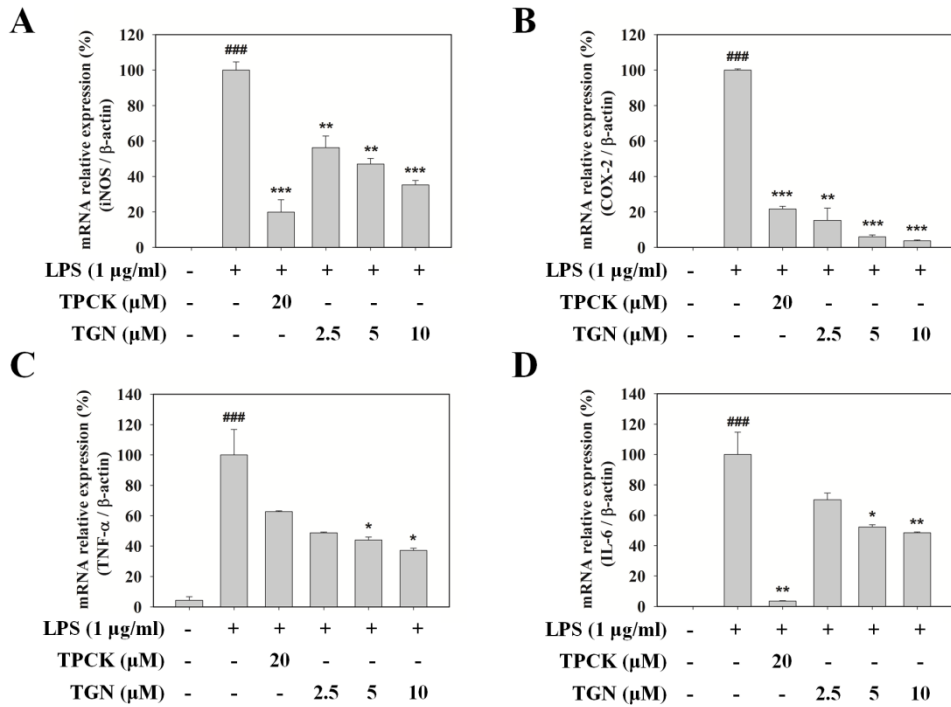
Figure 26. TGN inhibits inflammation-related mRNA expression levels .

(A, B, C and D) Cells were pretreated with the indicated concentrations of TGN for 6 h, followed by stimulation with LPS (1 µg/ml) for 6 h. Total RNAs were isolated and the relative mRNA expression levels of iNOS, COX-2, TNF-α and IL-6 were examined by real-time PCR. *$P<0.05$, **$P<0.01$ and ***$P<0.001$ indicate a significant difference compared with the LPS-only challenged group.

2.1.5. TGN suppresses LPS-stimulated activation of NF- κB

NF-κB is a crucial transcription factor that regulates pro-inflammatory mediators, including iNOS and COX-2 [110]. To determine whether TGN can suppress LPS-induced NF-κB transcriptional activity, an NF-κB SEAP reporter gene assay system was used. LPS treatment of RAW 264.7 cells harboring the pNF-κB-SEAP-NPT reporter construct for 16 h increased the SEAP expression approximately 6-fold over baseline, while pretreatment with TGN inhibited LPS-stimulated SEAP expression in a dose-dependent manner ($IC_{50} = 2.74 \pm 0.58$ μM) **(Fig. 27A)**. To further elucidate the molecular mechanism that leads to the inhibitory effect of TGN on LPS-induced NF-κB activation, IκB-α phosphorylation and degradation as well as nuclear translocation of p50 and p65, the major subunits of NF-κB, were examined by Western blot. A time course experiment showed that IκB-α phosphorylation was attenuated by 10 μM TGN after 10 and 15 min of LPS stimulation **(Fig. 27B)**. In addition, LPS-induced IκB-α degradation was also inhibited by 10 μM TGN after 10 and 15 min. In addition to results, treatment with LPS increased p50 and p65 protein expression in the nucleus, but pretreatment with TGN inhibited translocation of the p50 and p65 subunits from the cytoplasm into the nucleus compared with cells treated with LPS alone **(Fig. 27C)**. These results indicate that TGN suppresses iNOS and COX-2 expression through the prevention of NF-κB activation.
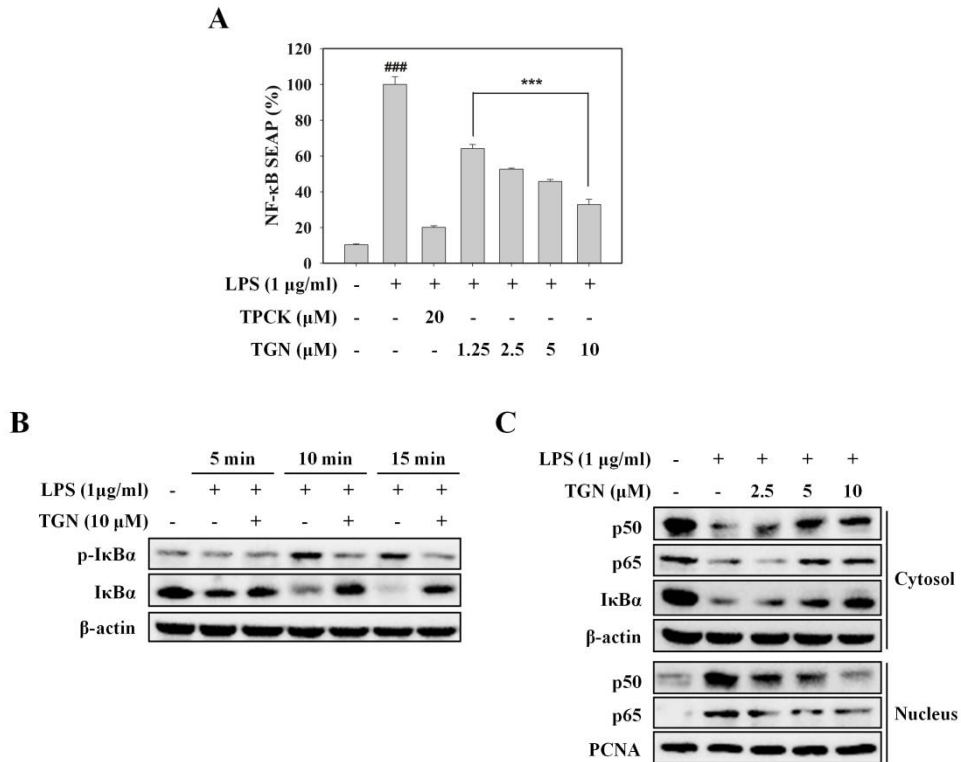
Figure 27. TGN suppresses LPS-stimulated NF-κB activation.

(A) RAW 264.7 cells harboring the pNF-κB-SEAP-NPT reporter construct were pretreated with the indicated concentrations of TGN 6 h before LPS stimulation. After incubation with LPS (1 μg/ml) for 16 h, NF-κB SEAP activity was measured as relative fluorescence units (RFUs). (B) RAW 264.7 cells were pretreated with 10 μM TGN for 6 h, and then exposed to LPS (1 μg/ml) for the specified time periods. Total protein extractions were used to determine the protein expression of p-IκB-α and IκB-α. (C) Cells were pretreated with 10 μM TGN for 6 h before LPS stimulation for 15 min. The cytoplasmic and nuclear extracts were analyzed by Western blot analysis with IκBα and NF-κB p65 and p50 antibodies.

2.1.6. HO-1 mediates the inhibitory effect of TGN on LPS-induced inflammatory responses

To determine whether HO-1 mediates the anti-inflammatory effects of TGN, iNOS, COX-2 and HO-1 expression by TGN were compared in a time course study following LPS treatment. Both iNOS and COX-2 expression reached peak levels at 12 to 24 h after LPS challenge, while HO-1 expression was not affected by treatment with LPS alone **(Fig. 28A)**. Treatment with TGN before LPS challenge prevented the increase of iNOS and COX-2 expression at 12 to 24 h after LPS treatment, keeping HO-1 at a high concentration. These results suggest that the anti-inflammatory properties of TGN are relevant to HO-1 induction. To confirm this correlation, SnPP, a HO-1-specific inhibitor, was used. SnPP dose-dependently reversed the inhibitory effect of TGN on NO production **(Fig. 28B)**. Furthermore, knockdown of HO-1 using siRNA reversed the suppression of NO production **(Fig. 28C)**, as well as iNOS and COX-2 expression by TGN in LPS-induced RAW 264.7 cells **(Fig. 28D)**. TGN-mediated inhibition of p50 and p65 nuclear translocation was also significantly blocked by HO-1 siRNA compared to control siRNA **(Fig. 28E)**. Taken together, these results reveal that TGN inhibits LPS-induced inflammatory responses such as iNOS and COX-2 expression and NF-κB activation via the up-regulation of HO-1 in macrophages.
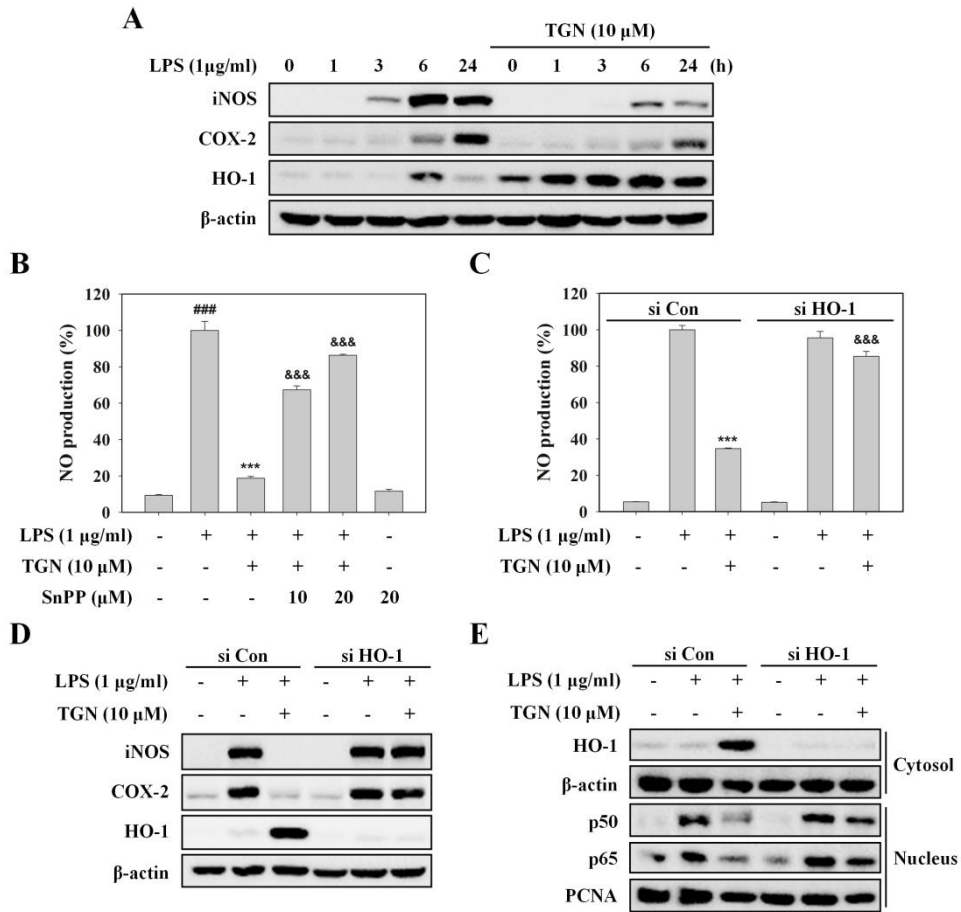
Figure 28. HO-1 mediates the inhibitory effect of TGN on LPS-induced inflammatory responses.

(A) Cells were pretreated with 10 μM TGN for 6 h and then stimulated with LPS (1 μg/mL) for the indicated times. Whole lysates were analyzed by Western blot analysis with iNOS, COX-2 and HO-1 antibodies. (B) RAW264.7 cells were pretreated with TGN in the presence of SnPP for 6 h and then stimulated with LPS (1 μg/ml) for 18 h. The quantities of NO in the medium were determined. Data are presented as the mean ± SD. [###]$P<0.001$ versus the unstimulated control group; [***]$P<0.001$ versus the LPS-only stimulated group; [&&&]$P<0.001$ versus the TGN plus LPS treated group. (C and D) Control siRNA (si Con) or HO-1-targeted siRNA (si HO-1) transfected cells were pretreated with 10 μM TGN for 6 h before

70

LPS (1 μg/ml) stimulation for 18 h. (C) The quantities of NO in the culture supernatants were determined. ***$P<0.001$ versus the LPS-only stimulated group; $^{\&\&\&}P<0.001$ versus the si Con-transfected group treated with TGN plus LPS. (D) Western blot analysis was performed to detect iNOS, COX-2 and HO-1 protein expression. (E) RAW 264.7 cells were transfected with si Con or si HO-1 for 48 h, and then pretreated with 10 μM TGN for 6 h before LPS (1 μg/ml) challenge for 15 min. Cytoplasmic or nuclear extracts were analyzed by Western blot to detect the expression of HO-1 or p50 and p65, respectively.

2.1.7. TGN inhibits TPA-induced iNOS and COX-2 expression in HaCaT cells and mouse skin

In order to demonstrate whether TGN acts as an anti-inflammatory compound on other cell types and on an *in vivo* model, the effects of TGN were examined on human HaCaT keratinocyte cells and a TPA-induced skin inflammation model in mice. Non-cytotoxic concentrations of TGN upregulated HO-1 and Nrf2 expression and inhibited LPS-induced iNOS and COX-2 protein expression dose-dependently in HaCaT cells, showing similar tendencies in macrophages **(Fig. 29A, B, and C)**. The HaCaT cells were treated with 1 μM TPA for 4 h after pretreatment with TGN. As shown in **Fig. 29D**, TPA treatment stimulated iNOS and COX-2 expression, while pretreatment with TGN suppressed TPA-induced inflammatory mediators. On the basis of these *in vitro* results, it was identified whether anti-inflammatory properties of TGN take place in the animal model of TPA-induced acute cutaneous inflammation as well. The topical application of 10 nmol TPA onto the shaved dorsal skin of mice increased iNOS and COX protein levels at 2 and 4 h, respectively. Treatment with 2.5 or 5 μmol TGN 30 min prior to TPA stimulation decreased the expression of both iNOS and COX-2. In particular, the higher topical dose (5 μmol) of TGN significantly inhibited iNOS and COX-2 expression. This result is similar to that of the positive control, 5 μmol dexamethasone **(Fig. 30)**. These results support the premise that TGN exerts a potent inhibitory effect on skin inflammation both *in vitro* and *in vivo*.
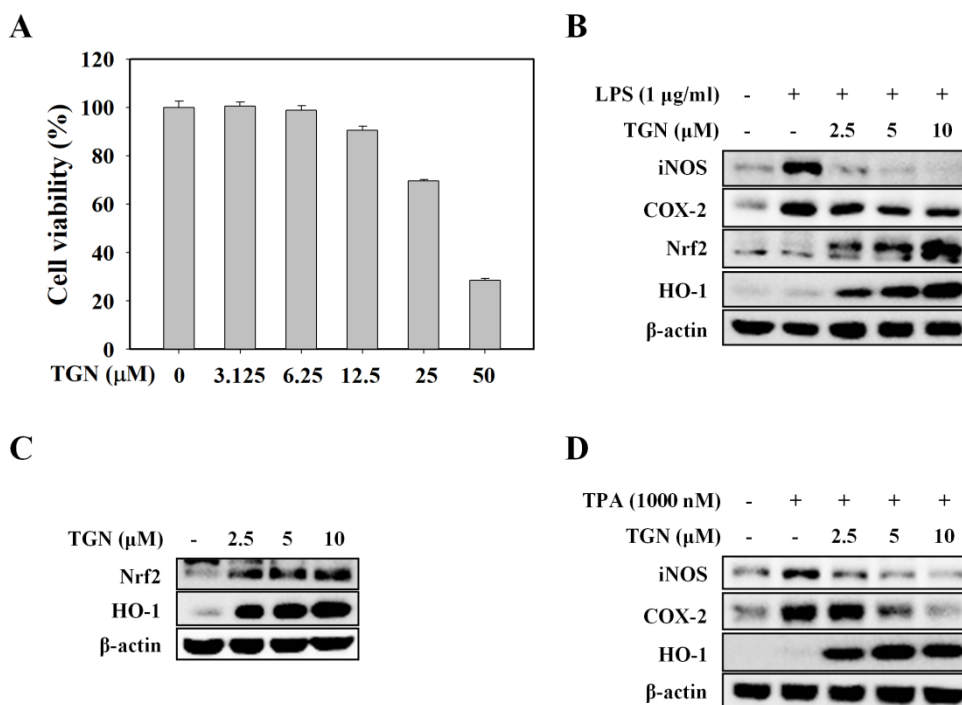
Figure 29. TGN has anti-inflammatory effects on HaCaT cells.

(A) HaCaT cells were treated with the indicated concentrations of TGN for 24 h, and cell viability was determined by an MTT assay. (B) Cells were pretreated with TGN for 6 h, then stimulated with LPS (1 μg/ml) for 18 h. Western blot analysis was performed to determine protein expression. (C) Cells were incubated with various concentrations of TGN for 6 h. (D) HaCaT cells were preincubated with TGN for 30 min and stimulated with TPA (1 μM) for 4 h. Total cell lysates were prepared for Western blot analysis.

TPA (10 nmol)	-	+	+	+	+
TGN (µmol)	-	-	2.5	5	-
Dexa (µmol)	-	-	-	-	5
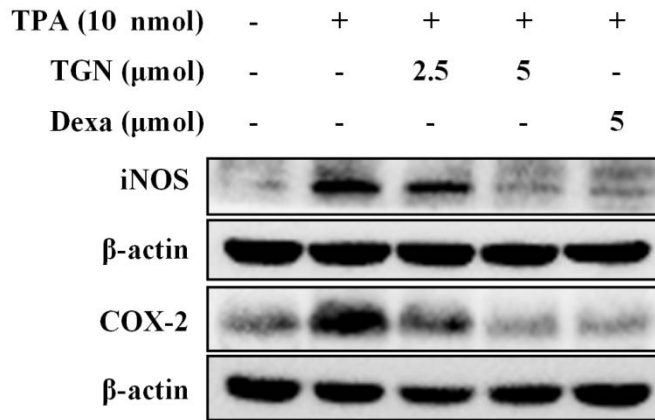
Figure 30. TGN inhibits TPA-induced skin inflammation in mice.

Female ICR mice (n=6 animals per group) were topically treated with 200 µl TGN (2.5 or 5 µmol) on their shaved back skin 30 min before the application of 10 nmol TPA. The mice were euthanized at 2 h and 4 h after the TPA treatment. The control group was treated topically with 200 µl DMSO/acetone (10:90, v/v) only. Dexamethasone 5 µmol was used as a positive control. The protein levels of iNOS (2 h) and COX-2 (4 h) from skin tissue were determined by Western blotting. The data shown are representative of three independent experiments.

2.1.8. Discussion

This study was designed to elucidate the involvement of HO-1 signaling in the anti-inflammatory effects of TGN in macrophages. We demonstrated that TGN upregulated HO-1 expression at the transcriptional level through the upstream activation of Nrf2 in RAW 264.7 macrophages. Furthermore, the upregulation of HO-1 expression through Nrf2 signaling mediated the TGN inhibition of iNOS and COX-2 expression by suppressing the NF-κB pathway in LPS-induced RAW 264.7 cells **(Fig. 31)**. This is the first study to reveal that TGN, a sesquiterpenoid from *T. farfara*, has anti-inflammatory properties mediated by HO-1 induction. In this study, TGN was also studied *in vivo* skin inflammation model for the first time.

Sesquiterpenoids, some of the main bioactive constituents in *T. farfara*, exhibit a wide range of pharmacological activities, including anti-cancer, anti-inflammatory, neuroprotective, anti-obesity, and anti-diabetic effects [73, 111-114]. In addition, tussilagone, the major sesquiterpene compound in this plant, has been reported to suppress LPS-induced NO, PGE_2, and TNF-α production in murine macrophages, and to inhibit the LPS-induced activation of NF-κB, MAPKs, and IRF-3 signaling in dendritic cells [72, 115]. A common feature of these studies is that HO-1 induction is found to play a key role in the effects of tussilagone. The α,β-unsaturated carbonyl group of this compound may play an important role in HO-1 induction. Previous studies have revealed that numerous naturally occurring compounds bearing an α,β-unsaturated carbonyl moiety, such as curcumin, caffeic acid phenethyl ester, and zerumbone, activate Nrf2 and subsequently induce HO-1

expression [47, 116]. This α,β-unsaturated carbonyl structure can act as a Michael reaction acceptor, modifying the cysteine thiols of Keap1 and in turn, releasing Nrf2 to translocate into the nucleus and regulating the induction of phase II enzymes [117, 118]. Several reports have emphasized the essential role of α,β-unsaturated carbonyl groups in inducing phase II enzymes [119-121]. Because TGN also possesses an α,β-unsaturated carbonyl moiety, it is proposed herein that TGN has the potential to induce HO-1 expression through the activation of Nrf2, thereby exerting anti-inflammatory effects. This hypothesis is supported by evidence indicating that TGN activated Nrf2 by promoting the degradation of Keap1 and that it increased HO-1 expression significantly, suggesting that TGN, as a Michael reaction acceptor, is a potential HO-1 inducer.

The induction of HO-1 is recognized as a potential therapeutic strategy to protect against oxidative stress and inflammatory responses [109]. Accumulating evidence supports the premise that HO-1 has an important role in regulating inflammatory processes. Several antioxidant phytochemicals and small molecules have been reported to inhibit inflammatory processes through the induction of HO-1 [122-124]. The detailed mechanisms that mediate the anti-inflammatory activities of HO-1 have not been fully elucidated; however, not only the degradation of proinflammatory heme by HO-1, but also CO and biliverdin/bilirubin, by-products of heme metabolism, may contribute to the regulation of inflammatory responses [109, 125]. Earlier studies revealed that the overexpression of HO-1/CO inhibits LPS-induced COX-2/PGE$_2$ synthesis in cerebrovascular endothelial cells and that HO-1/CO mediates the inhibitory effect of IL-10 on LPS-induced TNF-α

biosynthesis *in vitro* and *in vivo*, supporting the premise that HO-1 has a key role as a protector against inflammatory diseases [126, 127]. In agreement with these studies, our findings indicated that TGN significantly enhanced HO-1 expression at the transcriptional level and inhibited LPS-induced inflammatory responses. The results of the present study also revealed that the inhibition of HO-1 with SnPP or siRNA transfection abrogated the suppressive effects of TGN on inflammatory mediators in LPS-induced RAW 264.7 cells. These results support the premise that HO-1 acts as a modulator in inflammatory processes, although the contribution of HO-1 by-products to the anti-inflammatory properties of TGN needs further investigation. Taken together, TGN and its involvement in HO-1 upregulation may have therapeutic potential for the treatment of various inflammatory diseases.

The Nrf2 transcription factor is a crucial positive regulator of HO-1 gene expression, while Nrf2 is a negative regulator of NF-κB signaling, which produces inflammatory mediators [128, 129]. Recent studies have shown that the upregulation of Nrf2 by phytochemicals activates HO-1 expression but inhibits NF-κB in LPS-induced lung tissue, BV-2 microglial cells, and murine splenic lymphocytes [130-132]. HO-1 may link cross-talk between the Nrf2 and NF-κB signaling pathways in inflammatory processes [133, 134]. Our results demonstrated that TGN upregulated HO-1 expression through Nrf2 activation but inhibited NF-κB signaling and iNOS and COX-2 expression by blocking the nuclear translocation of NF-κB in LPS-induced macrophages. Moreover, transfection with siRNA against HO-1 presented evidence that upregulated HO-1 mediates the interplay between two important transcription factors, Nrf2 and NF-κB, during the

suppression of inflammatory responses, at least in part. Because Nrf2 and NF-κB individually or cooperatively regulate many signaling cascades, targeting the upregulation of HO-1 and the inhibition of NF-κB together with TGN may be a more useful pharmacological strategy for the maintenance of homeostasis in response to inflammatory diseases [135, 136].

Because TPA strongly induces inflammatory responses, the TPA-induced skin inflammation *in vivo* model is widely used to evaluate the pharmacological activities of potent anti-inflammatory agents [137]. The topical application of TPA to the skin increases the expression of proinflammatory mediators, including iNOS and COX-2 [138, 139]. Although TGN has been shown to suppress TPA-induced iNOS and COX-2 expression in human keratinocytes, it is necessary to prove its effects conclusively in an animal model. Pretreatment with TGN effectively reduced the protein levels of iNOS and COX-2 in TPA-stimulated mouse skin; these results were consistent with the findings of *in vitro* studies. Thus, these *in vivo* results provide evidence that TGN is beneficial for the pharmacological treatment of inflammatory skin diseases.
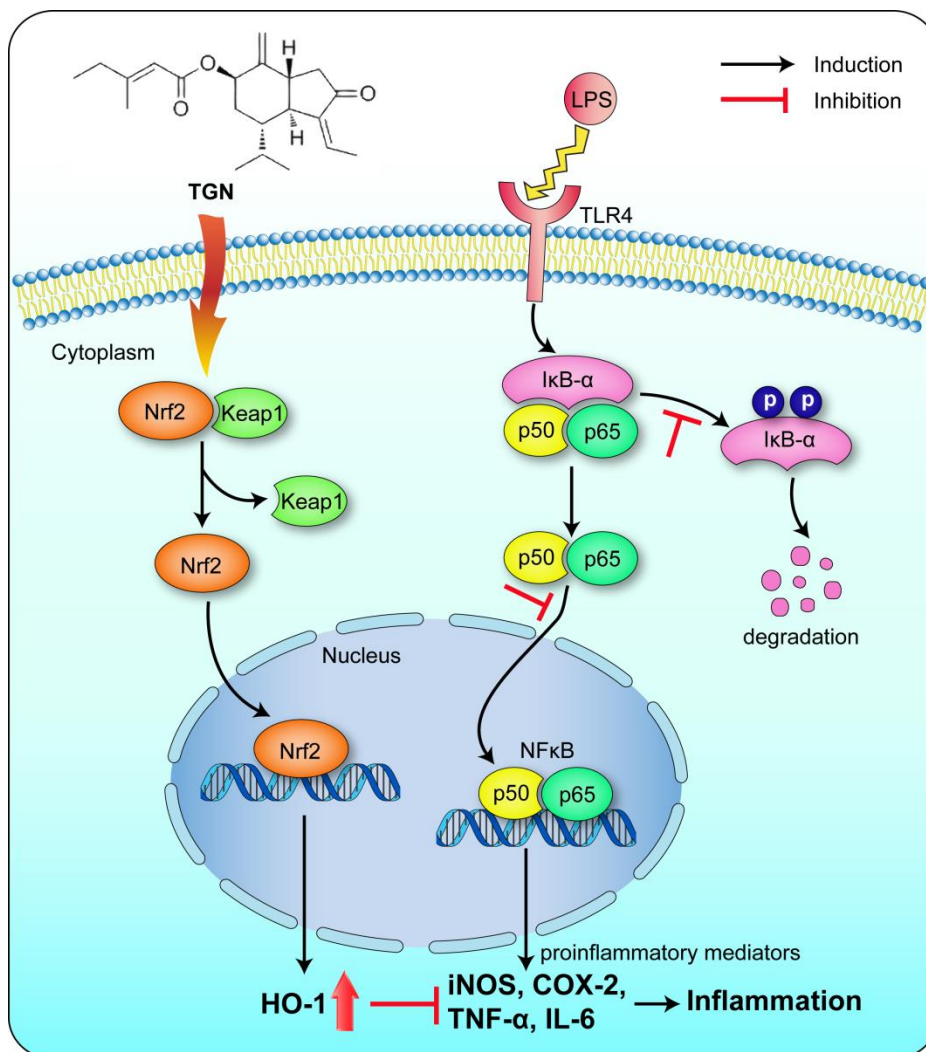
Figure 31. The proposed mechanism of Nrf2/HO-1-mediated anti-inflammatory effects of TGN by suppressing NF-κB pathway

2.2. TGN ameliorates psoriatic features in keratinocytes and an imiquimod-induced psoriasis-like dermatitis in mice mediated through Nrf2 activation

2.2.1. TGN inhibits TNF-α-induced NF-κB activation and the expression of psoriasis-related pro-inflammatory genes in keratinocytes

NF-κB is a crucial transcription factor that regulates immune and inflammatory responses in various diseases, including psoriasis [140]. To elucidate whether TGN can modulate TNF-α-induced NF-κB activation in human HaCaT keratinocyte cells, IκB-α degradation as well as nuclear translocation of p65, one of the major subunits of NF-κB, were determined by Western blot. Both TNF-α-induced IκB-α degradation and nuclear accumulation of p65 were inhibited by TGN in a dose-dependent manner **(Fig. 32A, B)**. Luciferase assay revealed that TGN pretreatment decreased NF-κB promoter activation by TNF-α challenge **(Fig. 32C)**. Next, it was examined whether TGN inhibited gene expression of pro-inflammatory cytokines involved in psoriasis. TNF-α upregulated the relative mRNA expression of IL17, IL17A, IL23, TNF-α, and CXCL8, while pretreatment with TGN suppressed the mRNA levels of these cytokines **(Fig. 33)**. Taken together, these results show that TGN inhibits TNF-α-induced inflammatory responses through impairment of NF-κB activation in keratinocytes.
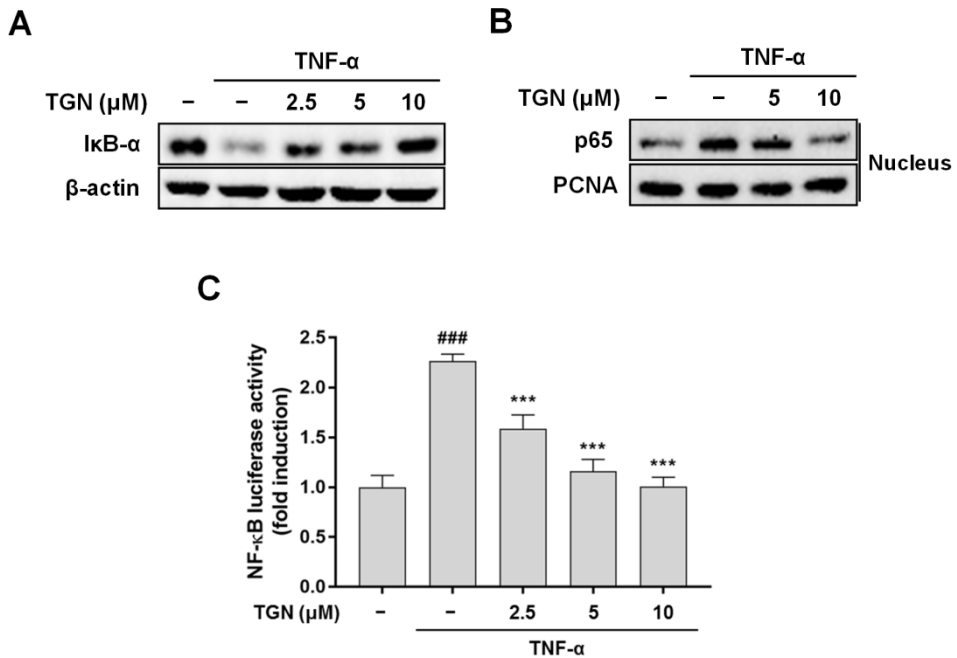
Figure 32. Inhibitory effects of TGN on TNF-α-induced NF-κB activation

(A and B) HaCaT cells were pretreated with the indicated concentrations of TGN for 1 h and then exposed to TNF-α for an additional 30 min. Total protein extractions were used to determine the protein expression of IκB-α (A) or nuclear proteins were extracted to determine the p65 expression in the nucleus (B). (C) HaCaT cells were pretreated with the indicated concentrations of TGN for 1 h and then exposed to TNF-α for an additional 24 h. NF-κB-luciferase activity was measured.

81
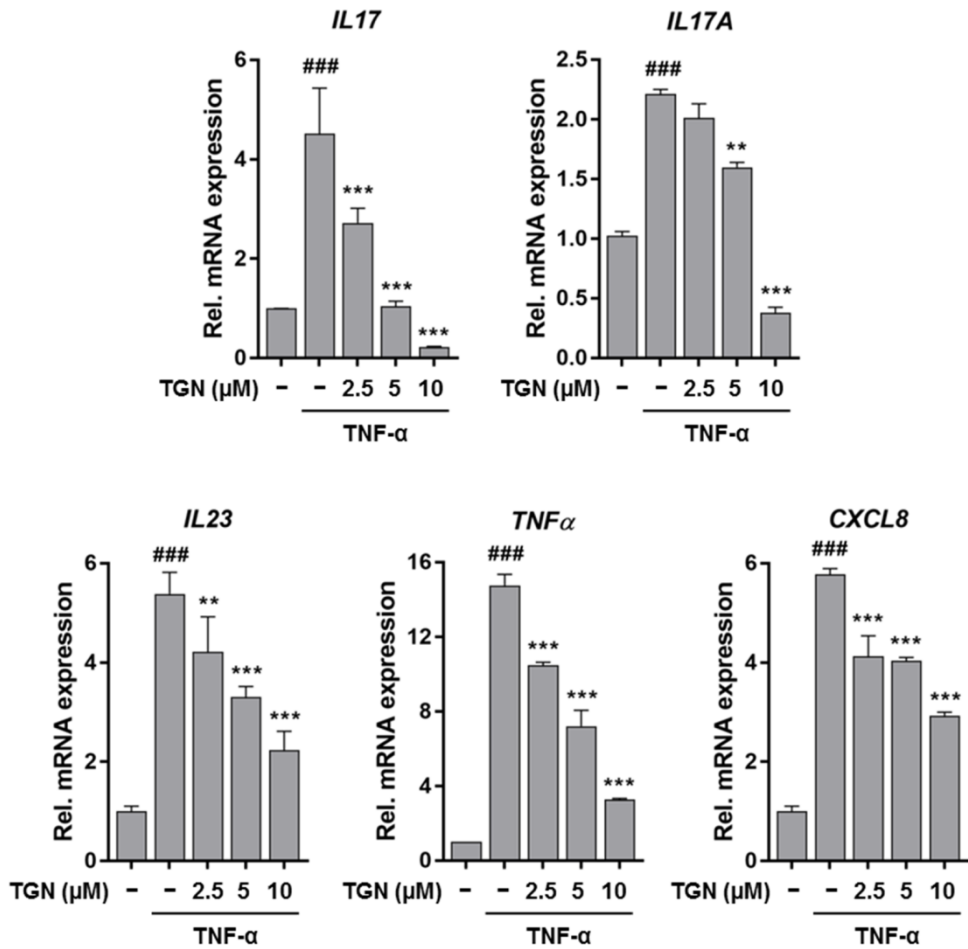
Figure 33. Inhibitory effects of TGN on the mRNA expression of inflammatory mediators

Cells were preincubated with the indicated concentrations of TGN for 1 h and then exposed to TNF-α for an additional 6 h. TNF-α-induced mRNA levels of IL-17, IL-17A, IL-23, TNF-α, and CXCL8 (IL-8) were analyzed by real-time PCR.

2.2.2. TGN suppresses IL-6-induced STAT3 activation and keratinocyte proliferation

STAT3 is a therapeutic target for psoriasis as a key regulator involved in the regulation of cell proliferation and in the pathogenesis of psoriasis [141, 142]. IL-6-induced phosphorylation and nuclear translocation of STAT3 were attenuated after treatment with TGN **(Fig. 34A)**. STAT3 luciferase activity was also reduced by TGN dose-dependently **(Fig. 34B)**. It was further examined whether TGN inhibited proliferation of keratinocytes and the expression of proliferation markers. After serum starvation for 24 h to equilibrate cells in the G0/G1 phase, HaCaT cells were stimulated with IL-6 in the presence or absence of TGN. TGN significantly inhibited IL-6-promoted cell proliferation as well as keratinocyte growth **(Fig. 35A)**. In addition, pretreatment with 10 µM TGN inhibited the cyclin D1 mRNA expression **(Fig. 35B)** and keratin 16 protein level **(Fig. 35C)** compared with cells treated with IL-6 alone. These results indicate that TGN suppresses STAT3 activation leading to inhibition of keratinocyte hyperproliferation.
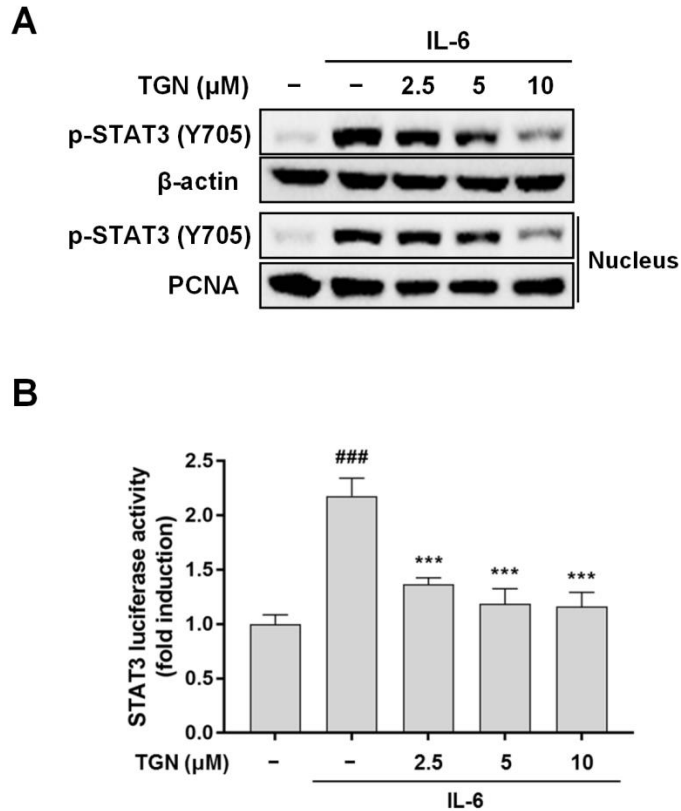
Figure 34. Inhibitory effects of TGN on IL-6-induced STAT3 activation

(A) Cells were stimulated with IL-6 for 30 min after pretreatment with TGN for 1 h. The levels of phosphorylated STAT3 in whole cell lysates and nuclear extracts were detected by a Western blot analysis. (B) HaCaT cells were transfected with NF-κB-regulated luciferase reporter construct. Twenty-four hours after transfection, the cells were treated with 25 ng/ml IL-6 for 24 h in the presence of TGN. The luciferase activity was performed using a dual luciferase assay.
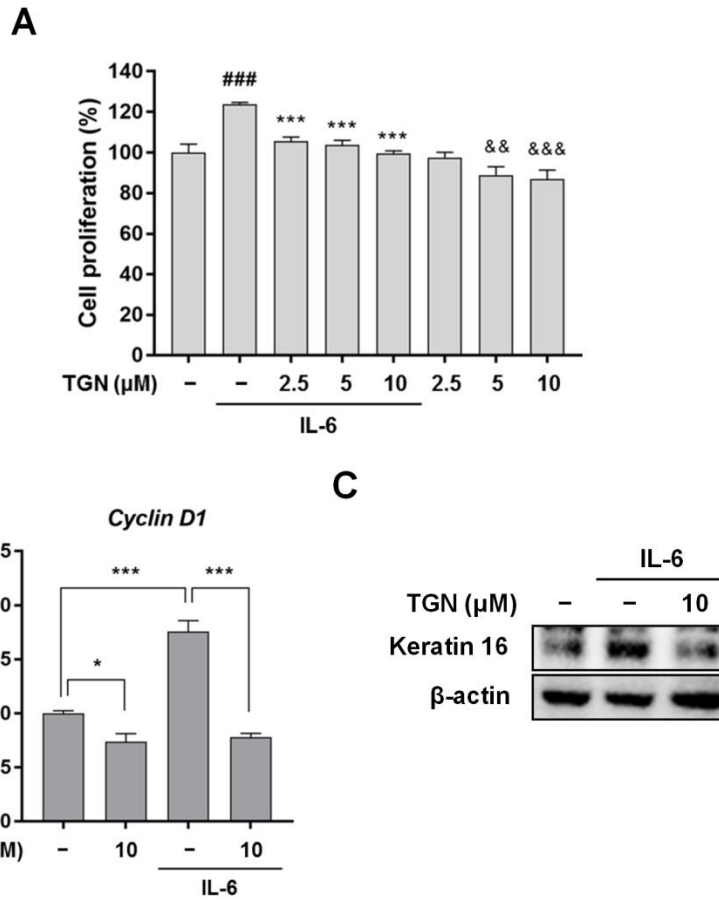
Figure 35. Inhibitory effects of TGN on IL-6-induced hyperproliferation

(A) IL-6-induced hyperproliferation of keratinocytes was measured by an MTT assay. (B) The mRNA expression of cyclin D1, a proliferation marker, was analyzed by real-time PCR. (C) The protein expression of keratin 16, a proliferation marker, was determined by Western blotting.

2.2.3. TGN activates Nrf2/ARE signaling pathway

Nrf2 activation is considered as a promising therapeutic strategy in skin diseases, including psoriasis [48, 68]. A previous study has shown that TGN upregulates Nrf2/HO-1 signaling in macrophages [143]. Thus, it was determined whether this regulatory action takes place in keratinocytes. TGN significantly promoted Nrf2 and HO-1 protein expressions and Nrf2 nuclear localization in HaCaT keratinocytes **(Figs. 36A, B, and C)**. To examine the effect of TGN on Nrf2 transcriptional activity, a luciferase reporter gene assay was conducted. ARE luciferase reporter activity reached a maximum level after 24 h **(Fig. 36D)** and increased dose-dependently at this time-point **(Fig. 36E)**. Furthermore, the mRNA levels of Ho-1 and Nqo1, the major target genes of Nrf2, dramatically increased after TGN treatment for 24 h in murine primary keratinocytes **(Fig. 37A)**. Next, the chromatin immunoprecipitation (ChIP) assay was carried out to verify whether Nrf2, which translocated into the nucleus, can directly bind to ARE on the Ho-1 and Nqo1 promotor regions. Results showed that more Nrf2 was bound to the ARE sequences of the Ho-1 and Nqo1 genes in primary keratinocytes treated with TGN for 24 h compared with the non-treated control cells. **(Fig. 37B)**. There were no significant differences between control (non-treated) and TGN-treated groups for the binding to the non-specific control regions of ARE. Overall, these findings suggest that TGN activates Nrf2 signaling pathway through direct Nrf2 binding to AREs present in the promotor of Nrf2-target genes and transcriptional activation.
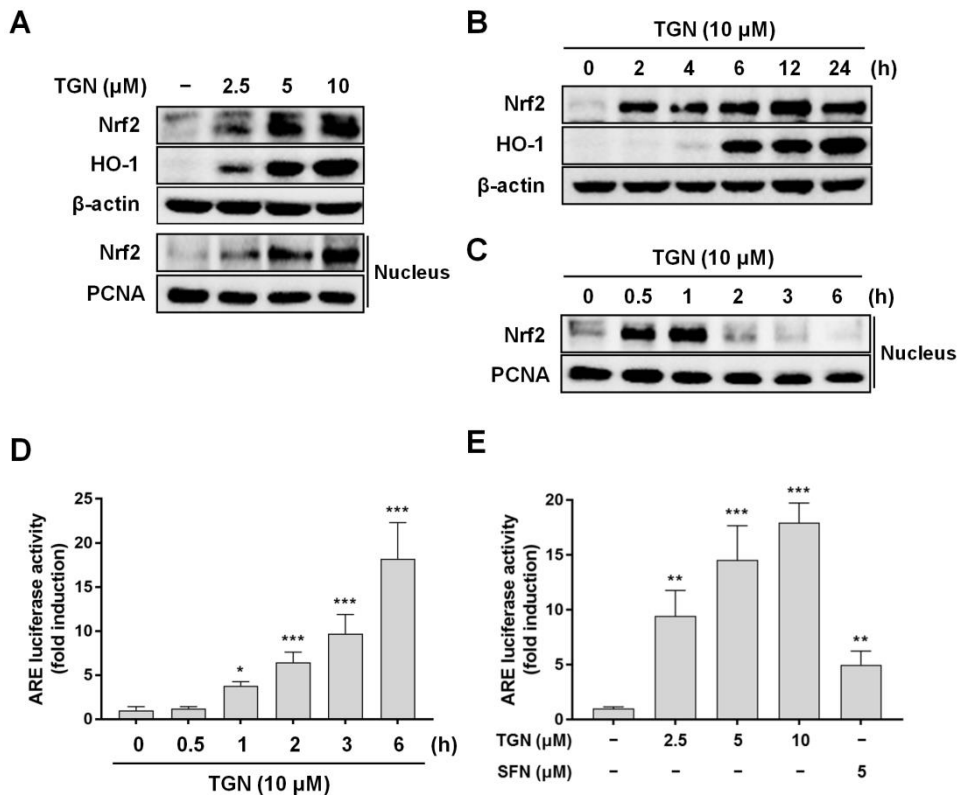
Figure 36. Effects of TGN on the activation of Nrf2/ARE signaling

(A–C) HaCaT cells were treated with the indicated concentrations (A) or times (B, C) of TGN. Nrf2 and HO-1 in the whole cell lysates and Nrf2 in the nucleus were determined by Western blotting. (D and E) The cells were exposed to the indicated times (D) or concentrations (E) of TGN, and ARE-luciferase activity was measured. The results shown are the means ± SD of three experiments. Significant difference from control group, *P <0.05, **P<0.01, and *** P<0.001

A

Ho-1

Nqo1

B
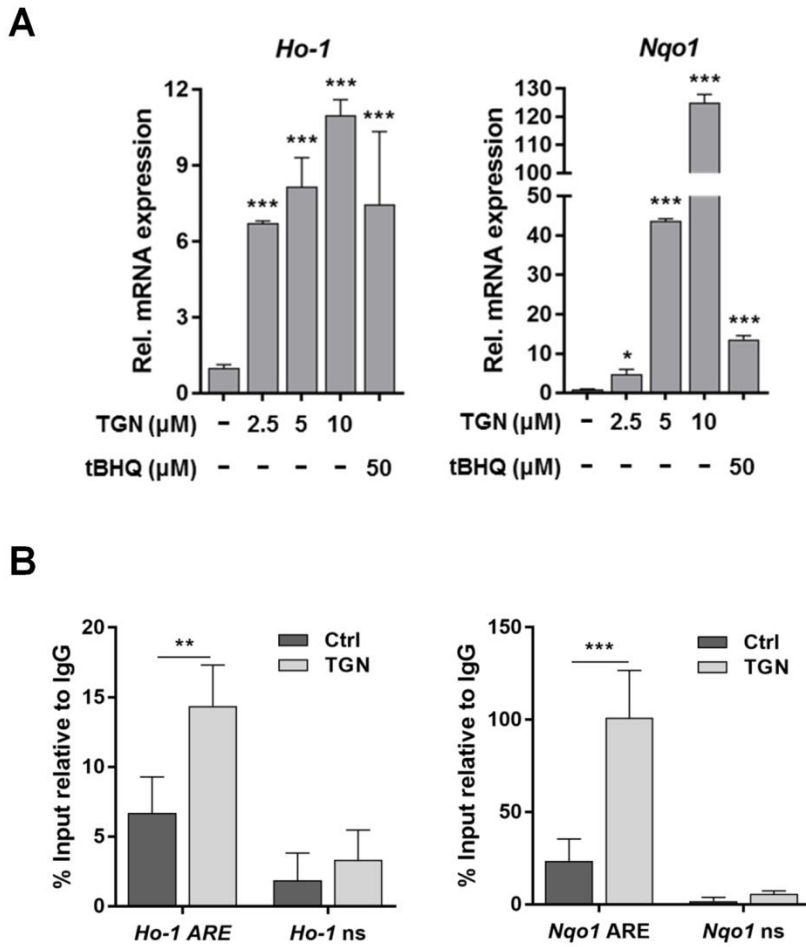
Figure 37. Effects of TGN on the induction of the Nrf2 target genes and ARE sequence-binding activity of Nrf2 in murine primary cultured keratinocytes

(A) Cells were treated with the indicated concentrations of TGN 24 h, and mRNA levels of *Ho-1* and *Nqo1* were analyzed by real-time PCR. *$P<0.05$, **$P<0.01$, and ***$P<0.001$ indicate a significant difference compared with the vehicle-treated control group. (B) Primary keratinocytes were incubated with 10 μM TGN for 24 h, and ChIP assay was conducted to assess binding of Nrf2 to the ARE in the promoters of the genes encoding *Nqo1* and *Ho-1*.

2.2.4. Inhibition of NF-κB and STAT3 by TGN is mediated through Nrf2 activation

To investigate the regulatory effect of Nrf2 on NF-κB and STAT3, HaCaT cells were transfected with small interfering RNA (siRNA) or exposed to SnPP, a HO-1-specific inhibitor. Knockdown of Nrf2 or HO-1 by siRNA and down-regulation of HO-1 by SnPP abrogated TGN-mediated inhibition of IκB-α degradation **(Figs. 38A, B)**. Similarly, silenced Nrf2 or HO-1 expression abolished the inhibitory effect of TGN on STAT3 phosphorylation **(Figs. 38C, D)**. These results indicate that Nrf2 activation and its target gene expression by TGN can regulate cytokine-induced activation of NF-κB and STAT3 in keratinocyte.
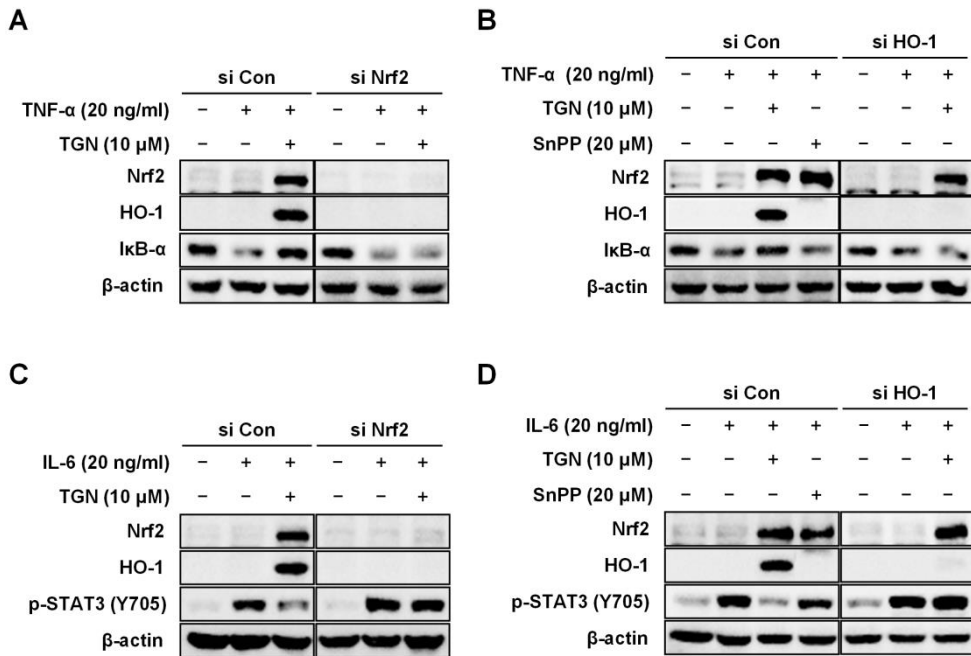
Figure 38. Nrf2/HO-1 signaling-mediated inhibition of NF-κB and STAT3

The cells were transfected with 50 nM of control siRNA (si Con), Nrf2-targeted siRNA (si Nrf2), or HO-1-targeted siRNA (si HO-1) for 48 h and then treated with 10 µM of TGN for 6 h. The cell lysates were prepared for Western blot analysis with specific antibodies against Nrf2, HO-1, IκB-α, and p-STAT3. β-actin was used as an internal control. The results shown are representative of three independent experiments.

2.2.5. Topical TGN treatment ameliorates IMQ-induced psoriasis-like skin inflammation in mice

As topical application of IMQ, a Toll-like receptor 7/8 ligand and potent immune activator, on mouse skin mimics human psoriasis lesions [38], *in vivo* anti-psoriatic effects of TGN were evaluated on the IMQ-induced psoriasis-like skin inflammation model in mice. To identify the therapeutic potential of TGN against psoriasis, mice were topically treated with 5% IMQ cream or control Vaseline cream on the shaved back skin and right ear for the first five consecutive days co-treated with 1 or 5 nmol/100 µl of TGN and IMQ for further nine days **(Fig. 39A)**. On the fifth day, the IMQ-treated mice resulted in remarkable thickened, erythematous, and scaly back skin compared with control group mice, reflecting psoriasis-like skin condition **(Fig. 39B)**. Phenotypical changes of the back skin and right ear **(Fig. 39C)** and Psoriasis Area Severity Index (PASI) score from skin **(Figs. 40A–D)** and ear **(Figs. 40E–G)** showed that topical treatment of TGN considerably attenuated IMQ-induced psoriatic traits. The spleen index (spleen-weight-to-body-weight ratio) also diminished in TGN-treated mice compared with mice treated with IMQ alone, suggesting the immunosuppressive property of TGN **(Figs. 41A, B)**.

91
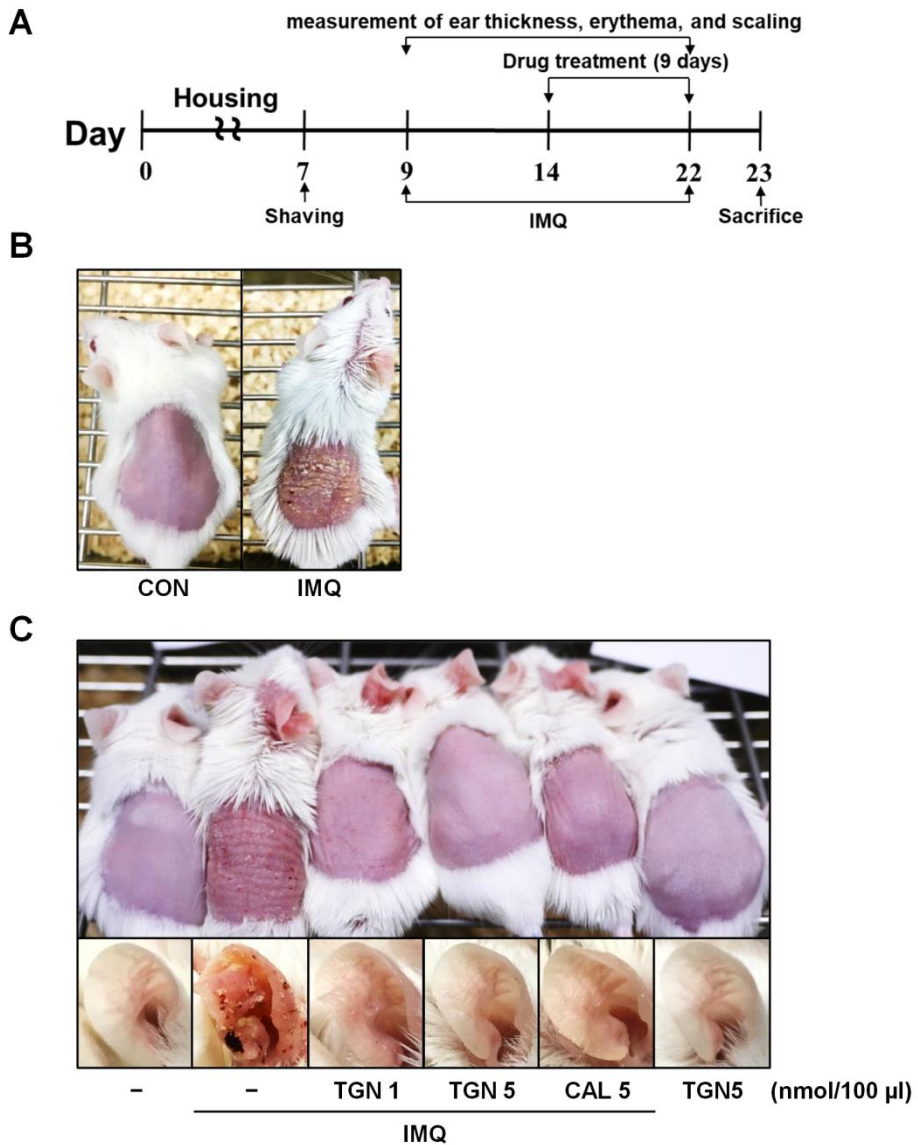
Figure 39. Effects of topical TGN on IMQ-induced psoriasis like dermatitis in a mouse model

(A) *In vivo* experimental scheme describing the treatment periods with IMQ and TGN. (B and C) Phenotypical presentation of mouse back skin and right ear on the 5th day (B) and 15th day (C) after IMQ treatment.
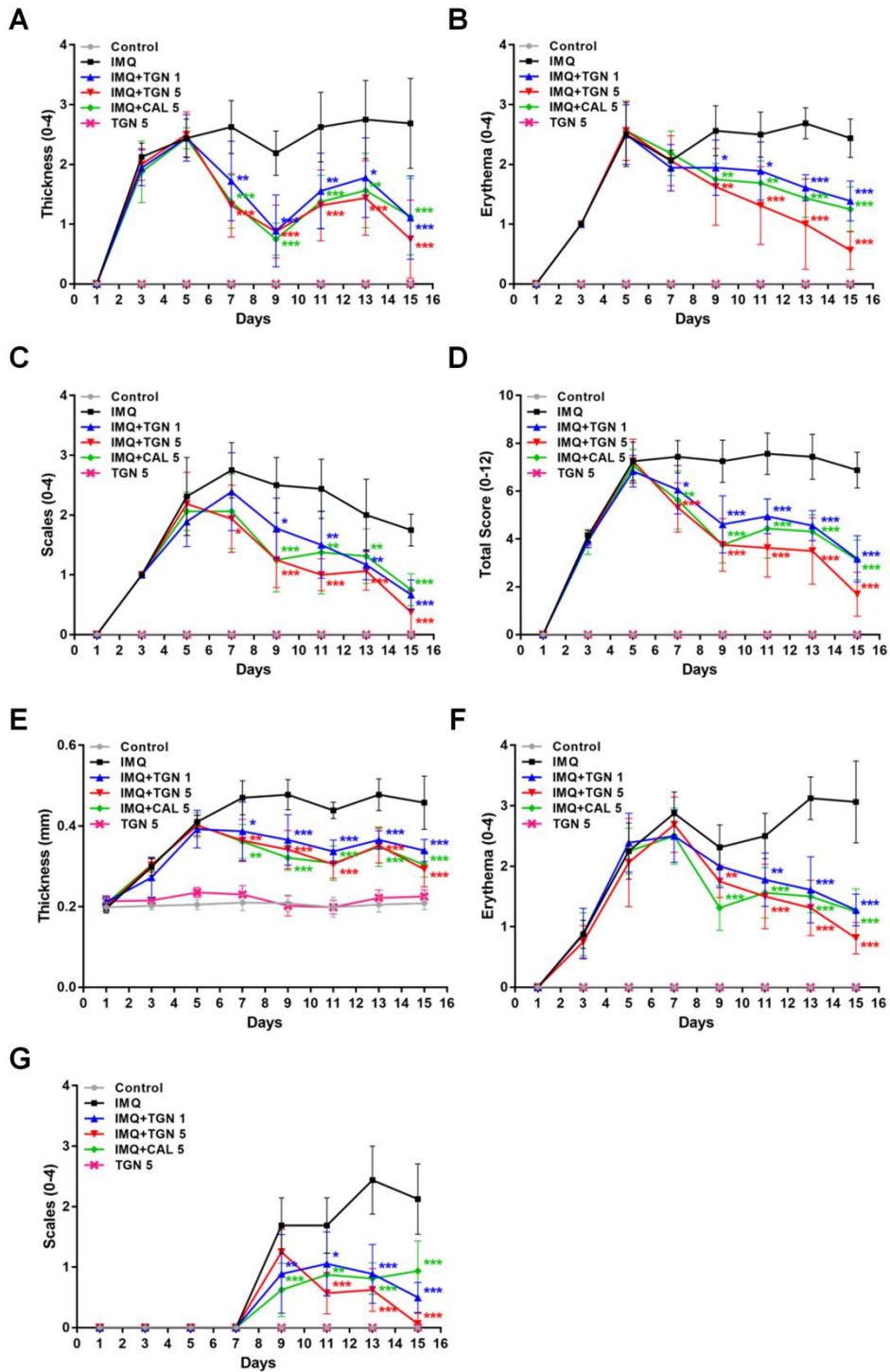
Figure 40. Quantification of the severity of psoriasis-like skin using the PASI score

Quantitative severity assessment of changes throughout the 14-day experimental period. (A–D) Thickness (A), erythema (B), and scaling (C) of the back skin were scored every alternative day. The cumulative score was calculated and depicted (D). (E–G) Thickness was measured with a caliper (E), and erythema (F) and scaling (G) of the right ear were scored every alternative day.
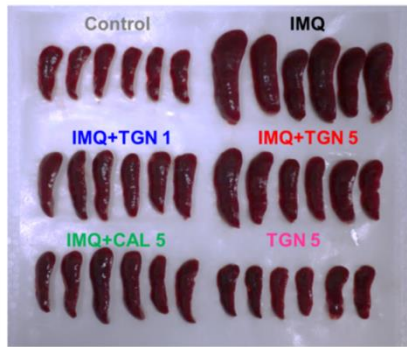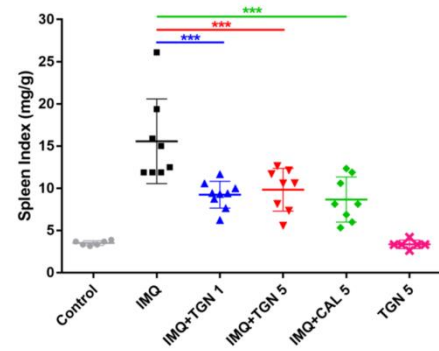
Figure 41. Immunosuppressive effect of TGN in IMQ-induced mice

(A) Representative morphology of spleens of each group (B) Spleen index (spleen weight/body weight) was calculated. The asterisk indicated that there was a statistical difference (***$P <0.001$) from IMQ group.

2.2.6. TGN reduces inflammatory immune genes and epidermal hyperproliferation in IMQ-induced psoriasis-like skin

To further confirm the anti-psoriatic efficacy of topical TGN treatment, skin tissues obtained from mice were analyzed. Histopathological analysis of back skin and ear sections with hematoxylin and eosin (H&E) staining showed reduction of IMQ-induced epidermal thickening (acanthosis) **(Figs. 42, 43, and 44)** and dermal infiltrating cells in TGN-treated skin **(Fig. 44)**. The expression of NF-κB p65 measured by immunochemistry staining was increased by IMQ treatment, whereas TGN treatment almost completely inhibited p65 expression **(Fig. 45A)**. Moreover, TGN application significantly attenuated the IMQ-induced mRNA levels of psoriasis-associated inflammatory cytokines (*Il17a*, *Il22*, *Il23a*, and *Tnf-α*) as well as antimicrobial peptides (*S100a7*, *S100a8*, *S100a9*, and *Defb4*) in skin **(Figs. 45B, C)**. Analysis of keratinocyte proliferation showed reduced Ki-67-positive cells in the epidermis of TGN-treated mice, compared with those of the IMQ alone-treated mice (**Fig. 46A**). Furthermore, Western blotting analysis revealed that IMQ-stimulated STAT3 phosphorylation was inhibited after topical treatment with TGN **(Fig. 46B)**. Taken together, these results support that IMQ-induced psoriasis-like skin lesions were ameliorated both *in vitro* and *in vivo* through inhibition of NF-κB and STAT3 and psoriasis-associated markers.
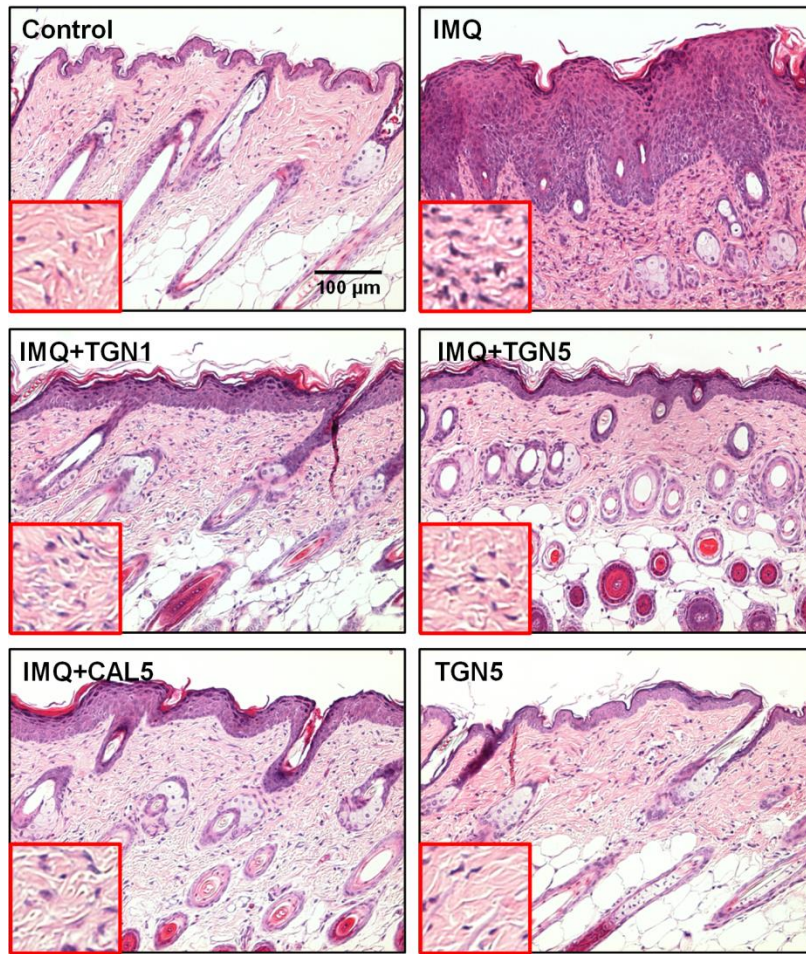
Figure 42. Histopathological changes of back skin of mice

H&E staining of the back skin of Balb/c mice treated for 14 consecutive days with control cream or IMQ or for 9 consecutive days with TGN or CAL (magnification, ×200). Insets with red box represent increased immune cell influx (magnification, ×400).
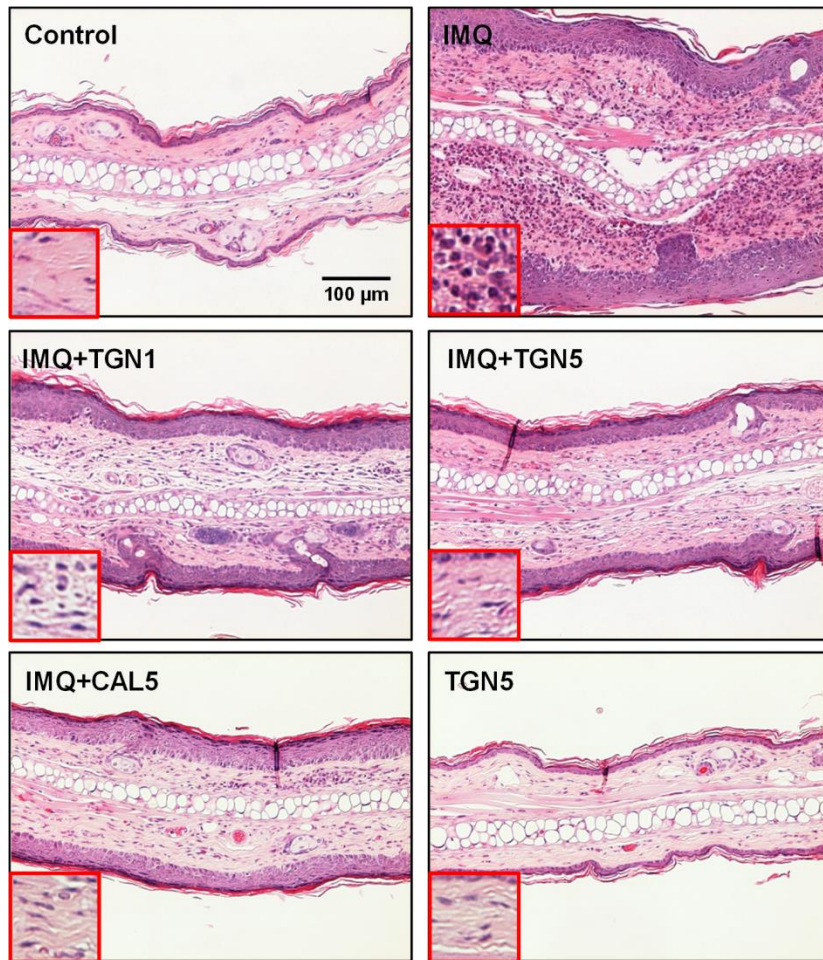
Figure 43. Histopathological changes of the ear of mice

H&E staining of the right ear of Balb/c mice treated for 14 consecutive days with control cream or IMQ or for 9 consecutive days with TGN or CAL (magnification, ×200). Insets with red box represent increased immune cell influx (magnification, ×400).
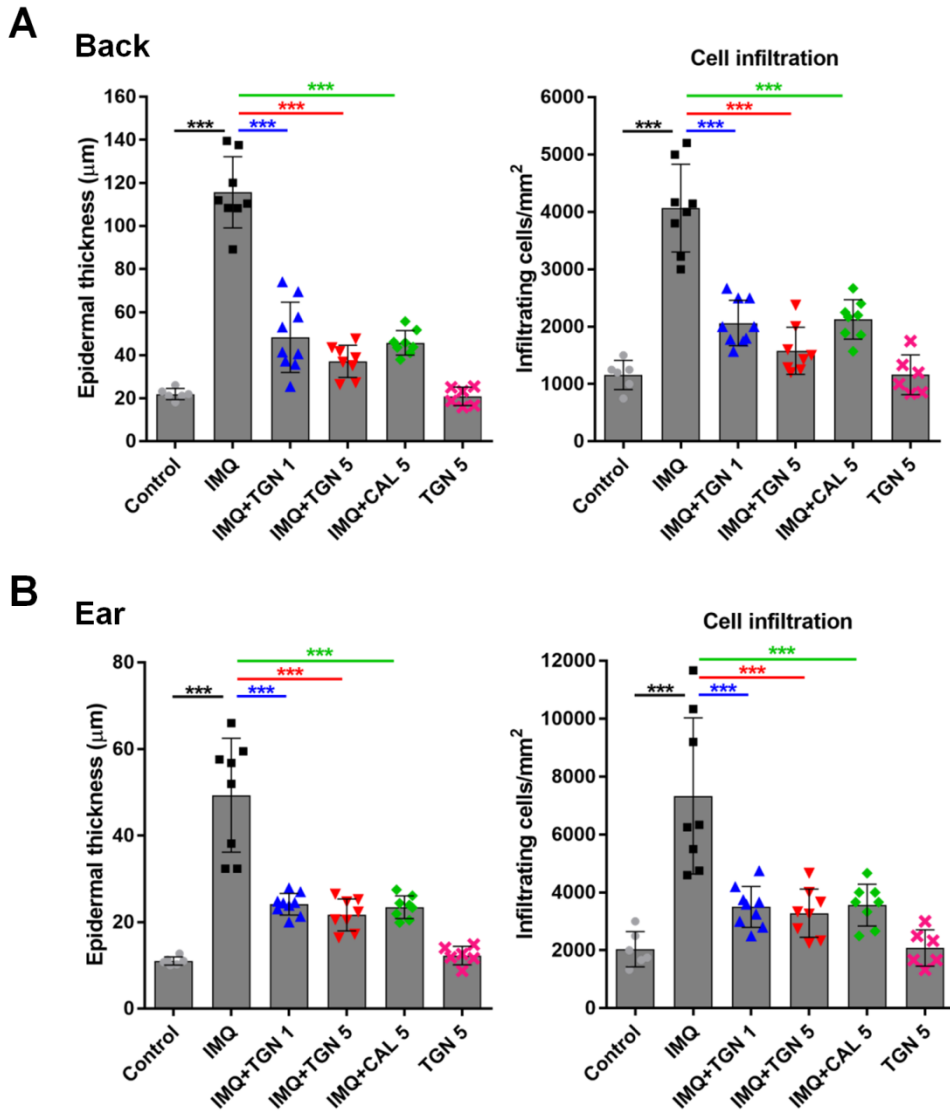
Figure 44. Quantification of psoriatic features in the back and ear skin sections

(A and B) Epidermal thickness and number of infiltrating cells in the back (A) and ear (B) skin sections were quantified.
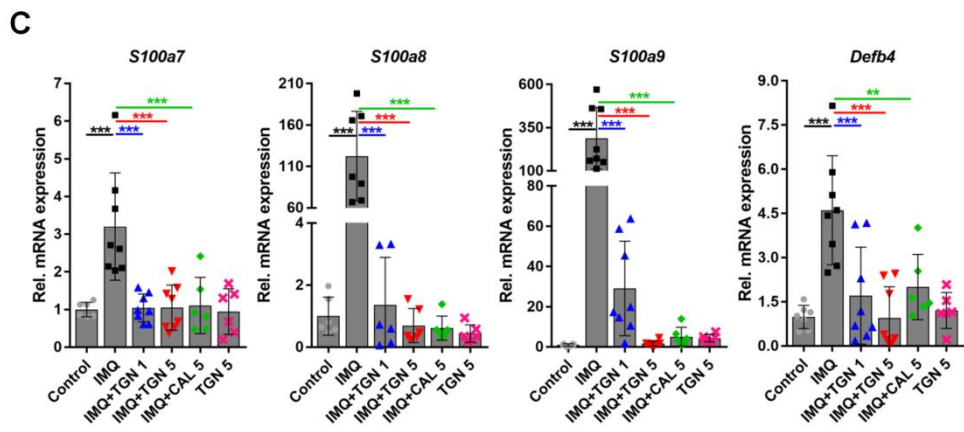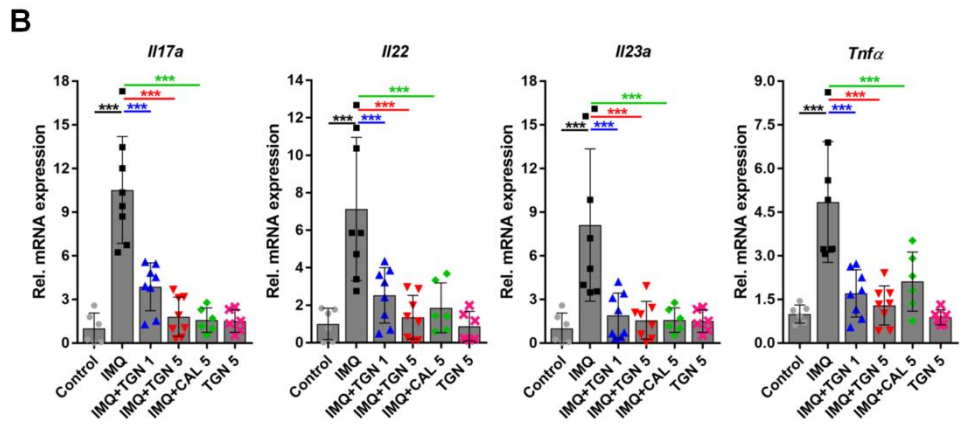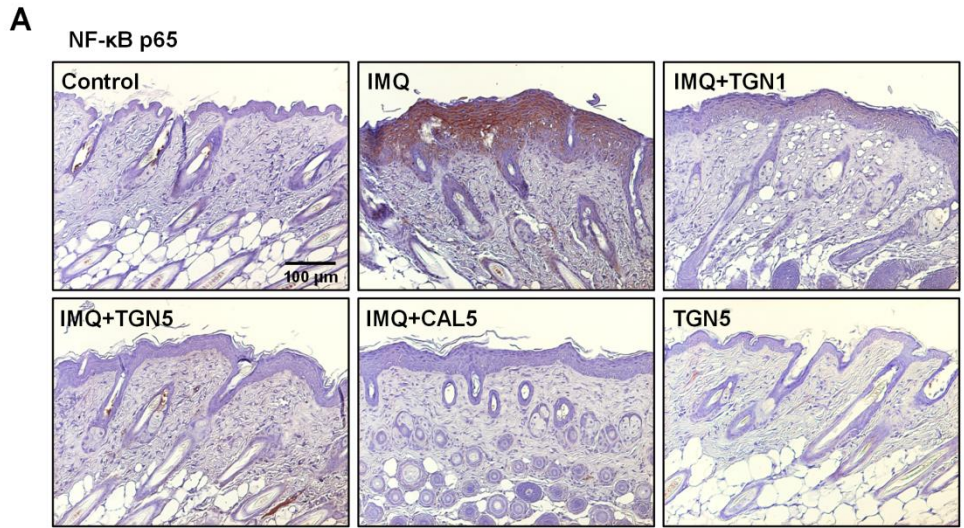
Figure 45. Inhibitory Effects of TGN on IMQ-induced NF-κB activation and inflammatory immune genes

(A) Immunohistochemical analysis of NF-κB p65 protein expression in the epidermis. (B and C) RNA from back skin of Balb/c mice was analyzed for expression of inflammatory cytokines (B) and antimicrobial peptides (C) by qRT-PCR. Each symbol represents mRNA expression relative to Gapdh mRNA levels in an individual mouse.
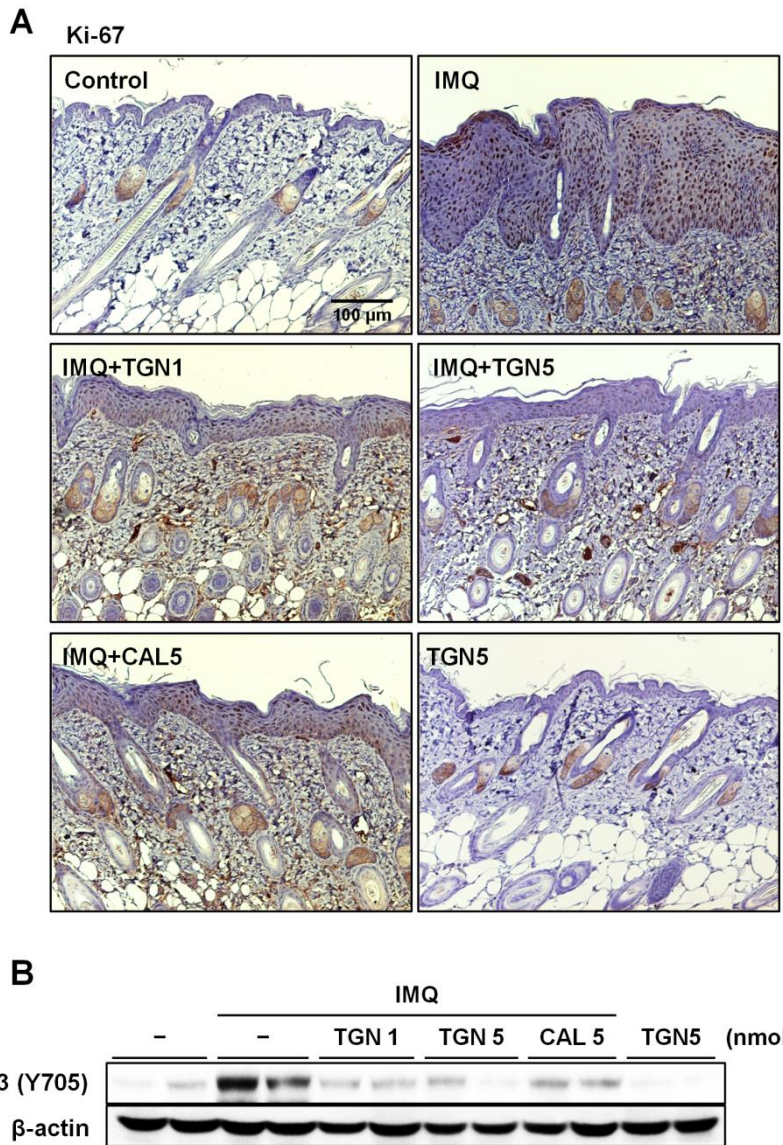
Figure 46. Inhibitory effects of TGN on the protein expression of proliferation marker and STAT3 in IMQ-treated mouse skin

(A) The protein expression of epidermal proliferation marker Ki-67 was analyzed by Immunohistochemical staining (magnification, ×200). (B) STAT3 phosphorylation was detected by Western blotting on protein extracts from back skin homogenates of mice.

2.2.7. Discussion

The present study was designed to investigate whether TGN, which showed anti-inflammatory effects and activated the Nrf2/HO-1 signaling pathway in the previous study, alleviates psoriatic features *in vitro* and in an IMQ-induced psoriasis-like dermatitis in mice. This study demonstrated that TGN attenuated cytokine-induced psoriatic activation of NF-κB and STAT3, which are crucial transcription factors involved in the pathogenesis of psoriasis. Furthermore, the activation of Nrf2/HO-1 by TGN mediated NF-κB and STAT3 inhibition **(Fig. 47)**. Topical administration of TGN exerted inhibitory effects on IMQ-induced psoriatic skin lesions as well as systemically immunosuppressive effect, providing a potential of TGN as an anti-psoriatic agent.

The pathophysiology of psoriasis is multifactorial, which is associated with a number of biochemical and immunological disturbances. It has been demonstrated that oxidative stresses are involved in the pathogenesis of psoriasis [144]. Skin is the major target of oxidative stress, as it is continuously exposed to exogenous stressors, such as UV radiation and other environmental stresses producing ROS. Skin metabolism, chronic inflammation, and skin tissue damage are also endogenous stresses that generate ROS. Continued ROS might result in excessive oxidative stress, leading to many skin diseases, including psoriasis [68]. Thus, an efficient antioxidative strategy stimulating an endogenous defense mechanism is important for treatment of psoriasis. Many cytoprotective proteins, including HO-1 and NQO1, are under the control of Nrf2, a master regulator of the

antioxidant response [69]. Dimethylfumarate (DMF), the main ingredient of oral fumaric acid esters (FAEs, Fumaderm), which has been used as a systemic therapy for the treatment of moderate to severe forms of psoriasis, is a potent Nrf2 activator through its capacity to directly modulate specific Keap1 cysteine residue [145]. Preclinical studies have demonstrated that DMF exhibits anti-inflammatory and cytoprotective activities that are partially mediated by the Nrf2 antioxidant response pathway [146]. Additionally, several studies revealed that pharmacological upregulation of HO-1 contributes to the attenuation of psoriatic features *in vitro* and *in vivo* [147-149]. TGN significantly activated Nrf2 and its downstream target gene HO-1 in HaCaT cells and primary cultured murine keratinocytes. Activation of Nrf2/HO-1 by TGN regulated NF-κB and STAT3, resulting in the suppression of inflammatory responses and keratinocyte hyperplasia, the main features of psoriatic lesions. The present results demonstrate that Nrf2 activation by TGN can be a therapeutic target for the treatment of psoriasis by modulating the transcription factors associated with psoriasis as well as promoting the defense system of the skin.

The IMQ-induced murine model is widely used to study psoriasis-like skin dermatitis in mice. IMQ is a ligand for Toll-like receptors (TLR7 and TLR8) and a potent immune activator. Topical application of IMQ produces psoriasis-like skin lesions in mice, which display many of the same phenotypic and histological characteristics as those observed in psoriasis in humans: induction of acanthosis, parakeratosis, and a mixed inflammatory infiltrate mediated by the elevations of IL-23/IL-17 axis [38]. It was also shown that the application of IMQ on human

nonlesional psoriatic skin resulted in psoriasis-like skin inflammation, although it differs somewhat from typical psoriasis in patients [150]. In the present study, IMQ was topically applied to the mouse's back skin and right ear for five consecutive days. On the fifth day of IMQ treatment, psoriasis-like skin conditions were observed, such as increased skin thickness and increased PASI score for erythema and scaling in the IMQ group compared to the control group. Co-treatment with IMQ and TGN for nine more days ameliorated both phenotypical and histological changes of psoriasis induced by IMQ. The therapeutic effect of TGN was comparable with the calcipotriol (CAL), a vitamin D analogue which is effective in psoriasis treatment. In addition, TGN inhibited NF-κB and STAT3 activation, reducing the expression of immune mediators and epidermal proliferation in skin tissue homogenates. These results are in agreement with the findings of *in vitro* studies.

The spleen is the largest secondary lymphoid organ in the immune system, and its enlargement with an increase in weight represents the increase of cells in the spleen and the elevation of immune reactions [38, 151]. Splenomegaly was observed after treatment with IMQ once daily for 14 days. Interestingly, topical administration of TGN significantly reduced the IMQ-induced spleen index, indicating the systemic immunosuppressive effect of TGN. Because TGN exerts therapeutic effects on psoriatic lesions through the modulation of psoriasis-associated transcription factors, it can be seen as a result of a systematic immune response. Further study is required to clarify the pharmacokinetic profile of TGN after topical application.

105

Vitamin D analogs, such as CAL, tacalcitol, and maxacalcitol, are one of the most popularly prescribed first-line topical treatments for psoriasis [152]. The biological activities of vitamin D analogs are mediated through the vitamin D receptor, a ligand-activated transcription factor, which regulates gene transcription in target cells such as keratinocytes and lymphocytes [152, 153]. Topical treatment with CAL decreased human beta defensin and proinflammatory cytokines by inhibiting NF-κB in keratinocytes from lesional psoriatic plaques and cultured human epidermal keratinocytes [154]. A recent study also demonstrated that topical CAL application exerted antipsoriatic effect in a murine model of psoriasis by controlling the IL-23/IL-17A axis and systemic burden of pathogenic T17 cells [155]. Here, CAL was used as a positive control for *in vivo* study. Topical treatment of TGN in mice showed comparable effects to CAL by regulating transcription factors involved in the pathogenesis of psoriasis. Several studies have indicated that CAL can induce significant ear swelling and atopic-dermatitis-like skin inflammation [156, 157]. Interestingly, the most-common side effect of CAL is a skin irritation (red, dry, and itchy skin) exhibiting similarities with atopic-dermatitis lesions [158]. If further study reveals that the side effects of TGN are less than CAL, TGN can be useful as a safe topical treatment for psoriasis from the medicinal plant.
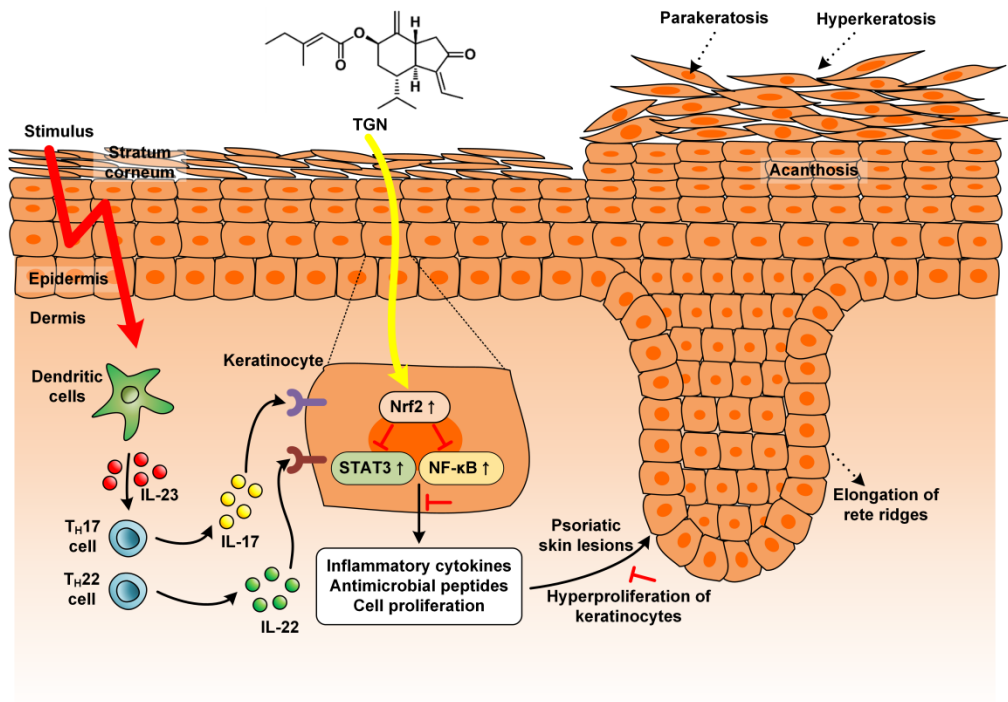
Figure 47. The proposed mechanism of Nrf2-mediated anti-psoriatic effects of TGN by suppressing NF-κB and STAT3

IV. CONCLUSION

The present study demonstrates that ECN and TGN, sesquiterpenoids isolated from the medicinal plant *T. farfara*, are potent, naturally occurring Nrf2 activators. Nrf2-mediated neuroprotection by ECN and amelioration of psoriasis by TGN were investigated.

The current study revealed that ECN exhibited neuroprotective effects against oxidative stress-induced cell damage in PC12 cells and dopaminergic neurodegeneration in mice. In addition, its mechanism of action through potential activation of the Nrf2/ARE signaling pathway has been elucidated. ECN activates the Nrf2 pathway through phosphorylation of Akt and interaction with Keap1. These results suggest that targeting Nrf2 activation by a potent, naturally derived Nrf2 activator, ECN, is a promising therapeutic approach for the prevention or treatment of neurodegenerative conditions.

TGN, a sesquiterpene with an α,β-unsaturated carbonyl group, significantly upregulates HO-1 expression by activating Nrf2. In addition, TGN-induced HO-1 is involved in the anti-inflammatory actions of TGN in LPS-stimulated RAW 264.7 cells. A key mechanism underlying the anti-inflammatory effects of TGN was also identified. TGN suppresses the NF-κB signaling pathway by preventing IκB-α degradation and phosphorylation and NF-κB nuclear translocation. Moreover, HO-1 induction by TGN contributes to the inhibition of the NF-κB pathway. These results suggest that TGN, which targets HO-1 induction and HO-1-mediated NF-κB inhibition, may be a promising therapeutic candidate for the development of anti-inflammatory agents derived from medicinal plants.

109

Based on these findings, TGN was applied to treat psoriasis, a chronic inflammatory skin disease. It was demonstrated that TGN diminishes the activation of NF-κB and STAT3, crucial signaling cascades involved in the pathogenesis of psoriasis, in keratinocytes and mice. A TGN-activated Nrf2 pathway has an essential role in the regulation of these transcription factors. Thus, pharmacological Nrf2 activation can be a new therapeutic target for the treatment of psoriasis through the signaling crosstalk with psoriasis-related transcription factors. Furthermore, in an IMQ-induced psoriasis-like dermatitis mouse model, topical TGN treatment not only provides local symptomatic benefit but can also contribute to control of systemic immune responses by attenuating the series of psoriatic pathogenesis. Taken together, TGN, a naturally derived compound that can activate Nrf2, will be of interest for the development new drugs for psoriasis.

V. EXPERIMENTAL SECTION

1. Materials

1.1. ECN

ECN was isolated from dried buds of *Tussilago farfara* and identified, as previously reported by Song et al. [159]. A compound was dissolved in dimethyl sulfoxide (DMSO) to obtain a stock solution, and the DMSO concentration was kept below 0.05% in the cell cultures so that it had no effect on the cells.

1.2. Isolation and identification of TGN

TGN was provided by Prof. Eun Kyoung Seo (Ehwa Womans University, Seoul, Korea). The dried flower buds of *T. farfara* (25 kg) were extracted with MeOH (3 × 95 L, 24 h) at room temperature. The solvent was evaporated *in vacuo* to afford a MeOH extract (4.9 kg), which was then suspended in distilled water and sequentially partitioned with *n*-hexane (3 × 6 L), EtOAc (3 × 6 L), and *n*-BuOH (3 × 6 L). The *n*-hexane extract (396 g) was subjected to silica gel column chromatography (CC) using gradient mixtures of hexanes-EtOAc (99:1→0:1) as the mobile phases to yield 13 fractions (*Frs. 1–20*). *Fr. 5* (66 g) was fractionated by CC (ODS-A; H_2O-MeOH 7:3→0:1) and purified by CC (Sephadex LH-20; MeOH 100%) to afford TGN (250.9 mg, 0.001% w/w). The structure of TGN was identified by interpretation of its 1D and 2D NMR spectroscopic data as well as by comparison with published values [160].

1.3. Preparation of TGN

TGN was obtained by hydrolysis of tussilagone (TG) which was preparatively separated from Farfarae Flos [159]. One gram of TG was dissolved in 70% aqueous acetonitrile and sodium hydroxide was added to 100 mM solution. The reaction mixture was stirred at 25°C for 1 h, followed by solvent extraction with chloroform. The lower layer (organic solvent) was evaporated and separated by counter-current chromatography (CCC). The CCC condition as follows: *n*-hexane as stationary phase; water (eluent A) and acetonitrile (eluent B) as mobile phase; linear gradient, 0–100 min (70–90% B) and 100–150 min (90% B) at a flow rate of 8 mL/min and a rotation speed of 450 rpm. Eluate from 138-152 min was collected and dried (345 mg), followed by structural determination. The ^{1}H and ^{13}C NMR spectra were compared with previous literature [160].

1.4. Chemicals and reagents

Fetal bovine serum (FBS), penicillin, and streptomycin were purchased from GenDepot (Barker, TX, USA). Horse serum (HS) was the product of GIBCO BRL (Grand Island, NY, USA). Ham's F-12K, Dulbecco's phosphate buffered saline, 3-(4,5-dimethylthiazol-2-yl)-2,5-diphenyltetrazolium bromide (MTT), 6-hydroxydopamine (6-OHDA), cycloheximide, actinomycin D, 2′,7′-dichlorofluorescein diacetate (DCF-DA), dithiothreitol (DTT), *N*-acetyl-L-cysteine (NAC), LY294002, U0126, SB203580, SP600125, protease inhibitor cocktail,

paraformaldehyde (PFA), diaminobenzidine (DAB), sucrose, apomorphine (APO), tribromoethanol (TBE), and *Escherichia coli* LPS were purchased from Sigma-Aldrich Co. (St. Louis, MO, USA). Hydrogen peroxide (H_2O_2) solution (30% purified) was purchased from Merck (Darmstadt, Germany). The primary antibodies for Nrf2, HO-1, p-Akt, Akt, iNOS, COX-2, p-IκB-α, IκB-α, p50, p65, and β-actin, as well as all secondary antibodies and tin protoporphyrin IX (SnPP), were obtained from Santa Cruz Biotechnology (Santa Cruz, CA, USA). The primary antibodies for Keap1 and PCNA were supplied by Genetex (Irvine, CA, USA). Rabbit anti-tyrosine hydroxylase (TH), rabbit anti-dopamine transporter (DAT) and polyvinylidene fluoride were obtained from Millipore (Marlborough, MA, USA). Trolox was provided by Cayman Chemical (Ann Arbor, MI, USA). The ARE-binding site-luciferase construct was a generous gift from Prof. Young-Joon Surh (Seoul National University, Seoul, Korea). The PGE_2 enzyme-linked immunosorbent assay kit and TPA were purchased from Cayman Chemical (Ann Arbor, MI). All other chemicals were purchased from Sigma-Aldrich Co. unless otherwise specified.

1.5. Cell culture

PC12 rat pheochromocytoma cell line was purchased from the American Type Culture Collection (Manassas, VA, USA). PC12 cells were cultured in Ham's F-12K medium, supplemented with 15% HS, 2.5% FBS. The RAW 264.7 murine macrophage cell line was purchased from the American Type Culture Collection

(Manassas, VA). Human HaCaT cells were originally obtained from Dr. Norbert E. Fusenig (German Cancer Research Center, Heidelberg, Germany) and subcultured in this laboratory. These cells were maintained in DMEM supplemented with 10% FBS. The RAW 264.7 cells harboring the pNF-κB-secretory alkaline phosphatase-NPT reporter construct were cultured under the same conditions, except that the medium was supplemented with 500 μg/mL Geneticin (G-418; GenDepot). Cells were maintained in the presence of 100 U/ml penicillin and 100 μg/ml streptomycin at 37 ℃ in a humidified atmosphere of 5% CO_2 and 95% air.

1.6. Animals

1.6.1. 6-OHDA-induced mouse model of PD

Male ICR mice (8 weeks old, 30–35 g) were purchased from Daehan Biolink Co., Ltd. (Eumseong, Korea). All animals were housed at a constant temperature of 23 ± 1 ℃ and a relative humidity of 60 ± 10% in a 12 h light/dark cycle. Animal treatment and maintenance were carried out in accordance with the Principle of Laboratory Animal Care (NIH publication No. 85-23, revised 1985) and the Animal Care and Use Guidelines of Kyung Hee University. All animal studies were performed according to the approved guidelines of the Institutional Animal Care and Use Committee of Kyung Hee University (approval ID: KHUASP(SE)-16-128).

1.6.2. TPA-induced skin inflammation in mice

Female ICR mice (five weeks old, 25–30 g) were purchased from Koatech Co. (Pyeongtaek, Korea). All animals were housed in a pathogen-free barrier zone of the Seoul National University Animal Laboratory at $22 \pm 2°C$ with $50 \pm 5\%$ humidity in a 12-h light/dark cycle. All animal studies were performed according to the approved guidelines of Seoul National University Institutional Animal Care and Use Committees (approval ID: SNU-151012-1).

1.6.3. IMQ-induced psoriasis-like dermatitis model in mice

Female Balb/c mice (7 weeks old, 17-20 g) were purchased from Koatech Co. (Pyeongtaek, Korea). All animals were housed in a pathogen-free barrier zone of the Seoul National University Animal Laboratory at $22 \pm 2°C$ with $50 \pm 5\%$ humidity in a 12-h light/dark cycle. All animal studies were performed according to the approved guidelines of Seoul National University Institutional Animal Care and Use Committees (approval ID: SNU-180206-1).

2. Methods

2.1. Measurement of cell viability

The cytoprotective effect of ECN on H_2O_2- or 6-OHDA-induced PC12 cells was

measured with an MTT-based colorimetric assay. In brief, cells were treated with indicated concentrations of ECN before exposure to H_2O_2 (500 μM) or 6-OHDA (250 μM) for 24 h. MTT solution was added at the end of the treatment to the cell culture media at 0.5 mg/ml final concentration and incubated for 2 h at 37 ℃ in the dark. The absorbance at 595 nm was determined with an EMax® microplate reader (Molecular Devices, Sunnyvale, CA, USA).

2.2. Western blot analysis

Total cell lysates were prepared using the lysis buffer [20 mM HEPES (pH 7.6), 350 mM NaCl, 20% glycerol, 0.5 mM EDTA, 0.1 mM EGTA, 1% Nonidet P-40 (NP-40), 50 mM NaF, 0.1 mM dithiothreitol (DTT), 0.1 mM phenylmethylsulfonyl fluoride (PMSF) and protease inhibitor cocktail]. Skin tissue was homogenized and lysed in T-PER Tissue Protein Extraction Reagent (Thermo Fisher Scientific Inc., Rockford, IL). To prepare cytosolic and nuclear extracts, cells were collected and washed with PBS. Cells were resuspended in the lysis buffer [10 mM HEPES (pH 7.9), 10 mM KCl, 0.1 mM EDTA, 0.1 mM EGTA, 1 mM DTT, 1 mM PMSF, and a protease inhibitor cocktail], incubated on ice for 15 min, and then 10% of NP-40 was added. The mixture was vortexed for 10 s and centrifuged at 15,000 rpm for 5 min, with this supernatant containing the cytoplasmic fraction. The nuclear pellets were resuspended in nuclear extraction buffer [20 mM HEPES (pH 7.9), 400 mM NaCl, 1 mM EDTA, 1 mM EGTA, 1 mM DTT, 0.5 mM PMSF, and a protease inhibitor cocktail] for 1 h on ice with vortexing at 10 min intervals and then

117

centrifuged at 15,000 rpm for 10 min. The protein concentration was quantified using the Bradford protein assay (Bio-Rad Laboratories, Richmond, CA, USA). Equal amounts of protein (30 μg) were loaded on 8% of SDS polyacrylamide gels and transferred to nitrocellulose membranes. The membranes were blocked by 5% bovine serum albumin in T-BST buffer (20 mM Tris, 137 mM NaCl, 0.1% Tween 20, pH 7.6) and incubated with primary antibodies overnight at 4 ℃. After washing, the membranes were incubated with horseradish peroxidase-conjugated secondary antibodies for 1 h at room temperature. The immunoblots were detected with EZ-Western detection kit (DoGEN, Seoul, Korea). The values above the figures represent the relative density of the bands normalized to that for β-actin or PCNA.

2.3. Quantitative real-time reverse transcriptase polymerase chain reaction (qRT-PCR)

Total RNA was isolated using the Trizol reagent kit (Invitrogen, Carlsbad, CA, USA). Both the quantity and purity of RNA were measured using the Nanodrop spectrophotometer (Thermo Scientific, Wilmington, DE, USA). Total RNA (1 μg) was synthesized into cDNA using the amfiRivert Platinum cDNA Synthesis Master Mix (GenDepot, Barker, TX, USA), in accordance with the manufacturer's instructions. PCR amplification of target genes was performed using forward and reverse primers and a SYBR Green working solution (iTaq™ Universal SYBR Green Supermix, Bio-Rad, Hercules, CA, USA) with an Applied Biosystems 7300 real-time PCR system and software (Applied Biosystems, Carlsbad, CA, USA).

The following primers were used: Nrf2, 5′-CTC GCT GGA AAA AGA AGT G-3′ (F; forward) and 5′-CCG TCC AGG AGT TCA GAG G-3′ (R; reverse); HO-1, 5′-CAC GCA TAT ACC CGC TAC CT-3′ (F) and 5′-CCA GAG TGT TCA TTC GAG A-3′ (R); iNOS, 5′-TCC TAC ACC ACA CCA AAC-3′ (F) and 5′′-CTC CAA TCT CTG CCT ATC C-3′ (R); COX-2, 5′-CCT CTG CGA TGC TCT TCC-3′ (F) and 5′-TCA CAC TTA TAC TGG TCA AAT CC-3′ (R); TNF-α, 5′-AGC ACA GAA AGC ATG ATC CG-3′ (F) and 5′-CTG ATG AGA GGG AGG CCA TT-3′′ (R); IL-6, 5′′-GAG GAT ACC ACT CCC AAC AGA CC-3′ (F) and 5′-AAG TGC ATC ATC GTT GTT CAT ACA-3′ (R); and β-actin, 5′-CCC ACT CCT AAG AGG AGG ATG-3′ (F) and AGG GAG ACC AAA GCC TTC AT-3′ (R); Gapdh, 5′-AGG TCG GTG TGA ACG GAT TTG-3′ (F) and 5′-GGG GTC GTT GAT GGC AAC A-3′ (R); Il17a, 5′-CTC CAG AAG GCC CTC AGA CTA C-3′ (F) and 5′-GGG TCT TCA TTG CGG TGG-3′ (R); Il22, 5′-ATG AGT TTT TCC CTT ATG GGG AC-3′ (F) and 5′-GCT GGA AGT TGG ACA CCT CAA-3′ (R); Il23a, 5′-AAC TCC TCC AGC CAG AGG ATC A-3′ (F) and 5′-TCT TGG AAC GGA GAA GGG GG-3′ (R) TNFα, 5′-TGC CTA TGT CTC AGC CTC TTC-3′ (F) and 5′-GAG GCC ATT TGG GAA CTT CT-3′ (R); S100a7, 5′-GAG GAG TTG AAA GCT CTG CTC TTG-3′ (F) and 5′-GTG ATG TAG TAT GGC TGC CTG CGG-3′ (R); S100a8, 5′-AAA TCA CCA TGC CCT CTA CAA G-3′ (F) and 5′-CCC ACT TTT ATC ACC ATC GCA A-3′ (R); S100a9, 5′-GCA CAG TTG GCA ACC TTT ATG-3′ (F) and 5′-TGA TTG TCC TGG TTT GTG TCC-3′

119

(R); Defb4, 5′-CTC CAC TTG CAG CCT TTA CC-3′ (F) and 5′-ATC TGT CGA

AAA GCG GTA GGG-3′ (R).

2.4. Luciferase assay

Cells were co-transfected with 0.5 µg of pRL-CMV control vector (Promega, Madison, WI, USA) and 5 µg of luciferase plasmid using iN-fect™ transfection reagent (iNtRON Biotechnology, Seongnam, Korea), according to the manufacturer's instructions. After 24 h of transfection, the cells were treated with ECN for an additional 6 h or 24 h. The luciferase activity was performed using a dual luciferase assay kit (Promega, Madison, WI, USA).

2.5. Transient transfection of small interfering RNA

The cells, which were 60–80% confluent, were transfected with 100 nM scrambled, small interfering RNA (siRNA), Nrf2 and HO-1 siRNA (Bioneer, Daejeon, Korea) using Lipofectamine RNAiMAX (Invitrogen, Carlsbad, CA, USA) according to the manufacturer's instructions. After a 48 h transfection, cells were treated with the compound or other chemicals and then used for subsequent experiments.

2.6. Measurement of ROS accumulation

PC12 cells were seeded into 96-well plates (1×10^4 cells/well) for 24 h, and then

the medium was changed to serum-free medium. The cells were pretreated with ECN (2.5, 5, or 10 μM) for different times (10, 30, 60, and 120 min) or NAC (5 mM for 1 h) and incubated with 50 μM DCF-DA for 30 min at 37 ℃. Fluorescence of DCF was detected by a multimode microplate reader (SpectraMax M5, Molecular Devices, Sunnyvale, CA, USA) at excitation and emission wavelengths of 485 and 538 nm, respectively.

2.7. Measurement of NO, PGE_2 production and cell viability

RAW 264.7 cells were seeded in 24-well plates at 1×10^5 cells per well and incubated for 24 h. The cells were treated with the indicated concentrations of TGN or AMT as the positive control 6 h before LPS (1 μg/ml) stimulation and then were incubated for an additional 18 h. The nitrite concentration in the culture medium was measured using Griess reagent to indicate nitric oxide production. Briefly, 100 μl of supernatant was mixed with an equivalent volume of the Griess reagent. The nitrite concentration was calculated from a standard curve of sodium nitrite solutions. The quantities of PGE_2 in the culture supernatant were measured using an immunoassay kit according to the manufacturer's instructions. Cell viability was measured with a 3-(4,5-dimethylthiazol-2-yl)-2,5-diphenyltetrazolium bromide (MTT)-based colorimetric assay. The absorbance values were determined with an EMax® microplate reader (Molecular Devices, Sunnyvale, CA).

2.8. NF-κB SEAP reporter gene assay

NF-κB SEAP activity was evaluated using transfected RAW 264.7 cells with the pNF-κB-SEAP-NPT plasmid. Transfected cells were pretreated with TGN for 6 h and were LPS was added for 16 h. The fluorescence from the product of the SEAP/MUP reaction was measured in relative fluorescence units (RFU) with a 96-well plate fluorometer (Gemini XS, Molecular Devices, Sunnyvale, CA) at an excitation of 360 nm and an emission of 449 nm.

2.9. Isolation and culture of murine primary epidermal keratinocytes

Isolation and cultivation of murine primary keratinocytes was performed using newborn (from 2 to 4 days old) mice. Mice were immersed first in 70% ethanol, then in sterile PBS, followed 70% ethanol and, finally, in PBS. Skin was incubated in 0.25% trypsin at 4°C overnight, then the epidermis was separated from the dermis, minced, and homogenized in complete Eagle's medium essential medium (EMEM) with 0.05 mM $CaCl_2$ (low calcium). The homogenate was filtered, and the solution containing MPKs was collected by centrifugation (1200 rpm at 4 °C for 5 min). Cells were seeded at a density of 5×10^4 cells per cm^2 on collagen-IV (2.5 g/cm^2)-coated dishes. The medium was changed the following day, and cells were grown to 90% confluency in defined keratinocyte serum-free medium (Invitrogen, Paisley, UK), supplemented with 10 ng/ml epidermal growth factor (EGF) and 10^{-10} M cholera toxin.

122

2.10. Chromatin Immunoprecipitation (ChIP)

Primary cultured murine keratinocytes were grown to 80–90% confluency in 14 cm culture dishes. Cross-linking was performed by incubating in a solution of 1% formaldehyde in PBS for 10 min at room temperature, followed by quenching with glycine for 5 min. Cells were then removed from the dish using a cell scraper in the presence of 4-benzenesulfonyl fluoride hydrochloride (AEBSF) in PBS. The cell suspension was then added to a 15 ml tube and centrifuged at 1,200 r.p.m. for 5 min at 4 ℃. The cell pellet was re-suspended in 120 ml of cell lysis buffer (50 mM Tris (pH 8.0), 10 mM EDTA, 1% (wt/vol) SDS, protease inhibitor mix (cOmplete Mini, 11836170001, Roche), 1 mM AEBSF and 20 mM Na-butyrate), vortexed, and incubated on ice for 5 min. DNA fragmentation was performed using a probe sonicator with cycles of 30 s with 30 s breaks in between (cycle 0.5, 30% power). Appropriate DNA fragmentation (100-500 bp) was confirmed using gel electrophoresis. The fragmented chromatin was then mixed with 800 ml of RIPA buffer (10 mM Tris (pH 7.5), 140 mM NaCl, 1 mM EDTA, 0.5 mM EGTA, 1% (vol/vol) Triton X-100, 0.1% (wt/vol) SDS and 0.1% (wt/vol) Na-deoxycholate, cOmplete Mini protease inhibitor mix, 1 mM AEBSF, and 20 mM Na-butyrate) and centrifuged at 12,000 x g for 10 min. The supernatant was divided into nine aliquots and used as input chromatin. The following antibodies were used for IP: anti-histone H3 (Abcam), anti-Nrf2 (Santa Cruz, Santa Cruz, CA, for endogenous and caNrf2), antiNrf2 (MyBioSource, San Diego, CA for endogenous Nrf2), and anti-rabbit IgG (Millipore, Molsheim, France). Prior to incubation with chromatin, 3 mg of the appropriate antibody was incubated with Dynabeads Protein A/G

(Thermo Fisher) diluted 1:10 in 100 ml of RIPA buffer at 4C for 2 h while rotating. The antibody-bead complexes were then captured using a DynaMag-2 magnet (Thermo Fisher), washed using RIPA buffer, and incubated with 100 ml of previously prepared chromatin overnight at 4 ℃ while rotating. The samples were magnetically captured, washed with RIPA buffer, and resuspended in DNA elution buffer (20 mM TrisHCl (pH 7.5), 5 mM EDTA and 50 mM NaCl, 20 mM Na-butyrate, 1% (wt/vol) SDS, and 50 mg/ml proteinase K). Samples were incubated at 68C for 2 h while shaking at 700 r.p.m., followed by the magnetic capture and removal of the supernatant containing the DNA into a new tube. DNA was purified by phenol-chloroform phase separation and precipitated in a solution of 70% ethanol with 0.1 M sodium acetate and 15 mg of glycogen at -80 ℃ for 2 h. After precipitation, DNA was centrifuged at 17,000 g for 30 min at 4 ℃, and the pellet was washed with 70% ethanol. Finally, the pellet was resuspended in 50 ml of TE buffer (10 mM Tris-HCl (pH 8.0) and 10 mM EDTA) and heated at 95 ℃ for 10 min. DNA was then analyzed by qPCR for the presence of DNA fragments containing the ARE sequence of interest.

2.11. Animal study

2.11.1. 6-OHDA-induced mouse model of PD

2.11.1.1. Surgery procedure

Mice were anesthetized by an intraperitoneal injection of TBE (312.5 mg/kg body weight) and fixed into a stereotaxic apparatus (myNeuroLab, St. Louis, MO, USA).

Each mouse received a unilateral injection of a 2 μl vehicle (saline with 0.1% (w/v) ascorbic acid, for control group) or 6-OHDA (16 μg/2 μl in 0.1% ascorbic acid-saline) into the right striatum (ST) (coordinates related to bregma in mm: anterior–posterior = 0.5, medial–lateral = 2.0, dorsal-ventral = –3.0). Surgery was performed one day after the last drug administration.

2.11.1.2. Drug administration

The mice were divided into four groups, with six mice for each group: (1) sham group (sham-operated plus intraperitoneally saline-treated group); (2) ECN 5 mg/kg group (sham-operated plus intraperitoneally ECN 5 mg/kg treated group); (3) 6-OHDA group (6-OHDA-lesioned plus intraperitoneally saline-treated group); (4) 6-OHDA + ECN 5 mg/kg group (6-OHDA-lesioned plus intraperitoneally ECN 5 mg/kg treated group). ECN dissolved in saline was administered to the mice once per day for seven consecutive days.

2.11.1.3. Rotarod test

The rotarod test was conducted as described previously [161], with modifications on the 14th day after 6-OHDA injection. The mice were trained on the rotarod apparatus (diameter 3 cm; Ugo Basile, Collegeville, PA, USA) at a fixed speed of 12 rpm for 180 s. After training twice, mice were tested at a rotation speed of 17 rpm. The time each mouse remained on the rotating bar before falling was recorded

with three trials, for a maximum of 180 s per trial. Data shown are the mean time spent on the rotarod over three test trials.

2.11.1.4. APO-induced rotation test

The rotation of all the mice induced by APO was tested on the 15th day after 6-OHDA lesion. Mice were placed in a hemispherical clear plastic bowl with a diameter of 40 cm and 360° turns in the direction opposite to the lesion (contralateral rotation) were counted for 25 min after subcutaneous injection of APO (4 mg/kg). Results were expressed as contralateral turns per 25 min.

2.11.1.5. Immunohistochemistry

After the completion of all behavioral testing, mice were transcardially perfused with 0.05 M PBS and then fixed with cold 4% PFA in a 0.1 M phosphate buffer. Brains were postfixed in a 0.1 M phosphate buffer containing 4% PFA overnight at 4 ℃ and then cryopreserved in 0.05 M PBS containing 30% sucrose. Frozen brains were cut into 30 μm thick coronal sections on a freezing microtome (Leica, Wetzlar, Germany) and stored in cryoprotectant (25% ethylene glycol, 25% glycerol, and 0.05 M phosphate buffer) at 4 ℃ until use. Free-floating sections were treated with H_2O_2 for 15 min, and then incubated with a rabbit anti-TH (1:1000 dilution) for SN and ST tissues or anti-DAT antibodies (1:500 dilution) for ST tissues overnight at

126

4 ℃ in PBS containing 0.3% Triton X-100 and normal goat serum. After washing with PBS, the sections were incubated with a biotinylated anti-rabbit IgG (1:200 dilution) for 90 min, followed by incubation with an avidin–biotin complex mixture (1:100 dilution) for 1 h at room temperature. The reaction was visualized by incubating sections with DAB for 3 min. The sections were rinsed in PBS, mounted onto gelatin-coated slides, dehydrated, and coverslipped using the histomount medium. The optical density of TH or DAT-positive fibers in ST was analyzed at ×40 magnification and the number of TH-positive cells in SN counted at ×100 magnification using the ImageJ software (Bethesda, MD, USA). The images were obtained using a microscope (Olympus Microscope System BX51, Olympus, Tokyo, Japan).

2.11.2. TPA-induced skin inflammation in mice

The dorsal skin of the mice was shaved using electric clippers. TGN and TPA were dissolved in 0.2 ml of dimethyl sulfoxide (DMSO)/acetone (10:90, v/v) and applied topically to the shaved area (approximately 15×15 mm). The mice were treated topically with 2.5 and 5 μmol TGN for 30 min. Skin inflammation was induced by the topical application of 10 nmol TPA. Control groups were treated with a vehicle (DMSO/acetone), and dexamethasone (5 μmol in 0.2 ml DMSO/acetone) was used as a positive control. The mice were euthanized by cervical dislocation at the indicated times, and the dorsal skins were excised and immediately frozen in liquid nitrogen for further protein isolation.

127

2.11.3. IMQ-induced psoriasis-like dermatitis model in mice

2.11.3.1. Treatments

The back skin of mice was shaved with an electric clipper and then treated with a depilatory cream to remove residual hair. After 48 h of resting, The mice were divided into six groups, with six to nine mice for each group: (1) Vehicle control group (Vaseline cream plus topical ethanol treated group); (2) IMQ group (IMQ plus topical ethanol treated group); (3) IMQ + TGN 1 nmol/100 μl group (IMQ plus topical TGN 1 nmol treated group); (4) IMQ + TGN 5 nmol/100 μl group (IMQ plus topically TGN 5 nmol treated group); (5) IMQ + calcipotriol (CAL) 5 nmol/100 μl group (IMQ plus topically CAL 5 nmol treated group); (6) TGN 5 nmol/100 μl group (Vaseline cream plus topically TGN 5 nmol treated group). TGN and CAL dissolved in ethanol was administered to the mice once per day for nine consecutive days. While control mice received a control cream, the IMQ-treated mice received on the right ear and the shaved back skin a daily topical dose of 20 and 62.5 mg of 5% IMQ cream (Aldara, 3M Pharmaceuticals), respectively, for five consecutive days to induce the disease before drug treatment. The IMQ group and IMQ + drug groups continued to receive the same dose of IMQ for a total of 14 consecutive days to achieve optimal chronic inflammation. From Day 6, IMQ + drug groups first received topical application of TGN or CAL and application of IMQ cream. The back and ear skin were topically treated with TGN or CAL dissolved in ethanol with the volume of 100 μl (on shaved back skin) or 20 μl (10 μl on each side of the right ear) daily from days 6–15.

2.11.3.2. Scoring severity of skin inflammation

All mice were monitored daily, and thickness, erythema, and scaling of back skin and ear were measured every alternate day throughout the entire 14 days of the experiment. Back and ear redness (erythema), presence of scales (scaling), and hardness of the skin were scored using a semiquantitative PASI scoring system from 0 to 4 based on their external physical appearance: 0 = no skin abnormalities, 1 = slight, 2 = moderate, 3 = marked, and 4 = severe. In addition, mouse ear skin thickening was assessed by measuring thickness using an electronic digital caliper (Mitutoyo, Japan). The cumulative score (erythema plus scaling plus thickening) served as a measure of the severity of inflammation (scale 0–12).

2.11.3.3. Histology and immunohistochemistry

After a total of 14 days or 9 consecutive days of TGN treatment, all mice were euthanized, and skin tissues were freshly harvested and fixed in 4% paraformaldehyde for histological and biochemical analysis. Skin tissues were embedded in paraffin, and the paraffin sections (3 μm) were stained with H&E or incubated with antibodies against Ki-67, NF-κB p65, and p-STAT3 (1:200 dilution) at room temperature for 40 min in Tris-buffered saline containing 0.05% Tween 20. The sections were developed using the HPR EnVision™ System (Dako, Glostrup, Denmark), and the peroxidase binding sites were detected by staining with 3,3'-diaminobenzidinetetrahydrochloride (Dako, Glostrup, Denmark). Finally, sections were counterstained with Mayer's hematoxylin and mounted then observed under a

microscope.

2.12. Statistical analysis

The results represent the mean ± the standard deviation (S.D.) from three different experiments. Statistical analyses were performed with a one-way analysis of variance (ANOVA) with Tukey's and/or Bonferroni's multiple comparisons test using GraphPad Prism 7.0 software (San Diego, CA, USA). P values less than 0.05 were considered statistically significant.

REFERENCES

[1] Gan, L; Cookson, MR; Petrucelli, L; La Spada, AR. Converging pathways in neurodegeneration, from genetics to mechanisms. *Nat Neurosci* **21** (2018) 1300.

[2] Lin, MT; Beal, MF. Mitochondrial dysfunction and oxidative stress in neurodegenerative diseases. *Nature* **443** (2006) 787-795.

[3] Block, ML; Zecca, L; Hong, J-S. Microglia-mediated neurotoxicity: uncovering the molecular mechanisms. *Nat Rev Neuro* **8** (2007) 57.

[4] Buendia, I ;Michalska, P; Navarro, E; Gameiro, I ;Egea, J ;León, R. Nrf2–ARE pathway: an emerging target against oxidative stress and neuroinflammation in neurodegenerative diseases. *Pharmacol Ther* **157** (2016) 84-104.

[5] Molteni, M; Rossetti, C. Neurodegenerative diseases: The immunological perspective. *J Neuroimmunol* **313** (2017) 109-115.

[6] Dias, V; Junn, E; Mouradian, MM. The role of oxidative stress in Parkinson's disease. *J Parkinsons Dis* **3** (2013) 461-491.

[7] Cheignon, C; Tomas, M; Bonnefont-Rousselot, D; Faller, P; Hureau, C; Collin, F. Oxidative stress and the amyloid beta peptide in Alzheimer's disease. *Redox Biology* (2017)

[8] Bertram, L; Tanzi, RE. The genetic epidemiology of neurodegenerative disease. *J Clin Invest* **115** (2005) 1449-1457.

[9] Obeso, JA; Rodriguez-Oroz, MC; Goetz, CG; Marin, C; Kordower, JH; Rodriguez, M; Hirsch, EC; Farrer, M; Schapira, AH; Halliday, G. Missing pieces in the Parkinson's disease puzzle. *Nat Med* **16** (2010) 653.

[10] Pickrell, AM; Youle, RJ. The roles of PINK1, parkin, and mitochondrial fidelity in Parkinson's disease. *Neuron* **85** (2015) 257-273.

[11] LeWitt, PA. Levodopa for the treatment of Parkinson's disease. *New Engl J Med* **359** (2008) 2468-2476.

[12] Connolly, BS; Lang, AE. Pharmacological treatment of Parkinson disease: a review. *JAMA* **311** (2014) 1670-1683.

[13] Blesa, J; Phani, S; Jackson-Lewis, V; Przedborski, S. Classic and new animal models of Parkinson's disease. *BioMed Research International* **2012** (2012)

[14] Schober, A. Classic toxin-induced animal models of Parkinson's disease: 6-OHDA and MPTP. *Cell Tissue Res* **318** (2004) 215-224.

[15] Zeng, X-S; Geng, W-S; Jia, J-J. Neurotoxin-induced animal models of Parkinson disease: Pathogenic mechanism and assessment. *ASN Neuro* **10** (2018) 1759091418777438.

[16] Hernandez-Baltazar, D; Zavala-Flores, L; Villanueva-Olivo, A. The 6-hydroxydopamine model and parkinsonian pathophysiology: Novel findings in an older model. *Neurología (English Edition)* **32** (2017) 533-539.

[17] Zhang, Z; Li, G;Szeto, SS; Chong, CM; Quan, Q; Huang, C; Cui, W; Guo, B; Wang, Y; Han, Y. Examining the neuroprotective effects of protocatechuic acid and chrysin on in vitro and in vivo models of Parkinson disease. *Free Radical Biol Med* **84** (2015) 331-343.

[18] Li, M; Zhou, F; Xu, T; Song, H; Lu, B. Acteoside protects against 6-OHDA-induced dopaminergic neuron damage via Nrf2-ARE signaling pathway. *Food Chem Toxicol* **119** (2018) 6-13.

[19] Motyl, J; Przykaza, Ł; Boguszewski, PM; Kosson, P; Strosznajder, JB. Pramipexole and Fingolimod exert neuroprotection in a mouse model of Parkinson's disease by activation of sphingosine kinase 1 and Akt kinase. *Neuropharmacology* **135** (2018) 139-150.

[20] Hu, X; Song, Q; Li, X; Li, D;Zhang, Q; Meng, W; Zhao, Q. Neuroprotective effects of kukoamine A on neurotoxin-induced parkinson's model through apoptosis inhibition and autophagy enhancement. *Neuropharmacology* **117** (2017) 352-363.

[21] Velmurugan, B; Rathinasamy, B;Lohanathan, B;Thiyagarajan, V;Weng, C-F. Neuroprotective Role of Phytochemicals. *Molecules* **23** (2018) 2485.

[22] Sandoval-Avila, S; Diaz, N; Gómez-Pinedo, U; Canales-Aguirre, A; Gutiérrez-Mercado, Y; Padilla-Camberos, E; Marquez-Aguirre, A; Díaz-Martínez, N. Neuroprotective effects of phytochemicals on dopaminergic neuron cultures. *Neurología (English Edition)* (2018)

[23] Kim, J; Lee, HJ; Lee, KW. Naturally occurring phytochemicals for the prevention of Alzheimer's disease. *J Neurochem* **112** (2010) 1415-1430.

[24] Tellone, E; Galtieri, A; Russo, A; Giardina, B; Ficarra, S. Resveratrol: a focus on several neurodegenerative diseases. *Oxid Med Cell Longev* **2015** (2015)

[25] Srivastav, S; Fatima, M; Mondal, AC. Important medicinal herbs in Parkinson's disease pharmacotherapy. *Biomed Pharmacother* **92** (2017) 856-863.

[26] Zhang, C; Li, C; Chen, S; Li, Z; Jia, X; Wang, K; Bao, J; Liang, Y; Wang, X; Chen, M. Berberine protects against 6-OHDA-induced neurotoxicity in PC12 cells and zebrafish through hormetic mechanisms involving PI3K/AKT/Bcl-2 and

Nrf2/HO-1 pathways. *Redox biology* **11** (2017) 1-11.

[27] Lin, C-Y; Tsai, C-W. Carnosic acid protects SH-SY5Y cells against 6-hydroxydopamine-induced cell death through upregulation of parkin pathway. *Neuropharmacology* **110** (2016) 109-117.

[28] Boehncke, WH; Schon, MP. Psoriasis. *Lancet* **386** (2015) 983-994.

[29] Hawkes, JE; Chan, TC; Krueger, JG. Psoriasis pathogenesis and the development of novel targeted immune therapies. *J Allergy Clin Immunol* **140** (2017) 645-653.

[30] Lowes, MA; Suarez-Farinas, M; Krueger, JG. Immunology of psoriasis. *Annu Rev Immunol* **32** (2014) 227-255.

[31] Lowes, MA; Russell, CB; Martin, DA; Towne, JE; Krueger, JG. The IL-23/T17 pathogenic axis in psoriasis is amplified by keratinocyte responses. *Trends Immunol* **34** (2013) 174-181.

[32] Martin, DA; Towne, JE; Kricorian, G; Klekotka, P; Gudjonsson, JE; Krueger, JG;Russell, CB. The emerging role of IL-17 in the pathogenesis of psoriasis: preclinical and clinical findings. *J Invest Dermatol* **133** (2013) 17-26.

[33] Cai, Y; Fleming, C; Yan, J. New insights of T cells in the pathogenesis of psoriasis. *Cell Mol Immunol* **9** (2012) 302-309.

[34] Muromoto, R; Hirao, T; Tawa, K; Hirashima, K; Kon, S; Kitai, Y; Matsuda, T. IL-17A plays a central role in the expression of psoriasis signature genes through the induction of IkappaB-zeta in keratinocytes. *Int Immunol* **28** (2016) 443-452.

[35] Greb, JE; Goldminz, AM; Elder, JT; Lebwohl, MG; Gladman, DD; Wu, JJ; Mehta, NN; Finlay, AY; Gottlieb, AB. Psoriasis. *Nat Rev Dis Primers* **2** (2016)

16082.

[36] Hawkes, JE; Adalsteinsson, JA; Gudjonsson, JE; Ward, NL. Research techniques made simple: murine models of human psoriasis. *J Invest Dermatol* **138** (2018) e1-e8.

[37] Hawkes, JE; Gudjonsson, JE; Ward, NL. The snowballing literature on imiquimod-induced skin inflammation in mice: a critical appraisal. *J Invest Dermatol* **137** (2017) 546-549.

[38] van der Fits, L; Mourits, S; Voerman, JS; Kant, M; Boon, L; Laman, JD; Cornelissen, F; Mus, AM; Florencia, E; Prens, EP; Lubberts, E. Imiquimod-induced psoriasis-like skin inflammation in mice is mediated via the IL-23/IL-17 axis. *J Immunol* **182** (2009) 5836-5845.

[39] Medzhitov, R. Origin and physiological roles of inflammation. *Nature* **454** (2008) 428-435.

[40] Mahida, YR. The key role of macrophages in the immunopathogenesis of inflammatory bowel disease. *Inflamm Bowel Dis* **6** (2000) 21-33.

[41] Fujihara, M; Muroi, M; Tanamoto, K; Suzuki, T; Azuma, H; Ikeda, H. Molecular mechanisms of macrophage activation and deactivation by lipopolysaccharide: roles of the receptor complex. *Pharmacol Ther* **100** (2003) 171-194.

[42] Barnes, PJ; Karin, M. Nuclear factor-kappaB: a pivotal transcription factor in chronic inflammatory diseases. *N Engl J Med* **336** (1997) 1066-1071.

[43] Maines, MD. Heme oxygenase: function, multiplicity, regulatory mechanisms, and clinical applications. *FASEB J* **2** (1988) 2557-2568.

[44] Maines, MD; Panahian, N. The heme oxygenase system and cellular defense mechanisms. Do HO-1 and HO-2 have different functions? *Adv Exp Med Biol* **502** (2001) 249-272.

[45] Maines, MD. The heme oxygenase system: a regulator of second messenger gases. *Annu Rev Pharmacol Toxicol* **37** (1997) 517-554.

[46] Pae, HO; Kim, EC; Chung, HT. Integrative survival response evoked by heme oxygenase-1 and heme metabolites. *J Clin Biochem Nutr* **42** (2008) 197-203.

[47] Li, C; Hossieny, P; Wu, BJ; Qawasmeh, A; Beck, K; Stocker, R. Pharmacologic induction of heme oxygenase-1. *Antioxid Redox Signal* **9** (2007) 2227-2239.

[48] Schafer, M; Werner, S. Nrf2–A regulator of keratinocyte redox signaling. *Free Radic Biol Med* **88** (2015) 243-252.

[49] Martin, D; Rojo, AI; Salinas, M; Diaz, R; Gallardo, G; Alam, J; De Galarreta, CM; Cuadrado, A. Regulation of heme oxygenase-1 expression through the phosphatidylinositol 3-kinase/Akt pathway and the Nrf2 transcription factor in response to the antioxidant phytochemical carnosol. *J Biol Chem* **279** (2004) 8919-8929.

[50] Chen, CY; Jang, JH; Li, MH; Surh, YJ. Resveratrol upregulates heme oxygenase-1 expression via activation of NF-E2-related factor 2 in PC12 cells. *Biochem Biophys Res Commun* **331** (2005) 993-1000.

[51] Devesa, I; Ferrandiz, ML; Guillen, I; Cerda, JM; Alcaraz, MJ. Potential role of heme oxygenase-1 in the progression of rat adjuvant arthritis. *Lab Invest* **85** (2005) 34-44.

[52] Zampetaki, A; Minamino, T; Mitsialis, SA; Kourembanas, S. Effect of heme oxygenase-1 overexpression in two models of lung inflammation. *Exp Biol Med (Maywood)* **228** (2003) 442-446.

[53] Wu, ML; Ho, YC; Lin, CY; Yet, SF. Heme oxygenase-1 in inflammation and cardiovascular disease. *Am J Cardiovasc Dis* **1** (2011) 150-158.

[54] Ke, B; Shen, XD; Ji, H; Kamo, N; Gao, F; Freitas, MC; Busuttil, RW; Kupiec-Weglinski, JW. HO-1-STAT3 axis in mouse liver ischemia/reperfusion injury: regulation of TLR4 innate responses through PI3K/PTEN signaling. *J Hepatol* **56** (2012) 359-366.

[55] Menter, A; Korman, NJ; Elmets, CA; Feldman, SR; Gelfand, JM; Gordon, KB; Gottlieb, A; Koo, JY; Lebwohl, M; Lim, HW; Van Voorhees, AS; Beutner, KR; Bhushan, R. Guidelines of care for the management of psoriasis and psoriatic arthritis. Section 3. Guidelines of care for the management and treatment of psoriasis with topical therapies. *J Am Acad Dermatol* **60** (2009) 643-659.

[56] Raychaudhuri, SP; Raychaudhuri, SK. Biologics: target-specific treatment of systemic and cutaneous autoimmune diseases. *Indian J Dermatol* **54** (2009) 100-109.

[57] Johnson-Huang, LM; Lowes, MA; Krueger, JG. Putting together the psoriasis puzzle: an update on developing targeted therapies. *Dis Model Mech* **5** (2012) 423-433.

[58] Vadasz, Z; Rimar, D; Toubi, E. The new era of biological treatments. *Isr Med Assoc J* **16** (2014) 793-798.

[59] Sykiotis, GP; Bohmann, D. Stress-activated cap'n'collar transcription factors

in aging and human disease. *Sci Signal* **3** (2010) re3.

[60] Joshi, G; A Johnson, J. The Nrf2-ARE pathway: a valuable therapeutic target for the treatment of neurodegenerative diseases. *Recent patents on CNS drug discovery* **7** (2012) 218-229.

[61] Buendia, I; Michalska, P; Navarro, E; Gameiro, I; Egea, J; Leon, R. Nrf2–ARE pathway: an emerging target against oxidative stress and neuroinflammation in neurodegenerative diseases. *Pharmacol Ther* **157** (2016) 84-104.

[62] Chen, P-C; Vargas, MR; Pani, AK; Smeyne, RJ; Johnson, DA; Kan, YW; Johnson, JA. Nrf2-mediated neuroprotection in the MPTP mouse model of Parkinson's disease: critical role for the astrocyte. *Proc Natl Acad Sci USA* **106** (2009) 2933-2938.

[63] Satoh, T; Okamoto, S-I; Cui, J; Watanabe, Y; Furuta, K; Suzuki, M; Tohyama, K; Lipton, S. Activation of the Keap1/Nrf2 pathway for neuroprotection by electrophillic phase II inducers. *Proc Natl Acad Sci U S A* **103** (2006) 768-773.

[64] Jazwa, A; Cuadrado, A. Targeting heme oxygenase-1 for neuroprotection and neuroinflammation in neurodegenerative diseases. *Curr Drug Targets* **11** (2010) 1517-1531.

[65] Kumar, H; Kim, I-S; More, SV; Kim, B-W; Choi, D-K. Natural product-derived pharmacological modulators of Nrf2/ARE pathway for chronic diseases. *Nat Prod Rep* **31** (2014) 109-139.

[66] Magesh, S; Chen, Y; Hu, L. Small molecule modulators of Keap1-Nrf2-ARE pathway as potential preventive and therapeutic agents. *Med Res Rev* **32** (2012) 687-726.

[67] Lim, HJ; Dong, G-z; Lee, HJ; Ryu, J-H. In vitro neuroprotective activity of sesquiterpenoids from the flower buds of *Tussilago farfara*. *J Enzyme Inhib Med Chem* **30** (2015) 852-856.

[68] Ben-Yehuda Greenwald, M; Ben-Sasson, S; Bianco-Peled, H; Kohen, R. Skin Redox Balance Maintenance: The Need for an Nrf2-Activator Delivery System. *Cosmetics* **3** (2016) 1.

[69] Baek, J; Lee, MG. Oxidative stress and antioxidant strategies in dermatology. *Redox Rep* **21** (2016) 164-169.

[70] Judzentiene, A; Budiene, J. Volatile Oils of Flowers and Stems of *Tussilago farfara* L. from Lithuania. *J Essent Oil Bear Pl* **14** (2011) 413-416.

[71] Barceloux, DG. Coltsfoot (*Tussilago farfara* L.). *Medical Toxicology of Natural Substances: Foods, Fungi, Medicinal Herbs, Plants, and Venomous Animals* (2008) 446-448.

[72] Hwangbo, C; Lee, HS; Park, J; Choe, J; Lee, JH. The anti-inflammatory effect of tussilagone, from *Tussilago farfara*, is mediated by the induction of heme oxygenase-1 in murine macrophages. *Int Immunopharmacol* **9** (2009) 1578-1584.

[73] Lim, HJ; Dong, GZ; Lee, HJ; Ryu, JH. In vitro neuroprotective activity of sesquiterpenoids from the flower buds of *Tussilago farfara*. *J Enzyme Inhib Med Chem* **30** (2015) 852-856.

[74] Kim, M-R; Lee, JY; Lee, H-H; Aryal, DK; Kim, YG; Kim, SK; Woo, E-R; Kang, KW. Antioxidative effects of quercetin-glycosides isolated from the flower buds of *Tussilago farfara* L. *Food Chem Toxicol* **44** (2006) 1299-1307.

[75] Uysal, S; Senkardes, I; Mollica, A; Zengin, G; Bulut, G; Dogan, A; Glamoclija,

J; Sokovic, M; Lobine, D; Mahomoodally, FM. Biologically active compounds from two members of the Asteraceae family: Tragopogon dubius Scop. and *Tussilago farfara* L. *J Biomol Struct Dyn* (2018) 1-13.

[76] Jang, H; Lee, JW; Lee, C; Jin, Q; Choi, JY; Lee, D; Han, SB; Kim, Y; Hong, JT; Lee, MK; Hwang, BY. Sesquiterpenoids from *Tussilago farfara* inhibit LPS-induced nitric oxide production in macrophage RAW 264.7 cells. *Arch Pharm Res* **39** (2016) 127-132.

[77] Lee, K-M; Kwon, TY; Kang, U; Seo, EK; Yun, JH; Nho, CW; Kim, YS. Tussilagonone-induced Nrf2 pathway activation protects HepG2 cells from oxidative injury. *Food Chem Toxicol* **108** (2017) 120-127.

[78] Lee, HJ. Effects of Natural products including Tussilagonone on gene Expression and Production of MUC5AC Mucin from human airway Epithelial Cells. *Yakhak Hoeji* **62** (2018) 145-152.

[79] Gottlieb, AB. Psoriasis: emerging therapeutic strategies. *Nat Rev Drug Discov* **4** (2005) 19-34.

[80] Johnson, DA; Johnson, JA. Nrf2—a therapeutic target for the treatment of neurodegenerative diseases. *Free Radical Biol Med* **88** (2015) 253-267.

[81] Zhang, DD. Mechanistic studies of the Nrf2-Keap1 signaling pathway. *Drug Metab Rev* **38** (2006) 769-789.

[82] Surh, Y-J. Cancer chemoprevention with dietary phytochemicals. *Nature Reviews Cancer* **3** (2003) 768.

[83] Calabrese, V; Santoro, A; Monti, D; Crupi, R; Di Paola, R; Latteri, S;Cuzzocrea, S; Zappia, M; Giordano, J; Calabrese, EJ. Aging and Parkinson's

Disease: Inflammaging, neuroinflammation and biological remodeling as key factors in pathogenesis. *Free Radical Biol Med* **115** (2018) 80-91.

[84] Lastres-Becker, I; García-Yagüe, AJ; Scannevin, RH; Casarejos, MJ; Kügler, S; Rábano, A; Cuadrado, A. Repurposing the NRF2 activator dimethyl fumarate as therapy against synucleinopathy in Parkinson's disease. *Antioxid redox signal* **25** (2016) 61-77.

[85] Wu, RP; Hayashi, T; Cottam, HB; Jin, G; Yao, S; Wu, CC; Rosenbach, MD; Corr, M; Schwab, RB; Carson, DA. Nrf2 responses and the therapeutic selectivity of electrophilic compounds in chronic lymphocytic leukemia. *Proc Natl Acad Sci USA* **107** (2010) 7479-7484.

[86] Lee, K-M; Kang, K; Lee, SB; Nho, CW. Nuclear factor-E2 (Nrf2) is regulated through the differential activation of ERK1/2 and PKC α/βII by Gymnasterkoreayne B. *Cancer Lett* **330** (2013) 225-232.

[87] Surh, Y-J. Nrf2, an essential component of cellular stress response, as a potential target of hormetic phytochemicals. *J Food Drug Anal* **20** (2012) 217-219.

[88] Bryan, HK; Olayanju, A; Goldring, CE; Park, BK. The Nrf2 cell defence pathway: Keap1-dependent and-independent mechanisms of regulation. *Biochem Pharmacol* **85** (2013) 705-717.

[89] Almazari, I; Park, J-M; Park, S-A; Suh, J-Y; Na, H-K; Cha, Y-N; Surh, Y-J. Guggulsterone induces heme oxygenase-1 expression through activation of Nrf2 in human mammary epithelial cells: PTEN as a putative target. *Carcinogenesis* **33** (2011) 368-376.

[90] Athauda, D; Foltynie, T. The ongoing pursuit of neuroprotective therapies in

Parkinson disease. *Nat Rev Neurol* **11** (2015) 25-40.

[91] Potashkin, J; Blume, S; Runkle, N. Limitations of animal models of Parkinson's disease. *Parkinsons dis* **2011** (2011)

[92] Bezard, E; Yue, Z; Kirik, D; Spillantini, MG. Animal models of Parkinson's disease: limits and relevance to neuroprotection studies. *Mov Disord* **28** (2013) 61-70.

[93] Blesa, J; Przedborski, S. Parkinson's disease: animal models and dopaminergic cell vulnerability. *Front Neuroanat* **8** (2014) 155.

[94] Simola, N; Morelli, M; Carta, AR. The 6-hydroxydopamine model of Parkinson's disease. *Neurotox Res* **11** (2007) 151-167.

[95] Marin, C; Aguilar, E. In vivo 6-OHDA-induced neurodegeneration and nigral autophagic markers expression. *Neurochem Int* **58** (2011) 521-526.

[96] Dauer, W; Przedborski, S. Parkinson's disease: mechanisms and models. *Neuron* **39** (2003) 889-909.

[97] Wang, Q; Shin, E-J; Nguyen, X-KT; Li, Q; Bach, J-H; Bing, G; Kim, W-K; Kim, H-C; Hong, J-S. Endogenous dynorphin protects against neurotoxin-elicited nigrostriatal dopaminergic neuron damage and motor deficits in mice. *J Neuroinflammation* **9** (2012) 124.

[98] Boix, J; Padel, T; Paul, G. A partial lesion model of Parkinson's disease in mice–Characterization of a 6-OHDA-induced medial forebrain bundle lesion. *Behav Brain Res* **284** (2015) 196-206.

[99] Heuer, A; Smith, GA; Lelos, MJ; Lane, EL; Dunnett, SB. Unilateral nigrostriatal 6-hydroxydopamine lesions in mice I: motor impairments identify

extent of dopamine depletion at three different lesion sites. *Behav Brain Res* **228** (2012) 30-43.

[100] Havrda, MC; Paolella, BR; Ward, NM; Holroyd, KB. Behavioral abnormalities and Parkinson's-like histological changes resulting from Id2 inactivation in mice. *Dis Model Mech* **6** (2013) 819-827.

[101] Daubner, SC; Le, T; Wang, S. Tyrosine hydroxylase and regulation of dopamine synthesis. *Arch Biochem Biophys* **508** (2011) 1-12.

[102] Vaughan, RA; Foster, JD. Mechanisms of dopamine transporter regulation in normal and disease states. *Trends Pharmacol Sci* **34** (2013) 489-496.

[103] Kordower, JH; Olanow, CW; Dodiya, HB; Chu, Y; Beach, TG; Adler, CH; Halliday, GM; Bartus, RT. Disease duration and the integrity of the nigrostriatal system in Parkinson's disease. *Brain* **136** (2013) 2419-2431.

[104] Penttinen, AM; Suleymanova, I; Albert, K; Anttila, J; Voutilainen, MH; Airavaara, M. Characterization of a new low-dose 6-hydroxydopamine model of Parkinson's disease in rat. *J Neurosci Res* **94** (2016) 318-328.

[105] Pardridge, WM. Drug transport across the blood–brain barrier. *J Cereb Blood Flow Metab* **32** (2012) 1959-1972.

[106] Pajouhesh, H; Lenz, GR. Medicinal chemical properties of successful central nervous system drugs. *NeuroRx* **2** (2005) 541-553.

[107] Poulin, P; Theil, FP. Prediction of pharmacokinetics prior to in vivo studies. 1. Mechanism-based prediction of volume of distribution. *J Pharm Sci* **91** (2002) 129-156.

[108] Poulin, P; Theil, FP. Prediction of pharmacokinetics prior to in vivo studies.

II. Generic physiologically based pharmacokinetic models of drug disposition. *J Pharm Sci* **91** (2002) 1358-1370.

[109] Paine, A; Eiz-Vesper, B; Blasczyk, R; Immenschuh, S. Signaling to heme oxygenase-1 and its anti-inflammatory therapeutic potential. *Biochem Pharmacol* **80** (2010) 1895-1903.

[110] Gloire, G; Legrand-Poels, S; Piette, J. NF-kappaB activation by reactive oxygen species: fifteen years later. *Biochem Pharmacol* **72** (2006) 1493-1505.

[111] Li, H; Lee, HJ; Ahn, YH; Kwon, HJ; Jang, CY; Kim, WY; Ryu, JH. Tussilagone suppresses colon cancer cell proliferation by promoting the degradation of beta-catenin. *Biochem Biophys Res Commun* **443** (2014) 132-137.

[112] Lim, HJ; Lee, HS; Ryu, JH. Suppression of inducible nitric oxide synthase and cyclooxygenase-2 expression by tussilagone from Farfarae flos in BV-2 microglial cells. *Arch Pharm Res* **31** (2008) 645-652.

[113] Li, W; Huang, X; Yang, XW. New sesquiterpenoids from the dried flower buds of *Tussilago farfara* and their inhibition on NO production in LPS-induced RAW264.7 cells. *Fitoterapia* **83** (2012) 318-322.

[114] Liu, LL; Yang, JL; Shi, YP. Sesquiterpenoids and other constituents from the flower buds of *Tussilago farfara*. *J Asian Nat Prod Res* **13** (2011) 920-929.

[115] Park, Y; Ryu, HS; Lee, HK; Kim, JS; Yun, J; Kang, JS; Hwang, BY; Hong, JT; Kim, Y; Han, SB. Tussilagone inhibits dendritic cell functions via induction of heme oxygenase-1. *Int Immunopharmacol* **22** (2014) 400-408.

[116] Shin, JW; Ohnishi, K; Murakami, A; Lee, JS; Kundu, JK; Na, HK; Ohigashi, H; Surh, YJ. Zerumbone induces heme oxygenase-1 expression in mouse skin and

cultured murine epidermal cells through activation of Nrf2. *Cancer Prev Res (Phila)* **4** (2011) 860-870.

[117] Dinkova-Kostova, AT; Holtzclaw, WD; Cole, RN; Itoh, K; Wakabayashi, N; Katoh, Y; Yamamoto, M; Talalay, P. Direct evidence that sulfhydryl groups of Keap1 are the sensors regulating induction of phase 2 enzymes that protect against carcinogens and oxidants. *Proc Natl Acad Sci U S A* **99** (2002) 11908-11913.

[118] Dinkova-Kostova, AT; Massiah, MA; Bozak, RE; Hicks, RJ; Talalay, P. Potency of Michael reaction acceptors as inducers of enzymes that protect against carcinogenesis depends on their reactivity with sulfhydryl groups. *Proc Natl Acad Sci U S A* **98** (2001) 3404-3409.

[119] Nakamura, Y; Yoshida, C; Murakami, A; Ohigashi, H; Osawa, T; Uchida, K. Zerumbone, a tropical ginger sesquiterpene, activates phase II drug metabolizing enzymes. *FEBS Lett* **572** (2004) 245-250.

[120] Farombi, EO; Shrotriya, S; Na, HK; Kim, SH; Surh, YJ. Curcumin attenuates dimethylnitrosamine-induced liver injury in rats through Nrf2-mediated induction of heme oxygenase-1. *Food Chem Toxicol* **46** (2008) 1279-1287.

[121] Jeong, GS; Pae, HO; Jeong, SO; Kim, YC; Kwon, TO; Lee, HS; Kim, NS; Park, SD; Chung, HT. The alpha-methylene-gamma-butyrolactone moiety in dehydrocostus lactone is responsible for cytoprotective heme oxygenase-1 expression through activation of the nuclear factor E2-related factor 2 in HepG2 cells. *Eur J Pharmacol* **565** (2007) 37-44.

[122] Yeh, PY; Li, CY; Hsieh, CW; Yang, YC; Yang, PM; Wung, BS. CO-releasing molecules and increased heme oxygenase-1 induce protein S-glutathionylation to

modulate NF-kappaB activity in endothelial cells. *Free Radic Biol Med* **70** (2014) 1-13.

[123] Foresti, R; Bains, SK; Pitchumony, TS; de Castro Bras, LE; Drago, F; Dubois-Rande, JL; Bucolo, C; Motterlini, R. Small molecule activators of the Nrf2-HO-1 antioxidant axis modulate heme metabolism and inflammation in BV2 microglia cells. *Pharmacol Res* **76** (2013) 132-148.

[124] Kim, AN; Jeon, WK; Lee, JJ; Kim, BC. Up-regulation of heme oxygenase-1 expression through CaMKII-ERK1/2-Nrf2 signaling mediates the anti-inflammatory effect of bisdemethoxycurcumin in LPS-stimulated macrophages. *Free Radic Biol Med* **49** (2010) 323-331.

[125] Pae, H-O; Chung, H-T. Heme oxygenase-1: its therapeutic roles in inflammatory diseases. *Immune Netw* **9** (2009) 12-19.

[126] Shih, RH; Yang, CM. Induction of heme oxygenase-1 attenuates lipopolysaccharide-induced cyclooxygenase-2 expression in mouse brain endothelial cells. *J Neuroinflammation* **7** (2010) 86.

[127] Lee, T-S; Chau, L-Y. Heme oxygenase-1 mediates the anti-inflammatory effect of interleukin-10 in mice. *Nat Med* **8** (2002) 240-246.

[128] Kim, J; Cha, YN; Surh, YJ. A protective role of nuclear factor-erythroid 2-related factor-2 (Nrf2) in inflammatory disorders. *Mutat Res* **690** (2010) 12-23.

[129] Alam, J; Stewart, D; Touchard, C; Boinapally, S; Choi, AM; Cook, JL. Nrf2, a Cap'n'Collar transcription factor, regulates induction of the heme oxygenase-1 gene. *J Biol Chem* **274** (1999) 26071-26078.

[130] Choi, RJ; Cheng, MS; Kim, YS. Desoxyrhapontigenin up-regulates Nrf2-

mediated heme oxygenase-1 expression in macrophages and inflammatory lung injury. *Redox Biol* **2** (2014) 504-512.

[131] Park, SY; Kim, JH; Lee, SJ; Kim, Y. Involvement of PKA and HO-1 signaling in anti-inflammatory effects of surfactin in BV-2 microglial cells. *Toxicol Appl Pharmacol* **268** (2013) 68-78.

[132] Checker, R; Patwardhan, RS; Sharma, D; Menon, J; Thoh, M; Bhilwade, HN; Konishi, T; Sandur, SK. Schisandrin B exhibits anti-inflammatory activity through modulation of the redox-sensitive transcription factors Nrf2 and NF-kappaB. *Free Radic Biol Med* **53** (2012) 1421-1430.

[133] Banning, A; Brigelius-Flohe, R. NF-kappaB, Nrf2, and HO-1 interplay in redox-regulated VCAM-1 expression. *Antioxid Redox Signal* **7** (2005) 889-899.

[134] Soares, MP; Seldon, MP; Gregoire, IP; Vassilevskaia, T; Berberat, PO; Yu, J; Tsui, TY; Bach, FH. Heme oxygenase-1 modulates the expression of adhesion molecules associated with endothelial cell activation. *J Immunol* **172** (2004) 3553-3563.

[135] Ganesh Yerra, V; Negi, G; Sharma, SS; Kumar, A. Potential therapeutic effects of the simultaneous targeting of the Nrf2 and NF-kappaB pathways in diabetic neuropathy. *Redox Biol* **1** (2013) 394-397.

[136] Buelna-Chontal, M; Zazueta, C. Redox activation of Nrf2 & NF-kappaB: a double end sword? *Cell Signal* **25** (2013) 2548-2557.

[137] Lewis, JG; Adams, DO. Early inflammatory changes in the skin of SENCAR and C57BL/6 mice following exposure to 12-*O*-tetradecanoylphorbol-13-acetate. *Carcinogenesis* **8** (1987) 889-898.

[138] Chun, KS; Cha, HH; Shin, JW; Na, HK; Park, KK; Chung, WY; Surh, YJ. Nitric oxide induces expression of cyclooxygenase-2 in mouse skin through activation of NF-kappaB. *Carcinogenesis* **25** (2004) 445-454.

[139] Hung, W-L; Liu, CM; Lai, CS; Ho, C-T; Pan, MH. Inhibitory effect of garcinol against 12-O-tetradecanoylphorbol 13-acetate-induced skin inflammation and tumorigenesis in mice. *J Funct Foods* **18** (2015) 432-444.

[140] Goldminz, AM; Au, SC; Kim, N; Gottlieb, AB; Lizzul, PF. NF-kappaB: an essential transcription factor in psoriasis. *J Dermatol Sci* **69** (2013) 89-94.

[141] Calautti, E; Avalle, L; Poli, V. Psoriasis: A STAT3-Centric View. *Int J Mol Sci* **19** (2018)

[142] Sano, S; Chan, KS; Carbajal, S; Clifford, J; Peavey, M; Kiguchi, K; Itami, S; Nickoloff, BJ; DiGiovanni, J. Stat3 links activated keratinocytes and immunocytes required for development of psoriasis in a novel transgenic mouse model. *Nat Med* **11** (2005) 43-49.

[143] Lee, J; Kang, U; Seo, EK; Kim, YS. Heme oxygenase-1-mediated anti-inflammatory effects of tussilagonone on macrophages and 12-*O*-tetradecanoylphorbol-13-acetate-induced skin inflammation in mice. *Int Immunopharmacol* **34** (2016) 155-164.

[144] Kadam, DP; Suryakar, AN; Ankush, RD; Kadam, CY; Deshpande, KH. Role of oxidative stress in various stages of psoriasis. *Indian J Clin Biochem* **25** (2010) 388-392.

[145] Brennan, MS; Matos, MF; Li, B; Hronowski, X; Gao, B; Juhasz, P; Rhodes, KJ; Scannevin, RH. Dimethyl fumarate and monoethyl fumarate exhibit differential

effects on KEAP1, NRF2 activation, and glutathione depletion in vitro. *PLoS One* **10** (2015) e0120254.

[146] Fox, RJ; Kita, M; Cohan, SL; Henson, LJ; Zambrano, J; Scannevin, RH; O'Gorman, J; Novas, M; Dawson, KT; Phillips, JT. BG-12 (dimethyl fumarate): a review of mechanism of action, efficacy, and safety. *Curr Med Res Opin* **30** (2014) 251-262.

[147] Zhang, B; Xie, S; Su, Z; Song, S; Xu, H; Chen, G; Cao, W; Yin, S; Gao, Q; Wang, H. Heme oxygenase-1 induction attenuates imiquimod-induced psoriasiform inflammation by negative regulation of Stat3 signaling. *Sci Rep* **6** (2016) 21132.

[148] An, J; Li, T; Dong, Y; Li, Z; Huo, J. Terminalia Chebulanin Attenuates Psoriatic Skin Lesion via Regulation of Heme Oxygenase-1. *Cell Physiol Biochem* **39** (2016) 531-543.

[149] Campbell, NK; Fitzgerald, HK; Malara, A; Hambly, R; Sweeney, CM; Kirby, B; Fletcher, JM; Dunne, A. Naturally derived Heme-Oxygenase 1 inducers attenuate inflammatory responses in human dendritic cells and T cells: relevance for psoriasis treatment. *Sci Rep* **8** (2018) 10287.

[150] Vinter, H; Iversen, L; Steiniche, T; Kragballe, K; Johansen, C. Aldara[®]-induced skin inflammation: studies of patients with psoriasis. *Br J Dermatol* **172** (2015) 345-353.

[151] Qin, S; Wen, J; Bai, XC; Chen, TY; Zheng, RC; Zhou, GB; Ma, J; Feng, JY; Zhong, BL; Li, YM. Endogenous n-3 polyunsaturated fatty acids protect against imiquimod-induced psoriasis-like inflammation via the IL-17/IL-23 axis. *Mol Med Rep* **9** (2014) 2097-2104.

[152] Barrea, L; Savanelli, MC; Di Somma, C; Napolitano, M; Megna, M; Colao, A; Savastano, S. Vitamin D and its role in psoriasis: An overview of the dermatologist and nutritionist. *Rev Endocr Metab Disord* **18** (2017) 195-205.

[153] Carlberg, C; Campbell, MJ. Vitamin D receptor signaling mechanisms: integrated actions of a well-defined transcription factor. *Steroids* **78** (2013) 127-136.

[154] Peric, M; Koglin, S; Dombrowski, Y; Groß, K; Bradac, E; Büchau, A; Steinmeyer, A; Zügel, U; Ruzicka, T; Schauber, J. Vitamin D analogs differentially control antimicrobial peptide/"alarmin" expression in psoriasis. *PLoS One* **4** (2009) e6340.

[155] Kusuba, N; Kitoh, A; Dainichi, T; Honda, T; Otsuka, A; Egawa, G; Nakajima, S; Miyachi, Y; Kabashima, K. Inhibition of IL-17–committed T cells in a murine psoriasis model by a vitamin D analogue. *J Allergy Clin Immunol* **141** (2018) 972-981.

[156] Kim, BS; Siracusa, MC; Saenz, SA; Noti, M; Monticelli, LA; Sonnenberg, GF; Hepworth, MR; Van Voorhees, AS; Comeau, MR; Artis, D. TSLP elicits IL-33–independent innate lymphoid cell responses to promote skin inflammation. *Sci Transl Med* **5** (2013) 170ra116.

[157] Li, M;Hener, P; Zhang, Z; Kato, S; Metzger, D; Chambon, P. Topical vitamin D3 and low-calcemic analogs induce thymic stromal lymphopoietin in mouse keratinocytes and trigger an atopic dermatitis. *Proc Natl Acad Sci USA* **103** (2006) 11736-11741.

[158] Gottlieb, AB. Therapeutic options in the treatment of psoriasis and atopic dermatitis. *J Am Acad Dermatol* **53** (2005) S3-S16.

[159] Song, K; Lee, KJ; Kim, YS. Development of an efficient fractionation method for the preparative separation of sesquiterpenoids from *Tussilago farfara* by counter-current chromatography. *J Chromatogr A* **1489** (2017) 107-114.

[160] Park, HR; Yoo, MY; Seo, JH; Kim, IS; Kim, NY; Kang, JY; Cui, L; Lee, CS; Lee, CH; Lee, HS. Sesquiterpenoids isolated from the flower buds of *Tussilago farfara* L. inhibit diacylglycerol acyltransferase. *J Agric Food Chem* **56** (2008) 10493-10497.

[161] Choi, JG; Park, G; Kim, HG; Oh, D-S; Kim, H; Oh, MS. In vitro and in vivo neuroprotective effects of walnut (Juglandis semen) in models of Parkinson's disease. *Intl J Mol Sci* **17** (2016) 108.

ABSTRACT IN KOREAN

산화 스트레스는 알츠하이머 및 파킨슨 병과 같은 신경 퇴행성 질환에서 병의 발병 기전에 기여하는 신경 세포의 기능 장애 또는 사멸을 초래하여, 주요한 병인으로 작용한다. 피부는 자외선 및 활성 산소종 (ROS)을 생성하는 외인성 스트레스 요인에 지속적으로 노출되므로 산화 스트레스의 주된 표적이 되는 신체 기관이다. 따라서, 체내 항산화 방어 기작을 활성화시키는 것은 신경 퇴행성 질환 및 만성 염증성 피부 질환인 건선의 치료에 있어 효과적인 전략이 될 수 있으며 항산화 반응의 주 조절자인 Nrf2 의 약리학적 활성화가 주요 표적이 될 수 있다. 본 연구에서는 약용식물 관동화의 세스퀴테르펜 화합물인 ECN 과 TGN 이 강력한 Nrf2 활성화 물질임을 밝혔다. 또한, ECN 과 TGN 을 대상으로 신경보호 및 항건선 효능과 관련 작용 기전을 규명하였고, 동물 모델을 이용하여 생체 내 효능을 확인하였다.

식물 유래 생리활성 물질을 일컫는 파이토케미컬 (Phytochemical)은 강력한 항산화 물질로 해독 효소 및 세포 보호 단백질의 발현을 유도하는 Nrf2 의 활성화제 역할을 하는 것으로 주목받고 있다. 세스퀴테르펜을 포함하는 테르페노이드 계열 화합물은 Keap1 단백질에 존재하는 반응성 시스테인 잔기의 마이클 반응을 통해 Nrf2 를 활성화시킬 수 있다. 이러한 특징으로 인해 다양한 테르페노이드가 보호 효과를 갖는 것으로 보고되어있다. 그러나, ECN

및 TGN 의 Nrf2 매개 약리학적 활성은 아직 밝혀지지 않았다. 본 연구의 목적은 1) Nrf2 활성화 물질로서의 ECN 및 TGN 의 효능을 평가하고, 2) ECN 의 신경 보호 활성 및 TGN 의 항건선 효능에 대한 분자 기전을 밝히고 동물 모델을 이용하여 생체 내 반응을 확인하고자 하였다.

ECN 은 산화 스트레스에 의해 유발된 세포 손상에 대한 보호 효과를 나타내었다. 또한, PC12 세포에서 Nrf2 및 heme oxygenase-1 (HO-1) 발현을 상향 조절하고 Nrf2 활성화의 상위 기전으로 Akt 의 인산화를 유도하였다. Nrf2 유전자의 하향 조절은 ECN 에 의한 보호 효과를 억제시킨 결과를 통해, 산화 스트레스에 대한 ECN 의 신경 보호 효과가 Nrf2 / HO-1 신호 전달을 매개로 한다는 것을 밝혔다. 6-OHDA 유발 파킨슨병 동물 모델에서, ECN 의 투여는 운동 장애 및 도파민성 신경 손상을 완화시켰다.

TGN 은 대식세포에서 HO-1 매개 염증 저항성을 나타냈고 12-O-tetradecanoylphorbol-13-acetate (TPA)로 유도한 급성 피부 염증 쥐 모델에서 염증 매개 단백질의 발현을 감소시켰다. 또한 TGN 은 NF-kB 및 STAT3 활성화를 억제하여 건선 관련 염증 인자들의 발현 및 각질 세포의 과다 증식을 감소시켰다. 이와 같은 TGN 에 의한 NF-kB 및 STAT3 의 억제는 Nrf2 활성화를 통해 매개됨이 확인되었다. TGN 의 국소처리는 쥐에서 이미퀴모드 유발

153

건선성 피부 염증을 개선시켰다. 또한 TGN 은 쥐의 피부 조직에서 염증성 면역 유전자의 발현과 표피 과다 증식을 억제하였다.

본 연구 결과들을 종합하여 볼 때, 관동화 유래 세스퀴테르펜 화합물 ECN 과 TGN 은 강력한 Nrf2 활성화 물질로 작용하며, Nrf2 활성화를 매개로 하여 신경보호와 관련된 퇴행성 질환 및 건선의 예방 또는 치료 소재로서 가치 있을 것으로 기대된다. 이는 향후 관동화 유래 천연물 신약 개발에 있어 기초가 되는 중요한 연구로 사료된다.